EFFECT OF REACTION CONDITIONS AND ORGANIC ADDITIVES ON THE MORPHOLOGIES OF SYNTHETIC CALCIUM CARBONATES

A Thesis Submitted to
the Graduate School of Engineering and Sciences of
İzmir Institute of Technology
in Partial Fulfillment of the Requirements for the Degree of

MASTER OF SCIENCE

in Chemistry

by
Esra ALTAY

January 2006
İZMİR

We approve the thesis of **Esra ALTAY**

Date of Signature

.....
17 January 2006

Asst. Prof. Dr. Talal R. A. SHAHWAN
Supervisor
Department of Chemistry
İzmir Institute of Technology

.....
17 January 2006

Assoc. Prof. Dr. Metin TANOĞLU
Co-Supervisor
Department of Mechanical Engineering
İzmir Institute of Technology

.....
17 January 2006

Assoc. Prof. Dr. Hürriyet POLAT
Department of Chemistry
İzmir Institute of Technology

.....
17 January 2006

Asst. Prof. Dr. Mehtap EMİRDAĞ EANES
Department of Chemistry
İzmir Institute of Technology

.....
17 January 2006

Assoc. Prof. Dr. Hasan BÖKE
Department of Architectural Restoration
İzmir Institute of Technology

.....
17 January 2006

Assoc. Prof. Dr. Ahmet E. EROĞLU
Head of Department
İzmir Institute of Technology

.....

Assoc. Prof. Dr. Semahat ÖZDEMİR
Head of the Graduate School

ACKNOWLEDGEMENT

First and foremost I offer my sincerest gratitude to my supervisor Assist. Prof. Talal Shahwan who has supported me throughout my thesis with his patience and knowledge. The door to Assist. Prof. Talal Shahwan‘s office was always open whenever I had a question about my research. His substantial discussions and many perceptive comments have greatly improved this work. I attribute the level of my Masters degree to his encouragement and effort and without his generous donation of his time and ongoing guidance, this thesis would not have been completed. I have felt extremely lucky to be a member of the group and to have such a wonderful advisor and mentor.

I would also like to express my sincere thanks with much appreciation to my co-supervisor Assoc. Prof. Metin Tanoğlu for generously sharing his time and knowledge in our cooperative work He has offered critical comments, suggestions and insightful remarks.

My appreciation and thanks for the accomplishment of this study are directed to group members of Materials Research Center, Mine Bahçeci, Evrim Yakut and Gökhan Erdoğan, who contributed their time, effort, and expertise to help during the SEM and XRD analyses and mechanical tests. Also, special thanks to Elçin Kaya for her useful and helpful assistance during my studies in Materials Research Laboratory.

I am pleased to acknowledge TUBITAK for its partial financial support (Project No. 104T089).

I am also grateful to my friends in IYTE. I have made lasting friendships and have worked with many talented and intelligent people. Without the numerous people whom I have spent time togehter, graduate school would not have been as enjoyable.

Especially, I would like to give my special thanks to my family for helping me get through the difficult times, for all the emotional support, for the care they provided, and for their patience and love.

ABSTRACT

In this study, the effects of experimental conditions on the facile morphosynthesis of $CaCO_3$ were investigated. The analyzed conditions included the pH, concentration, mixing and aging temperature, and aging time. After establishing the optimal conditions for calcite and aragonite formation, the effects of organic additives, i.e., PVP, PDDA, PEG, CTAB and EDTA, on the stability and morphology of both polymorphs were examined. Finally, the applicability of calcite as a filling material in polyester was tested.

The results indicated that calcite was optimally synthesized at pH 9.0, 0.05 M initial reactant concentration, and 30^{o}C mixing and aging temperatures while the aging time was 24h. The morphologies of produced calcites were dominated by rhombohedra and cubic with particle size range of 5-6 μm. On the other hand, the precipitation of $CaCO_3$ dominated with aragonite requires mixing and aging temperatures of 70-90 in addition to shorter aging times. Within such experimental condition, aragonites displayed *needle-like* and *branch-like* morphologies with ca. 95% aragonite fraction and aspect ratio of around 8.

The applied additives demonstrated various effects on the morphology of precipitated $CaCO_3$. These effects ranged from changing the particle morphology of calcite and aragonite up to suppression of aragonite formation.

Finally the application of calcite as a filler in polyester polymer is discussed in light of a comparative determination of mechanical and thermal properties.

ÖZET

Bu çalışmada, deneysel koşulların $CaCO_3$ ın basit morfosentezi üzerindeki etkileri araştırılmıştır. Kalsit ve aragonit oluşumu için optimum koşulların belirlenmesinin ardından bazı organik katkı maddelerinin (PVP, PDDA, PEG, CTAB ve EDTA) her iki polimorfun kararlılığı ve morfolojisi üzerindeki etkisi incelenmiştir. Son olarak, kalsitin poliester reçinede dolgu maddesi olarak kullanılabilirliği test edilmiştir.

Elde edilen sonuçlara göre kalsit için optimum sentez koşulları; pH 9.0, başlangıç konsantrasyon değeri 0.05 M, bekletme süresi 24 saat, karıştırma ve bekletme sıcaklığı 30^oC olarak belirlenmiştir. Oluşan kalsit partikülleri 5-6 μm ortalama partikül büyüklüğü ile etkin olarak rhombohedral ve kübik morfolojilerde bulunmaktadır. Öteyandan, çökelen $CaCO_3$ içerisinde aragonitin yüksek oranda bulunması için daha kısa bekletme süresi ve 70-90 ^oC karıştırma ve bekletme sıcaklıkları gerekmektedir. Belirtilen deneysel koşulda aragonitler yaklaşık %95 aragonit ve 8 uzunluk/genişlik oranı ile iğne ve dal morfolojileri göstermektedir.

Katkı maddelerinin uygulanması, çökelen $CaCO_3$ morfolojisi üzerinde çeşitli etkiler göstermiştir. Bu etkiler, kalsit ve aragonitin partikül morfolojisi değişimi ve aragonit oluşumunun bastırılmasıyla sonuçlanmıştır.

Son olarak, kalsitin poliester polimer içinde dolgu maddesi olarak uygulanması mekanik ve termal özellikleri kıyaslanarak tartışılmıştır.

TABLE OF CONTENTS

LIST OF FIGURES

LIST OF TABLES

CHAPTER 1

INTRODUCTION

1.1 Calcium Carbonate and its Polymorphs

Calcium carbonate is one of the most abundant minerals on Earth. The Earth's crust contains 7% calcium carbonate as marble or limestone (Tai and Chen 1998). Nature deposits calcium carbonate as the major constituent of rocks, as mineral in the form of stalactites and stalagmites, as aqueous solution in the form of rivers and oceans, and in the form of skeletons and shells of plants and animals (Petrucci and Harwood 1997, Cölfen 2003). The link between these natural resources is the calcium carbonate cycle.

In the calcium carbonate cycle, plants and animals build up their skeletons and shells by absorbing calcium carbonate, from the water where calcium carbonate subsists as aqueous solution of calcium hydrogen carbonate $Ca(HCO_3)_2$. Following the death of these animals and plants such as crustacea, coccoliths, algea and corals, sedimentary deposit formation occurs on seabeds. Chalk and limestone formation develops during the sedimentation process. As a result of recrystallisation process of limestone under the high pressure and temperature conditions, marble is formed. Erosion may start the cycle by leading the carbonate rocks to be dissolved under the influence of wind, temperature and water (WEB_1 2005).

The particular interest in calcium carbonate system is caused by the polymorphism of calcium carbonate. It nucleates in three anhydrous crystalline forms - calcite, aragonite and vaterite – which have different particle morphologies or shapes (Tai and Chen 1998). Calcite is the most stable form of calcium carbonate and is formed at ambient temperature and atmospheric pressure. Aragonite is less stable than calcite and therefore less common. Vaterite is extremely scarce and rarely seen mineral (Westin and Rasmuson 2005a). Less stable forms of calcium carbonate can be stabilized kinetically. As a result of this, precipitates of calcium carbonate can be found as a mixture of polymorphs or with one form predominating (Tai and Chen 1998).

Even though the two different mineral species, calcite and aragonite, of calcium carbonate are chemically identical, they exhibit different crystal structures and symmetries. There is a certain dimension of radius (0.98 Å) which distinguishes between the two possible crystal system, rhombohedral and orthorhombic. The radius of the constituent cation determines the crystal structure of a carbonate. The carbonates having smaller cations form rhombohedral structures while such containing larger cations occupy orthorhombic structures. For examples, magnesium, manganese, and iron are small cations and their carbonates magnesite, rhodocrosite, and siderite, respectively, have rhombohedral crystal system. On the other hand, strontianite and cerrusite belong to the orthorombic crystal system, since their cations lead and strontium, respectively, are larger than the critical radius. However, in the case of calcium carbonate, the proximity of calcium radius (0.99 Å) to the critical radius, leads to the ability of calcium carbonate in either system. Therefore, calcite is rhombohedral while aragonite crystallizes according to the orthorhombic crystal system.

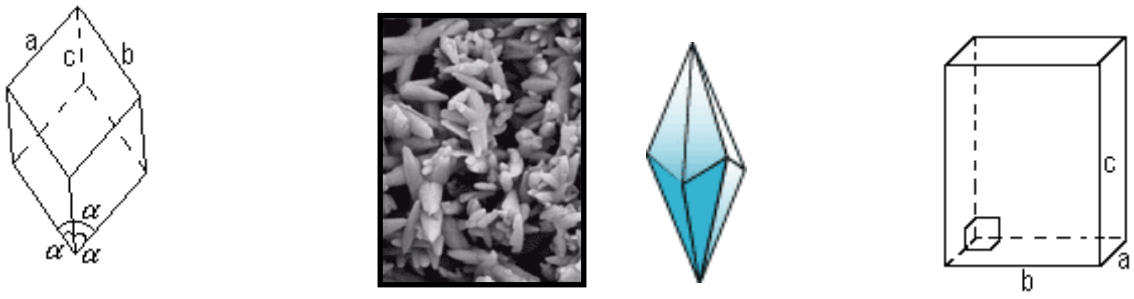

(a) (b) (c)

Figure 1.1. a) a rhombohedral unit crystal, b) a trigonal-scalenohedral form of calcite, and c) an orthorhombic unit cell (Source: WEB_2 2005)

Calcite crystals have equivalent axes and interfacial angles such that a=b=c and $\alpha=\beta=\gamma$ (Figure 1.1 (a)). The coordination number for calcite is 6. Although the most common form of calcite is rhombohedron, thousands of different shapes of calcite formed by combining the basic forms of the positive rhombohedron, negative rhombohedron, steeply, moderately and slightly tilting rhombohedrons and various scalenohedrons have been identified until today. Figure 1.1 (b) displays the trigonal - scalenohedral form of calcite as powder and as a single crystal.

Aragonite crystals have three inequivalent axes $a \neq b \neq c$ and and three equivalent interfacial angles such that $\alpha=\beta=\gamma=90^{o}$ (Figure 1.1 (c)). The coordination number for aragonite is 9. Aragonite begins to transform into calcite at 300-400^{o}C (WEB_2 2005), while vaterite does at about 457 ^{o}C (Wei et al. 2003). However, if the polymorphs are in contact with water, these temperatures may lower to room temperature. At 550 - 600^{o}C, calcite is transformed into calcium oxide (CaO) or lime (WEB_2 2005).

1.2 Nucleation and Crystal Growth Processes of $CaCO_3$

Polymorphs of a given substance can exhibit markedly different physical properties, i.e. solubility, hardness, melting point, density…etc. In industry, polymorphism is an important phenomenon, since different applications may require different polymorphs of a substance.

Precipitation and crystal growth are complex subjects with a vast literature. Many factors are important in determining the size and shape of the final particles. Supersaturation, temperature of reaction, subsequent aging, and the presence of additives are among the most important parameters.

1.2.1 Nucleation Process

In the formation and growth of crystals energetic factors play fundamental roles. Two components contribute to the total energy for the formation of a crystal; which are the surface and volume of such crystal. When crystals just start to form the ratio of surface area to volume is large, thus the surface energy contribution is very important.

According to the laws of thermodynamic, in order for a crystal to grow in an aqueous environment, the total free energy of the crystalline phase must be less than that of the liquid phase. The total energy of a phase (G_{total}) can be defined by the sum of the surface energy per unit volume (G_s) and the volume (G_v) components. For a crystal the total energy term can be illustrated as:

$$G_{total} = G_s 4r^2 - G_v 4/3r^3 \qquad (1.1)$$

If a crystal is larger than a certain size, called as the critical growth radius (r_c), growth will proceed spontaneously, because lower energy results. On the other hand, if radii of nuclei included in crystals are less than r_c, the first term in the equation dominates the total energy change. The nucleation state of crystal growth will not proceed in a direction of increasing crystal energy. This energy threshold is called as the nucleation energy. Supersaturation of liquids would assist to overcome this energy barrier and it makes the formation and growth of crystals possible (WEB_3 2005).

A supersaturated solution initiates formation of a new solid phase through nucleation (Westin and Rasmuson 2005a). Supersaturation, S, means that the solution contains more solute than present at equilibrium. It provides a relative measure of the systems deviation from its nonequilibrium state. Equation (1.2) illustrates such a relation between the solubility product of a solid phase and the supersaturation of the system.

$$\ln S = \frac{\Delta\mu}{RT} = \ln \frac{a_{CO_3} a_{Ca}}{(a_{CO_3} a_{Ca})_{eq}} = \ln \frac{a_{CO_3} a_{CO_3}}{Ksp} \qquad (1.2)$$

where $\Delta\mu$ is the difference in chemical potential between nonequilibrium and equilibrium state, a is the activity of ions.

The solubility of calcium carbonate differs depending on its polymorph. The corresponding solubility constants at 25^{o}C are;

Lg $K_{sp,calcite}$ = -8.475
Lg $K_{sp,aragonite}$ = - 8.36
Lg $K_{sp,vaterite}$ = -7.913

According to Ostwald' s law of stages, at a sufficiently high supersaturation the most soluble (the least stable) form crystallizes first. The next most soluble form develops by the transformation of the first form through a process of dissolution and crystallization (Gutjahr et al. 1996). Figure 1.2 depicts such mechanism. At the beginning (point A), system is supersaturated with respect to both forms I and II, and since form I is the higher-energy form, it will crystallize first. After this, form II should also begin to crystallize. The crystallization of form I will proceed until the concentration of the solution reaches the solubility of form I (point B). At this point, the system is supersaturated with respect to form II and the crystallization of this form will

continue until the concentration of solution drops below the solubility of form I. After that, form I will begin to dissolve. Further crystallization of form II will be correlated with more dissolution of form I until form I is completely transformed to form II. The presence of any other polymorphic forms with solubilities below form II results in a continuation of the above process until the system contains only the most stable (the least soluble) form.

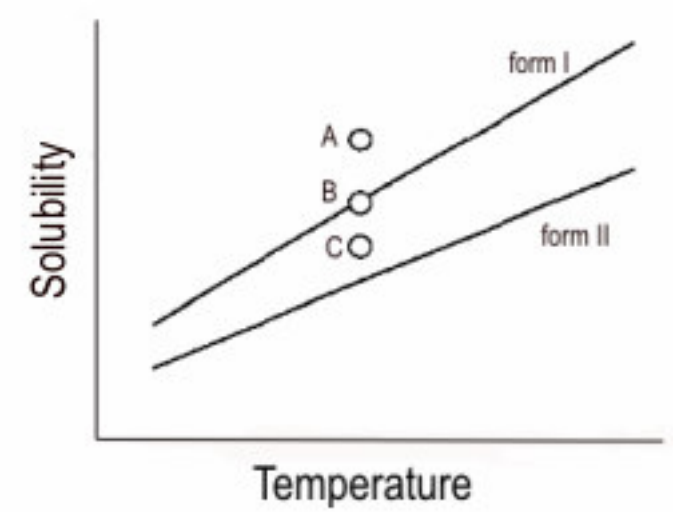

Figure 1.2. The effect of supersaturation on the crystallization of polymorphs. The circles indicate different supersaturations (Source: Khoshkhoo and Anwar 1993).

The induction time is defined as the time interval passing after the system is supersaturated till particles to be observed. The classical theory of crystallization divides the induction time to three discernible stages; which are the relaxation time, the nucleation time and the growth time. In the course of calcium carbonate precipitation, polymorphous abundance of calcium carbonate in the bulk solution usually changes in each stage (Westin and Rasmuson 2005a).

In the relaxation time, which is the unstable stage, the cluster distribution responds to the imposed supersaturation. In the case of calcium carbonate, when the ionic activity product (IAP) of the system exceeds the solubility product (K_{sp}) of amorphous calcium carbonate (ACC), spontaneous precipitation by the mixing of two concentrated solutions of calcium and carbonate results in a gelatinous matter. This amorphous phase is highly unstable, therefore it will transform into a mixture of crystalline polymorphs (calcite, aragonite and vaterite) within few minutes in solution.

Since the transformation rate is controlled by the nucleation and growth rates of more stable polymorphs, the IAP in the surrounding solution will stay constant at the solubility product value of ACC until it is completely dissolved. At the end of the first stage, ACC is dissolved completely, the IAP of the solution decreases as the newly formed particles grow by consumption of calcium and carbonate ions (Andreassen 2005).

In the nucleation time, which is the metastable stage, stable nuclei are produced. During this stage, vaterite and/or aragonite gradually transforms to the stable form (calcite). At this stage the IAP reaches the Ksp value of the least stable polymorphs, it remains stable until this phase is completely dissolved. Complete dissolution of vaterite and/or aragonite induces steep decrease in the IAP value to K_{sp} of calcite (Abdel-Aal and Sawada 2003).

In the growth time, which is the stable stage, no more change is observed. The value of IAP stabilizes at the solubility product of calcite and stable nuclei grow to a detectable size.

The transformations in the bulk solution proceed by a recrystallization mechanism, i.e., the dissolution of less stable polymorph and the growth of more stable polymorph, where the growth of stable crystals is the rate-determining process (Figure 1.3).

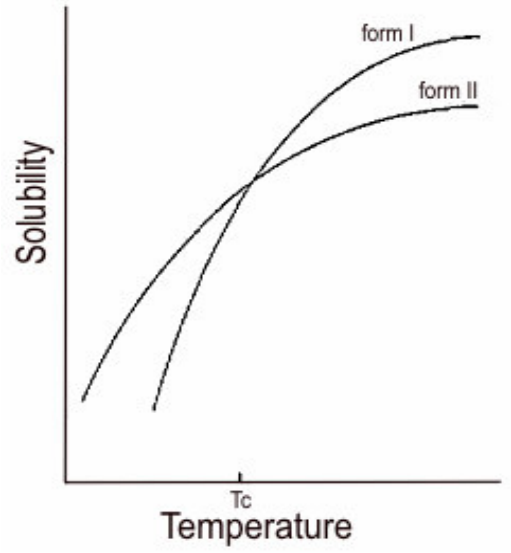

Figure 1.3. Solubility relationship between two polymorphic forms as a function of temperature close to the phase transition temperature Tc (Source: Khoshkhoo and Anwar 1993)

The thermodynamic stability of the polymorphic forms may change by the temperature. Only the lowest-free-energy form is thermodynamically stable at a given temperature. As an example, Figure 1.3 represents such a change in terms of solubilities. In the crystallization studies of the polymorphs thermodynamic stabilities must be considered (Khoshkhoo and Anwar 1993). Elevating the temperature above 60^{o}C stabilizes aragonite polymorph of calcium carbonate kinetically.

1.2.2 Crystal Growth

There are some approaches advanced to account for the mechanism of building of crystal, despite none of them represents the exact mechanism. In the progress of crystallization, first a small cluster of atoms that establishes the pattern and composition of the crystal is formed. Electrical forces in the crystal structure attract more atoms onto the seed crystal and induce of which to grow into a recognizable size.

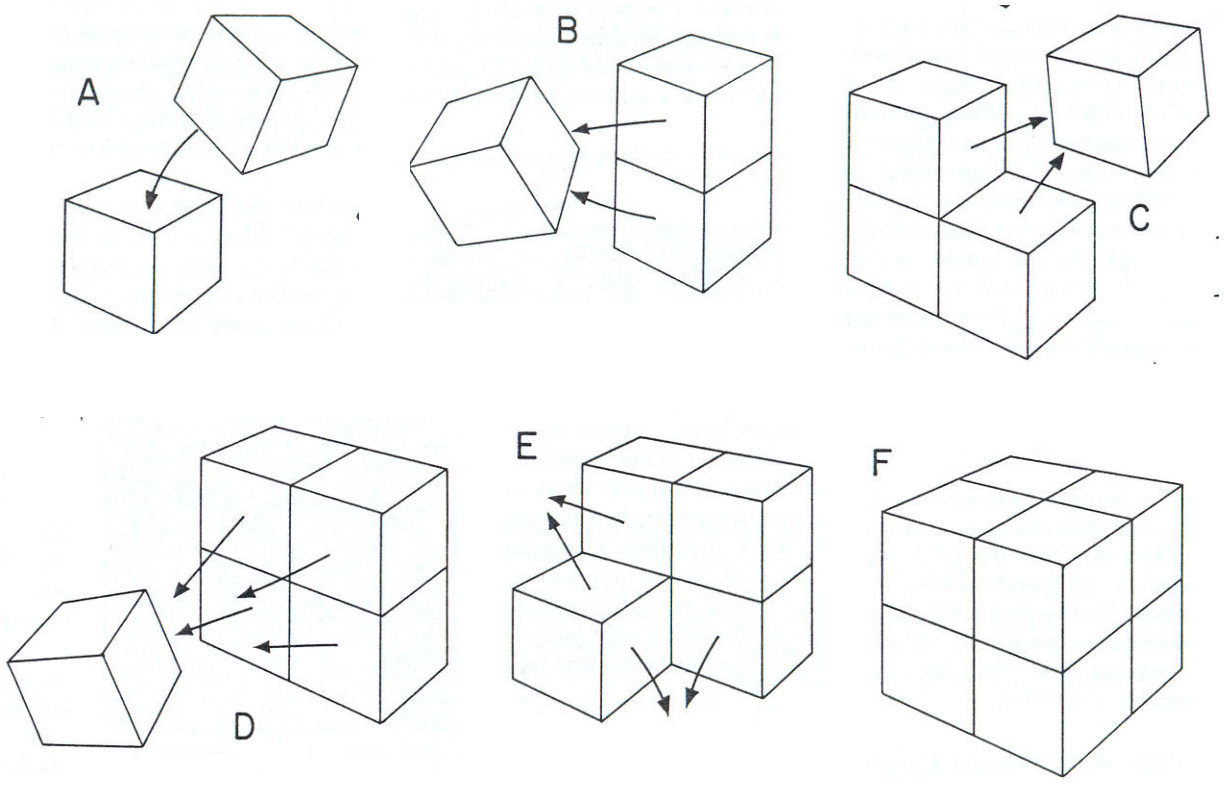

Figure 1.4. Growth process of a crystal from a cubic-shaped seed particle (Source: Sinkankas 1964)

Figure 1.4 represents a possible crystal growth mechanism developing from a cube-shaped or block-shaped seed. Since the beginning seed crystal (A) is a cube, the atomic attractions on each of its faces are assumed to be the same. Therefore, another block getting closer to the seed is attracted by any of them. The third one prefers to be drawn to the broader side of the growing seed since two faces exert more attraction than the single faces (B). Since the corners apply stronger attraction, the next block prefers corner to be attracted to any other place on the seed (C). The following steps D and E repeat the steps B and C, respectively (Sinkankas 1964).

1.2.2.1 Spiral Growth

As the crystal grows, the attraction of any corner or upraised part is so much stronger than elsewhere upon the face, thus incoming atoms are drawn to steps solely until the solid layer is formed. Other coming atoms start a new layer falling upon the new face. Such a process may be too slow for many crystals and they may create artificial steps by developing imperfections.

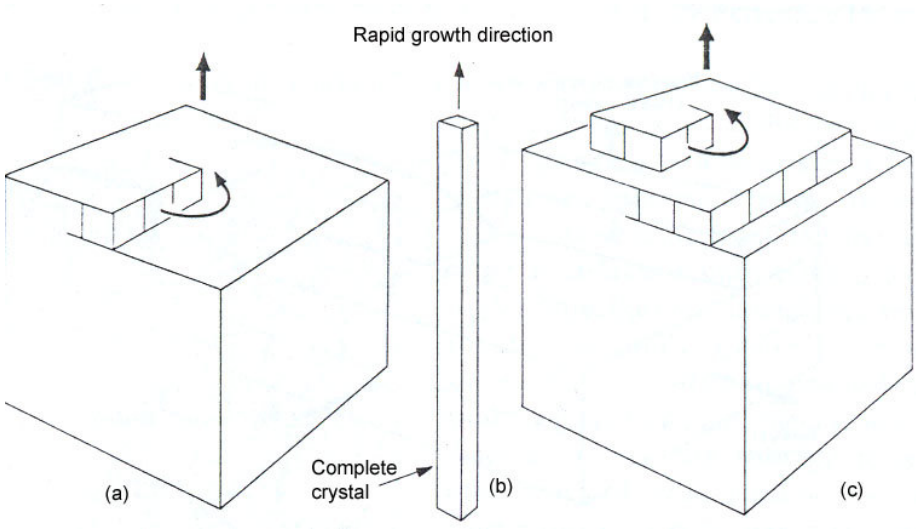

Figure 1.5. a) Spiral growth begins at a dislocation on a crystal face, causing formation of a step, b) Possible shape of the complete crystal, c) Formation of a step induces rapid growth along the face, and the step sweeps around in a spiral (Source: Sinkankas 1964).

Figure 1.5 represents a dislocation formed on a crystal face, which causes a formation of a step, as a result the formerly smooth layer is offset. The arrow in Figure 1.5 (c) indicates how the small shelf attracts atoms or ions faster and consequently grows around in a spiral ramp that rises upward indefinitely. Even though this crystal begins as a cube, it is more likely to finish as a slender crystal, perhaps like that shown in the Figure 1.5 (b). Despite this form of crystal growth is an imperfection, it is an important method of crystal growth being found on crystals of various species (Sinkankas 1964).

1.2.2.2 Growth Rates

In every crystal, growth proceeds with the same rate along certain directions, and is either slower or faster along others. No crystal grows at exactly the same rate in every direction. Figure 1.6 shows the rates of growth in spherical and cubic crystals.

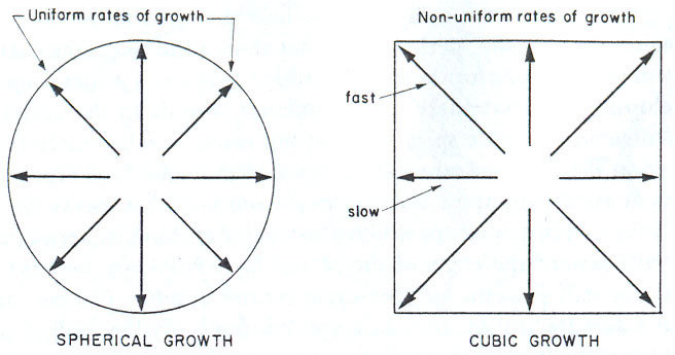

(a)

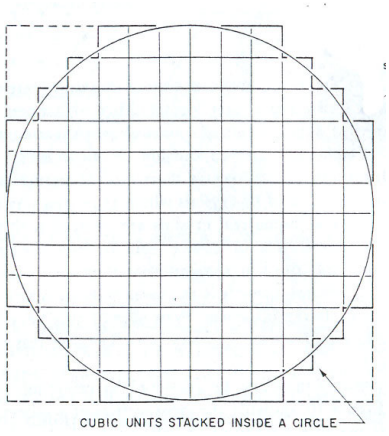

(b)

Figure 1.6. Rates of growth in spherical and cubic shaped crystals (Source: Sinkankas 1964)

Figure 1.6 (b) shows the general growth diagram of a sphere. As this almost-spherical crystal grows, all corners exercise the powerful attraction and atoms or ions attracted will fill them. In some growth cycles, corners fill out as shown by dotted lines, and the crystal restores itself to cubic shape. Therefore, attractions of ions in the crystal tend to keep the outer part covered by flat planes. However, sometimes growth is so rapid, which causes the faces to become rough. But some natural crystals have curved faces due to partial dissolution rather than growth.

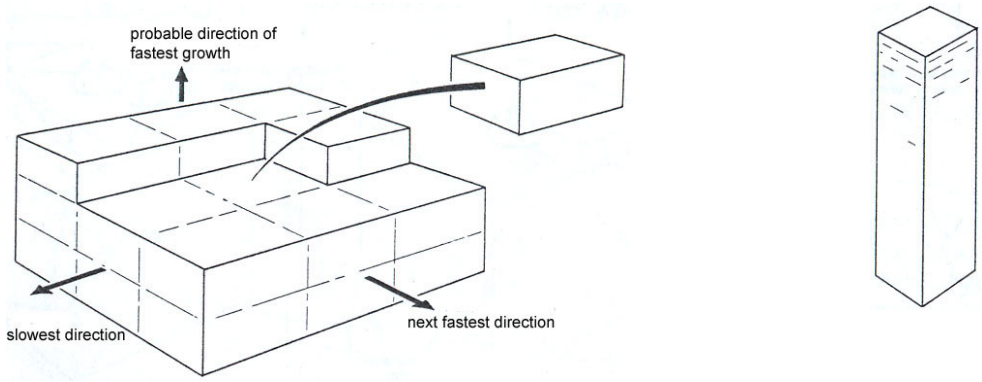

(a) (b)

Figure 1.7. Possible crystal growth mechanism from a brick-like shaped seed particle (Source: Sinkankas 1964).

If a building block has a brick-like shape rather than a cube one, the greatest attractive force will be on the largest face of the brick-like unit, less on the long and narrow face, and least on the ends (Figure 1.7 (a)). Then the finished crystal will most likely be a column stretching vertically (Figure 1.7 (b)). But, in the case where the attraction value on either of the other sides is highest, the final crystal shape might be possibly a flattened or tabular (Sinkankas 1964).

1.2.2.3 Development of Faces

Crystal growth is not always steady in any given direction, since they are extremely sensitive to slight changes in their environment. Sometimes the presence of an impurity in trace amounts in a solution may induce unequal growth, resulting in

over-development of some faces and loss of others. Figure 1.8 (a) shows a cube-shaped crystal that is rapidly changing its form due to the slower growth upon corners. In Figure 1.8 (b), the same reason converts the octahedron seed crystal into a cube (Sinkankas 1964).

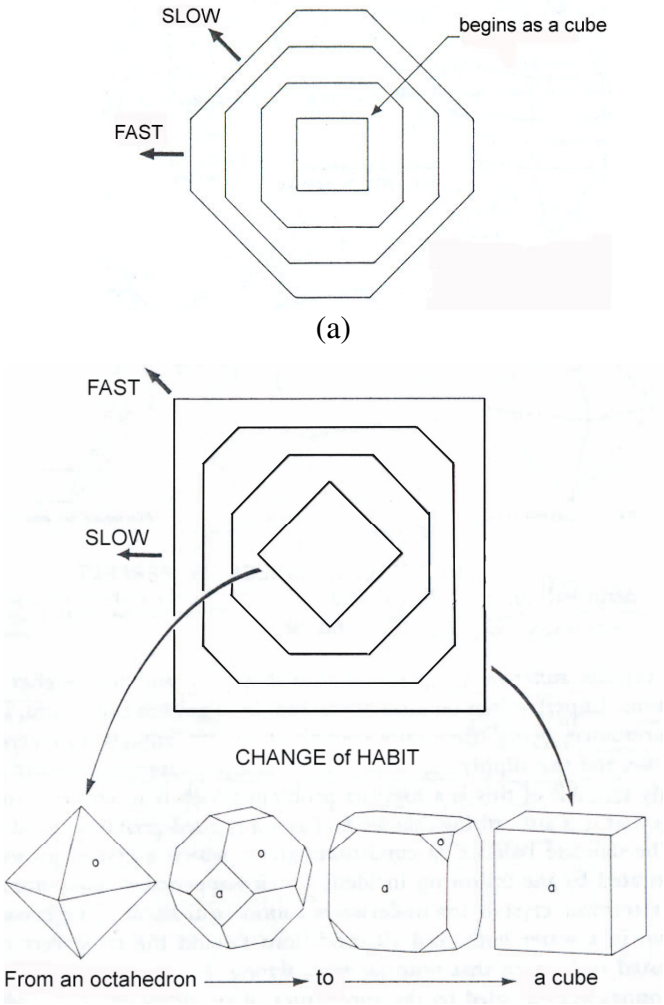

Figure 1.8. a) A cubic-shaped crystal, and b) an octahedron shaped crystal changing their forms due to the slower growth of corners (Source: Sinkankas 1964)

The geometry of the seed crystal tends to reflect itself in the finished crystal. The larger crystal is a greatly magnified version of the minute beginning unit. However, it is also possible that the final product has little resemblance to the original seed shape due to the development of some faces in certain directions at the expense of others (Sinkankas 1964).

1.2.3 Effects of Additives

As mentioned previously, when $CaCO_3$ precipitates in a highly supersaturated solution, a metastable phase often forms first and subsequently transforms into a more stable one. This process is a solvent mediated process. Finally rhombohedral calcite is obtained, which is the most thermodynamically stable phase of $CaCO_3$. Such transformations may be hindered or suppressed kinetically by solution additives, so that also the less stable phase is found at conditions, which are not compatible with its thermodynamic stability conditions (Xie et al. 2005).

The presence of additives can be thought to influence the crystallization of calcium carbonate by several different mechanisms. Interaction between additive molecules and calcium and carbonate ions individually lowers the concentration of freely available ions in solution medium and decreases the actual thermodynamic driving force for nucleation. For instance, the stability of complexes between calcium ions and metal complexing additives increases with the size of the so-called chelate ring formed. Thus, the influence on the driving force is expected to depend on the additive and its concentration. However, the additives can also influence the kinetics of nucleation. It is commonly assumed that homogeneous nucleation is preceded by the formation of more or less solid like clusters. The additives may directly interact with these clusters and thus hinder their formation (Westin and Rasmuson 2005a).

The molecules of an additive may have greater affinity with certain faces of a particular polymorph and will adsorb strongly onto these faces. This adsorption would result in inhibition of the deposition of oncoming solute molecules. The selective adsorption could result in the complete inhibition of nucleation or the retardation of the growth of the affected polymorphs to the advantage of others. Polymorphs less affected will continue to grow (Khoshkhoo and Anwar 1993).

1.2.3.1 Inhibition Models

There are various models for the interpretation of inhibitions by additives.

The Langmuir-Volmer model is one of them, which assumes a reversible adsorption of additives at specific surface sites, terraces, steps, or kinks (Gutjahr et al. 1996). A Langmuir isotherm describes the adsorption,

$$\theta_i = k_i c_i / (k_i c_i + 1) \tag{1.3}$$

where θ_i is the fraction of surface sites covered by the additive, c_i is the concentration of the additive in the solution and k_i is a constant .

Increasing coverage causes the growth rate, r_i, to decrease, which is given by:

$$r_i = r (1-\theta_i) \tag{1.4}$$

where r is the growth rate without additive. Then the relative decrease in the growth rate can be obtained by the equation,

$$(r-r_i) / r_i = k_i c_i \tag{1.5}$$

Another model assumes an immobile, i.e., irreversible adsorption of additives on the terrace (Gutjahr et al. 1996). The additives trap further steps. The velocity of the steps declines according to the equation,

$$\nu_p = \nu_x (1 - \rho_c / \rho) \tag{1.6}$$

where, ν_p is the velocity of a step with radius of curvature ρ, ν_x is the velocity of a straight step, ρ_c is the radius of the critical nucleus.

This route may result in a lower growth rate. Growth may stop completely at low supersaturation, if the critical radius becomes greater than the mean distance of additives on the terrace.

Different binding energies of ions at the kink sites of crystals, which may lead to different residence times of the impurity ions at the kinks results a different inhibition efficiency.

For controlling the polymorph of $CaCO_3$ the initial nucleation processes play an important role in controlling the final crystal. It is indicated that interactions of additives raise the critical energy value due to the repulsion and interfacial structure mismatch of the nucleating phase with nuclei. Since the dominating physical parameter of the nucleation energy is the surface energy, the influence of additives on nucleation may require to be evaluated in terms of an influence on the solid–liquid interfacial energy. However being able to discuss primary nucleation process requires more about properties of the prenuclei structure of which very little is known about (Westin and Rasmuson 2005a).

In spite of the presence of some approaches, there remain many unknowns as to how the additives affect the crystallization process. The final crystalline phase could arise through a series of steps, initiated by the formation of an amorphous phase that undergoes subsequent phase transformations (Naka and Chujo 2001). Controlling the precipitation conditions offers possibility to isolate the different polymorphic forms by harvesting crystals at an appropriate time.

1.3 Industrial Applications of Calcium Carbonate

In addition to the importance of $CaCO_3$ from a natural-process perspective, it is also an important system in industry (Tai and Chen 1998). Calcium carbonate makes an attractive model mineral for studies in the laboratory, because its crystals are easily characterized and the morphology of $CaCO_3$ has been subjected to control in biomineralization processes (Naka and Chujo 2001).

In general, the synthesis of calcium carbonate can be achieved using the following precipitation processes (Büchel et al. 2000):

$CaCl_2 + Na_2CO_3 \rightarrow CaCO_3 + 2NaCl$

$Ca(OH)_2 + CO_2 \rightarrow CaCO_3 + H_2O$

$Ca(OH)_2 + Na_2CO_3 \rightarrow CaCO_3 + 2NaOH$

$Ca(NO_3)_2 + 2NH_3 + CO_2 + H_2O \rightarrow CaCO_3 + 2NH_4NO_3$

Both natural (ground) calcium carbonate and synthetic (precipitated) calcium carbonate can be used in a wide range of applications (WEB_1 2005). Ground calcium carbonate (GCC) is mainly used in the construction industry, e.g. in road building and in the cement industry. It is also utilized in the manufacture of quicklime.

When limestone, chalk or marble, is used it has to be ground to a desired particle size for any of its applications. However, grinding does not remove the undesirable coloring material. Despite there are bleaching processes that can remove the coloring material, such processes are not preffered due to their expense this makes the highly pure precipitated $CaCO_3$ (PCC) more economically feasible and thus more desired for a number of specific industrial applications (WEB_4 2005).

Using of calcium carbonate minerals in industrial applications may bring following functions into the system (Büchel et al. 2000):

- to make the product less expensive,
- to improve an existing property or add a property absence in the unfilled product,
- to make the manufacture of the product easier.

Some industrial fields utilizing precipitated calcium carbonate (PCC) are summarized below.

1.3.1 Paper Industry

The use of calcium carbonate has grown appreciably, since sizing in the paper industry is inverted from acid to neutral. Today, calcium carbonate is the most widely used mineral in papermaking (WEB_1 2005). Worldwide, almost 75% of the PCC is used in paper industry, which corresponds approximately to 90% of the filler used for papermaking (Büchel et al. 2000). PCC is also used as a coating pigment to impart brightness and ink receptivity (WEB_4 2005).

The quality aspects of alkaline paper made with PCC are as follows:

Permanence: The presence of PCC reduces the degradation and subsequent discoloration of fibers. The acidic radicals in the atmosphere are neutralized by PCC

and kept from attacking the fibers, which prevents the reduction in strength and discoloration. For printing papers used for books, this permanence is crucial.

Brightness: Normally, clays with brightness of 76 - 90% are utilized for the acid-sized papers. Titanium dioxide usage increases the brightness, but this is expensive. The use of PCC provides at least 95% brightness in alkaline papers such value can be 3% higher than the brigthness obtained from GCC (Figure 1.9) as fraction of filler is approximately 0.25.

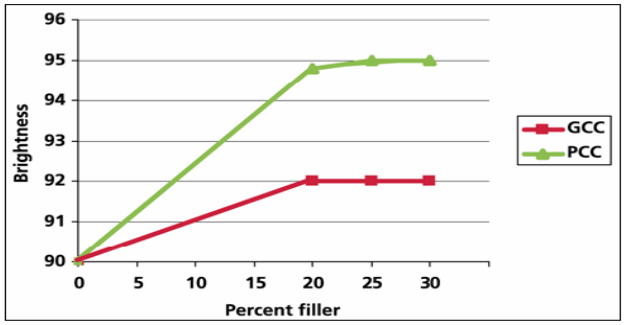

Figure 1.9. Brightness of paper with PCC vs GCC (Source: WEB_4 2005)

Opacity: Higher opacity supplies reduction in the ink show-through when the paper is printed. The use of PCC in alkaline papers can carry the opacity of paper to a higher degree than the GCC does (Figure 1.10).

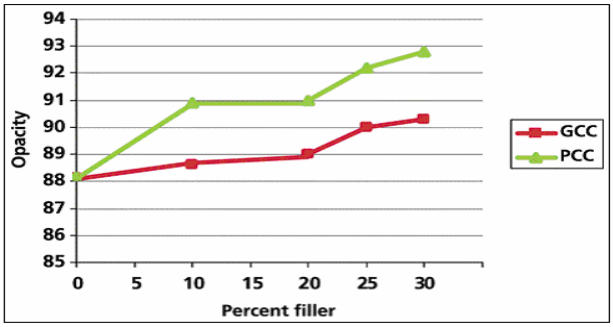

Figure 1.10. Opacity of paper with PCC vs GCC (Source: WEB_4 2005)

Bulk: Bulk is the actual, physical thickness of a piece of paper, usually expressed in thousandths of an inch. It affects the flexibility of paper; too thick paper causes difficulties during their usage. The use of PCC in alkaline papers increases the

bulk of the papers by 2-5%. In Figure 1.11 stiffness corresponds to the bulk of the paper, since stiffness increases as bulk increases.

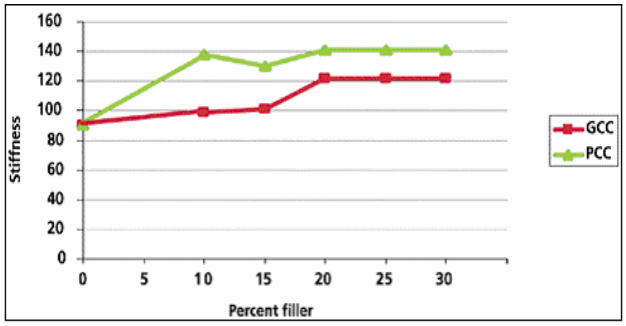

Figure 1.11. Bulk of paper with PCC vs GCC (Source: WEB_4 2005)

1.3.2 Plastic Industry

Calcium carbonate is a common mineral used for polymer compounding. It corresponds to more than 60% of the filler and reinforcements market by weight. It is mainly used for PVC, unsaturated polyesters, polypropylene and polyethylene compoundings. Calcium carbonate is not only used as a filler to reduce cost but it also submits a range of technical effects.

As an example, in plasticised PVC coated PCC utilization provides high surface gloss and smooth surface finish. Figure 1.12 compares the smooth surface finishes supplied by CPCC and GCC formulations (WEB_4 2005). The presence of larger particles in GCC formulation induces the scattering of light.

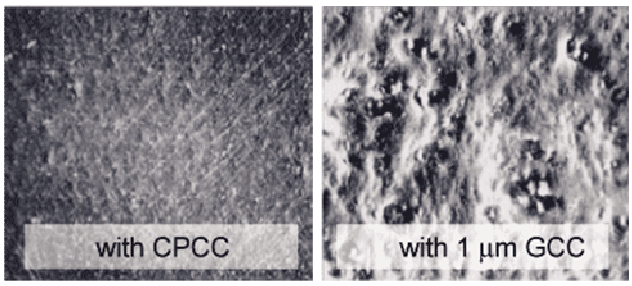

(a) (b)

Figure 1.12. Utilization of $CaCO_3$ in plasticised PVC; (a) Coated PCC formulation, (b) GCC formulation (Source: WEB_4 2005)

1.4 Composite Materials

Polymers have unique properties, such as low density, low electrical and thermal conductivities, low mechanical stiffness, that are sometimes necessary to be improved. Fillers in various shape and sizes are added into polymers to enhance the mechanical, electrical, thermal, optical properties to ease the processing and to reduce cost of polymers.

A composite can be defined as a material formed by combining two or more materials (a selected filler or reinforcing agent and a compatible matrix binder), to have unique and new properties. The constituents of the composite material do not dissolve or blend into each other and they retain their chemical and physical properties (WEB_ 5 2005).

Polymeric composites can be classified based on thermoplastic and thermoset matrix. Thermoplastics can be repeatedly solidify and melt as the temperature is decreased or increased, respectively, while thermosets transform into an infusible and insoluble material when they are cured chemically, in general, with the application of heat. Polyester resins are the most common resin systems among thermosetting polymers. Their low cost, ease of use and their versatility make polyesters applicable in many industrial applications. In addition to these advantages, they have high impact and good weathering resistance. Polyester resins are employed in laminates, castings, art objects, industrial construction, insulation, embodiments, molding compounds, coatings, and adhesives (Mansour and Abd-el-Messieh 2001).

Fillers and reinforcing elements that are used in the fabrication of composites are available in the particulate and fibrous forms based on their shapes. They are produced as organic, inorganic, metallic or ceramic materials. The type and the function of some fillers used in polymers are given in Table 1.1.

Fillers are employed in polyester resins: (i) to reduce the cost, (ii) to increase hardness, thermal conductivity and chemical resistance, (iii) to decrease the thermal expansion, (iv) and (v) to improve the insulation properties. Applications of various fillers such as quartz, clays and $CaCO_3$ in polyester do not affect the crosslinking performance, while alumina trihydrate or silica reduces the flammability and enhance electrical characteristics (Mansour and Abd-El-Messieh 2001).

Table 1.1. Types of fillers used in polymers and their functions (Öktem 1991)

TYPE	FILLER	FUNCTION
Organic Particulate	Carbon black	as reinforcing agent, processing aid, pigment, UV stabilizer, for producing conductivity
	Powdered rubber	for increasing toughness
Organic Fibrous	Aramid, ultra high molecular weight polyethylene (UHMWPE), HDPE	for high modulus, thermally resistant
	Cellulosics	as laminating material
Inorganic Particulate	Silica, silicates, clays, mica, $CaCO_3$, Al_2O_3	for low cost
	Molibdenium disulfide	as lubricant
	Barium ferrite	for its magnetic properties
	Barium sulfate	for chemical resistance and X-ray opacity
	Metal powders (aluminum, copper, bronze, brass, iron, silver, steel and zinc)	for metallizing effects, increased electrical and thermal conduction, radiation resistance
Inorganic Fibrous	Asbestos	for increasing tensile strength, flame resistance, heat abrasion, chemical resistance
	Glass	for chemical resistant and high strength

The mechanical characteristics of a composite material are significantly affected by interfacial interactions in addition to properties of components of the composite material. The physical and chemical interaction at the polymer-filler interface can affect the mechanical and physical properties of the composite. Molecular interactions at the interphase, thickness of the interphase and strength of the interphase determine the stress transfer between fibers and matrix. Good stress transfer between the matrix and filler is required for an optimum adhesion between the filler and the polymer. Poor adhesion or the absence of adhesion results in no stress transfer across the interface; as a result the load will be carried by the matrix polymer only. The presence of optimum adhesion results the stress transfer that allows the filler to share the stress and reinforcing effect is supplied. Dispersion problem can be controlled and the mechanical strength of composites can be enhanced by the application of some coupling agents to improve adhesion across the interface (Zhou et al. 2004).

Various types of surface modifiers such as fatty acids, phosphates, silanes, titanates or zirconates are employed to coat $CaCO_3$ in order to reduce the high surface energy of calcium carbonate, its particle-particle interactions, and agglomerate formation (Osman et al. 2004). Silane coupling agents contain unsaturated groups that can copolymerize with the unsaturated groups present in the polymer resin (Öktem 1991). The general formula of the silane coupling agents is shown in Figure 1.13, where R is the organofunctional group of the silane coupling agent and R´ is an either a halide, alkoxy or acyloxy group.

Figure 1.14 illustrates the interaction between a mineral surface and a silane coupling agent, schematically.

In the silanization process, first silanols form in the presence of water as a result of hydrolization of R´ groups in silane coupling agents. Then hydrogen bonds are formed between the silanols and the mineral surface. Finally, silanols condense to for siloxane and they bond to the surface through oxane bonds.

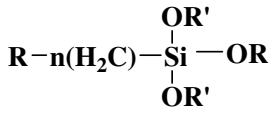

Figure 1.13. The general formula of the silane coupling agents (Demjén et al. 1997)

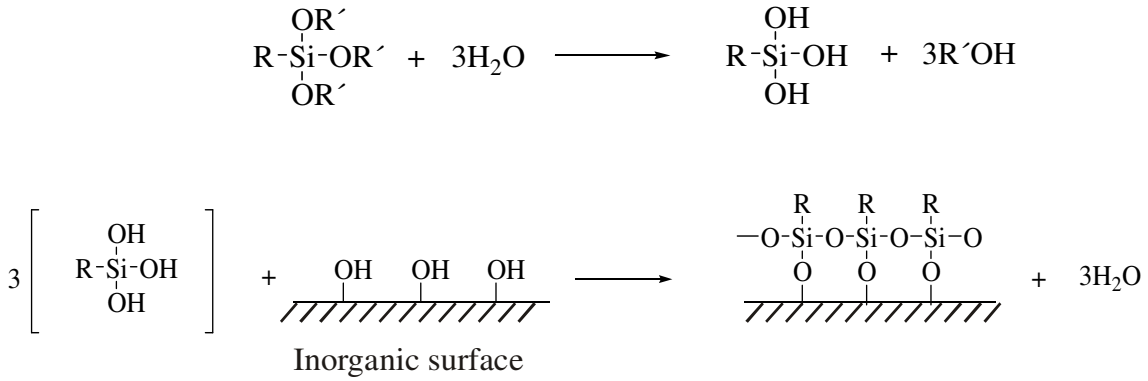

Figure 1.14. A possible mechanism between a silane coupling agent and a filler surface in the presence of water (Öktem 1991)

1.5 The Present Study

1.5.1 The Aim of the Study

In this study the primary goal was to reveal the effect of experimental conditions on the type of synthesized polymorph and the corresponding morphologies of $CaCO_3$. The experimental conditions examined in this work include concentration of the starting materials (Na_2CO_3 and $CaCl_2$), pH, mixing temperature, aging temperature and aging time. Following these experiments which elucidated the optimized conditions for the synthesis of calcite and aragonite polymorphs, the effect of organic additives on the morphology and aspect ratio of each polymorph was examined. The organic additives applied in this work included PVP, CTAB, PEG, EDTA and PDDA. Finally, the applicability of calcite as a filling material in a polyester resin was investigated. The effect of calcite addition on the mechanical properties of the composite material was evaluated and compared to those for pure polyester.

Throughout this study, the following techniques were used in the characterization of the synthesized materials:

- X-ray Powder Diffraction (XRD); applied to identity the outcoming polymorph of $CaCO_3$
- Fourier Transform Infrared Spectroscopy (FTIR); used to study the vibrational modes of the synthesized polymorphs
- Scanning Electron Microscopy (SEM); applied to reveal the morphological structure and evaluate the aspect ratio of the crystals of the synthesized material
- Mechanical Testing Machine; used to determine the mechanical properties; stress, strain behavior, tensile strength and modulus of the composite materials.

1.5.2 Literature Review

Since earlier of the 1990's, control of inorganic crystallization in aqueous solution has been subjected to thousands of studies. For crystallization of $CaCO_3$ the effect of pH, temperature, foreign ions and the effect of various types of organic matrixes are such parameters to be investigated widely.

Wray and Daniels 1957 described the experimental conditions for three polymorphs of calcium carbonate. Using calcium nitrate (calcium chloride gave the similar results) and sodium carbonate without controlling the solution pH and composition, high fraction aragonite was isolated at temperature above ca. 50^oC and vaterite at about 30^oC at digestion time of 0.1 hour. As a general trend higher temperature favors the formation of aragonite, and longer aging promotes the formation of calcite.

Yu et al. 2004 reported the experimental conditions to form plate - like calcite with particle size of 6-12 μm, as 0.5 M 1.28 mL of Na_2CO_3 and $CaCl_2$, at pH 10 with the aging time of 24 h. Interesting result obtained at which study that 80^oC aging temperature at the same condition lead to the formation of rhombohedra calcite particles with the particle size of 4-10 μm.

If pH was taken as a parameter in a constant - composition environment study at a fixed temperature of 24^{o}C, supersaturation of 5.5 and concentration ratio of 1, vaterite is obtained as major product in the pH range between 8.5 and 10. The fraction of aragonite and calcite increased with an increase in pH value. Aragonite had a maximum yield at pH 11 (Hu and Deng 2004) and calcite at pH 12.5. pH lower than 11 at low temperatures (~ 7^{o}C) suppressed the aragonite and promoted calcite, while nearly pure aragonite was obtained at 58^{o}C for a pH lower than 10 (Tai and Chen 1998). Swinney et al. 1982, however, obtained high purity aragonite at a pH around 10.

Effects of many additives including inorganic and organic ones have been investigated to obtain polymorphs of calcium carbonate with an optimum size and shape. Magnesium ion is the most common additive to obtain pure aragonite. Mg/Ca ratio of 4 was reported to be required for the precipitation of aragonite rather than calcite (Mann et al. 1990). Hu and Deng 2004 prepared needle-like and branch like aragonite using $MgCO_3$ and $CaCl_2$ aqueous solutions, which indicated that optimum amount of magnesium ion addition required to increase aragonite fraction, since further addition sligtly decreased the aspect ratio. Uniform needle-like aragonite particles with a mean length of 45 μm and aspect ratio of ~10 obtained by the 3 h. aging of a mixed solution containing 0.25 mol dm^{-3} $CaCl_2$ and 0.75 mol dm^{-3} urea at 90^{o}C without pH adjustment were reported (Wang et al. 1999). It is interesting that, separately heating of solutions to 90^{o}C before mixing lead to formation of flower-type vaterite particles, while aging the solution under magnetic stirring that prepared same as the conditions of aragonite lead to the formation of rhombohedral calcite particles. Poly (acrylate) in calcium solution obtained by the effect of radical initiator on the sodium acrylate caused aragonite precipitation at 30^{o}C (Naka and Chujo 2001). Poly (Aspartic acid – Leucine) is another additive reported to yield aragonite formation (Addadi and Weiner 1985).

In addition to magnesium ion, Ni^{2+}, Co^{2+}, Fe^{2+}, Ba^{2+} and St^{2+} also were indicated to favor aragonite formation while Pb^{2+}, Mn^{2+} and KH_2PO_4 favor the calcite formation (Tai and Chen 1998). Poly (vinyl alcohol) is highly selective for vaterite (Naka and Chujo 2001).

PVP is a widely studied water-soluble, nonionic, inert polyamide polymer by researchers. Wei et al. 2003 found that the presence of PVP has no effect on the polymorphs of $CaCO_3$ precipitation, but has a morhological effect on vaterite and calcite at high PVP concentration. The mixture of 0.1 M of 100 mL Na_2CO_3 and $CaCl_2$ including 100 g/L PVP prepared with magnetic stirring incubation and without pH

adjustment suppressed the crystallization of $CaCO_3$, leading to the formation of smaller crystal sized (i.e., <30 μm) and finer shaped of calcite. The same study reported that the time needed for vaterite to transform into calcite in PVP aqueous solution was much shorter than the solutions in the absence of PVP. Even though PVP alone has no effect on $CaCO_3$ morphology and crystal phase, as used accompanied by an anionic surfactant i.e., sodium dodecyl sulfate, flat sheet and flower-shaped crystals were obtained in the SDS/PVP system while aggregates of nanometer-sized crystals of $CaCO_3$ were obtained in SDS system in the reaction condition of 0.1 M initial concentrations of Na_2CO_3 and $CaCl_2$ at 24 h. aging time and 26±1 ^oC aging temperature. In this system the coexistence of aragonite and calcite at such a temperature was also confirmed (Wei et al. 2004a). PVP was also studied with sodium dodecyl benzene sulfonate (SDBS) anionic surfactant in the experimental condition of 0.1 M 100 mL of Na_2CO_3 and $CaCl_2$, the aging time of 10 h. and aging temperature of 26± 0.2^oC at pH=7 (Wei et al. 2004b). Increase in SDBS concentration without changing the amount of 1 g/L PVP altered the morphology of calcium carbonate from rhombohedral calcite to peach-nucleus-like calcite, futher increase lead to spherical vaterite particles.

Yu et al. 2004 investigated the effects of PEG (polyethylene glycol), CTAB (cethyl trimethylammoniumbromide), PVA (polyvinyl alcohol) and PAA (polyacrylic acid) on the $CaCO_3$ morphology and crystal phase. At 25^oC, all except PAA exhibited no obvious influence on the calcium carbonate crystallization; however, increase in temperature to 80^oC lead to various results. At 80^oC PEG resulted in irregular shapes, aragonite whiskers were obtained in the presence of CTAB, dendrite – shaped calcium carbonate with high fraction of calcite was produced in the presence of PVA. Irregular – shaped ellipsoidal particles formed in the presence of PAA at 25^oC enhanced by elevating the temperature to 80^oC and induced the formation of monodispersed calcite particles (~3 μm).

CTAB, a typical cationic surfactant, also applied to the system of calcium carbonate as a mixture of dihydrophilic block copolymer PEO-b-PMAA in Qi et al. 2002. While calcite spheres and dumbbells were produced in the presence of PEO-b-PMAA system, presence and increase of CTAB lead to the peanut and pine - cone shaped calcite crystals. They indicated that as a result of further increase in CTAB concentration calcite crystals gradually recovered their rhombohedral {104} faces.

Verdoes et al. 1992 reported that polyacrylic acid and a copolymer of polymaleic and polystyrene sulfonic acid increase the induction time of vaterite. Citric

acid (CIT) and diethylenetriamine pentaaceticacid (DTPA) decreases the growth rate of aragonite while ethylenediaminetetra aceticacid (EDTA) has a weaker effect (Westin and Rasmuson 2005b).

$CaCO_3$ is among the most studied filler with various types of polymers. There are several studies on the influence of increasing volume fraction of ground-micron sized commercial calcite fillers on the mechanical properties of polyolefins. Generally, increase in filler volume fraction increases the elastic modulus. All other tensile properties such as the yield stress and strain almost invariably decline with increasing filler volume fraction (Osman et al. 2004). Mansour and Abd-El-Messieh 2002 reported the comparative studies of clay, calcium carbonate and quartz fillers on the properties of styrenated polyesters. Quartz and clay imparted the highest compressive values to the polymer composites when the filler content was 60%, while $CaCO_3$ and quartz composited imparted the highest tensile strenght values as compared with clay. Osman et al. 2004 studied the effect of stearic acid - coated calcite on the properties of low-density polyethylene (LDPE). Stearic-coated calcite increased the stiffness and yield stress of LDPE while decreased all its other tensile properties. To avoid the decrease in tensile properties due to the excess amount of coating agent, optimal amount of surfactant to coat the filler surface with an organic monolayer might have been required. Demjén et al. 1997 examined the effects of eight silane coupling agents on the mechanical properties of PP/$CaCO_3$ composites by applying two surface treatment methods; dry blending and adsorption from n-butanol solution. The application of aminofunctional silane coupling agents lead to increased strength and decreased deformability. Aminofunctional silane coupling agents adheres well to the filler surface and they react also with the polymer. The amount of coupling agent forming a monolayer coverage values for the $CaCO_3$ changed between 0.3 and 1.0 wt%. For 3-(Trimethoxysilyl) propyl methacrylate (MPTMS) this value was found as 0.3%. MPTMS could be completely removed from the surface of $CaCO_3$ indicating very weak adhesion.

1.5.3 Applied Characterization Techniques

1.5.3.1 X-Ray Diffraction (XRD)

X-rays are electromagnetic radiation of wavelength about 1 Å (10^{-10} m), which is about the same size as an atom and enabled crystalline structure at the atomic level to be probed.

X-ray diffraction is a versatile, non-destructive technique used for identifying the crystalline phases present in solid materials and powders and for analyzing structural properties (such as stress, grain size, phase composition, crystal orientation, and defects) of the phases.

The method uses a beam of X-rays to bombard a specimen from various angles. X-ray photons scatter by interaction with the electron cloud of the material. When an X-ray beam hits an atom, the electrons around the atom start to oscillate with the same frequency as the incoming beam. In almost all directions we will have destructive interference, that is, the combining waves are out of phase and there is no resultant energy leaving the solid sample. However the atoms in a crystal are arranged in a regular pattern, and in a very few directions we will have constructive interference. The waves will be in phase and there will be well-defined X-ray beams leaving the sample at various directions. Hence, a diffracted beam may be described as a beam composed of a large number of scattered rays mutually reinforcing one another (WEB_6 2005).

By varying the angle of incidence, a diffraction pattern emerges that is characteristic of the sample.

The lattice planes, i.e., the crystal, must be properly oriented for the reflection to occur. The direction and intensity of the scattered (diffracted) beams depends on the orientation of the crystal lattice with respect to the incident beam. Any face of a crystal lattice consists of parallel rows of atoms separated by a unique distance (d-spacing), which are capable of diffracting X-rays.

The pattern produced by the diffraction of x-rays through the closely spaced lattice of atoms in a crystal is recorded and then analyzed to reveal the nature of that lattice, i.e. how the atoms pack together in the crystalline state and what the interatomic distance and angle are etc. This generally leads to an understanding of the material and molecular structure of a substance.

The X-ray patterns generated by this technique shows concentric rings of scattering peaks corresponding to the various d-spacings in the crystal lattice. The positions and the intensities of the peaks are used for identifying the underlying structure (or phase) of the material.

The unit cell and space group must be determined to solve the structure. Crystals are the structures ordered in three dimesions. They can be described as a repetition of identical unit cells, which are made up of the smallest possible volume. The dimensions of a unit cell can be described by 3 axis (a, b, c) and 3 angles between them (α, β, γ). A given set of planes with indices h, k, l cut the a-axis of the unit cell in h sections, the b axis in k sections and the c axis in l sections. A zero indicates that the planes are parallel to the corresponding axis. The process of reflection is described here in terms of incident and reflected (or diffracted) rays, each making an angle θ with a fixed crystal plane. Reflections occur from planes set at angle θ with respect to the incident beam and generate a reflected beam at an angle 2θ from the incident beam (WEB_7 2005). The unit cell is determined from the diffraction of the x-rays using the Bragg equation (Cullity 1978):

$$n\lambda = 2\,d\sin\theta \qquad (1.7)$$

where: n = an integer - 1,2,3…,etc,

λ = wavelength in Å (1.54 Å for copper),

d (d-spacing) = interatomic spacing in Å and

θ = the angle between the incident ray and the scattering planes

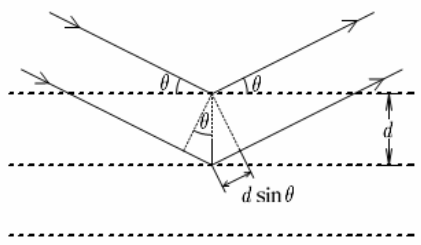

Figure 1.15. Reflection of x-rays from two planes of atoms in a solid (Source: WEB_8 2005)

As shown in Figure 1.15, the path length difference for waves reflected from successive planes is $2d\sin\theta$. Constructive interference of the reflected waves occurs when this distance is an integral of the wavelength.

An X-ray diffractometer involves a source of monochromatic radiation and an X-ray detector located on the perimeter of a graduated circle centered on the powder specimen. The geometry of a typical X-ray diffractometer is shown in Figure 1.16. In an X-ray tube, the high voltage maintained across the electrodes draws electrons toward a metal target (the anode). X-rays are produced at the point of impact, and radiate in all directions. Tubes with copper targets, which produce their strongest characteristic radiation ($K_{\alpha 1}$) at a wavelength of 1.5418 Å are commonly used. Divergent slits, located between the X-ray source and the specimen, and divergent slits, located between the specimen and the detector, limit scattered (non-diffracted) radiation, reduce background noise, and collimate the radiation. The detector and specimen holder are mechanically coupled with a goniometer, thus a rotation of the detector through 2θ degrees occurs in cooperation with the rotation of the specimen through θ degrees (WEB_9 2005). The powdered sample provides (theoretically) all possible orientations of the crystal lattice, the goniometer provides a variety of angles of incidence, and the detector measures the intensity of the diffracted beam. The resulting analysis is described graphically as a set of peaks with % intensity on the Y-axis and goniometer angle on the X-axis. The exact angle and intensity of a set of peaks is unique to the crystal structure being examined.

Bulk samples, powders, single crystals, polycrystalline materials, and thin films can be analyzed by this technique.

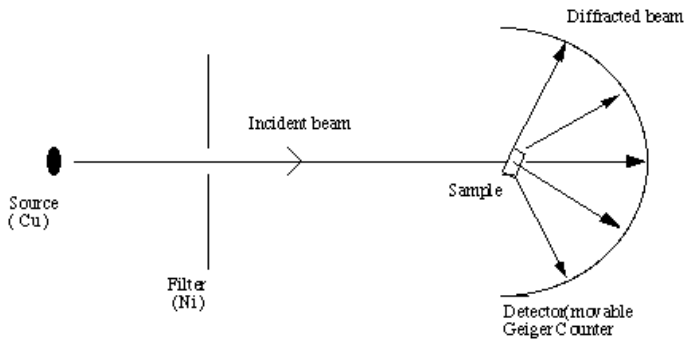

Figure 1.16. Schematic of an X-ray powder diffractometer (Source: WEB_10 2005)

1.5.3.2 Scanning Electron Microscopy / Energy Dispersive X-Ray Spectroscopy (SEM / EDS)

Scanning electron microscope (SEM) is a type of electron microscope that produces high-resolution images of a sample surface. Scanning electron microscopy is central to microstructural analysis and therefore important to any investigation relating to the processing, properties, and behavior of materials that involves their microstructure. The SEM provides information relating to topographical features, morphology, phase distribution, compositional differences, crystal structure, crystal orientation, and the presence and location of electrical defects. The SEM can also determine elemental composition of samples with the addition of an x-ray or electron spectrometer and phase identification through analysis of electron diffraction patterns. SEM is a versatile technique due to the multiple signals generation, simple image formation process, wide magnification range, and excellent depth of field.

In the SEM electron beam is accelerated with moderately high energy and positioned onto the sample by electromagnetic fields. When the incoming electrons hit on a point on the surface of the specimen they interact with atoms in the specimen by several mechanisms. Inelastic interaction is one of them by which energy is transferred to the sample from the beam. Elastic interaction is referred to a change in trajectory of the beam electrons as preserving their energies. Occurance of inelastic and elastic interactions at the same time results changing trajectories of the beam electrons from the original focused probe and losing their energies. This simultaneous energy loss and change in trajectory produces an interaction volume within the bulk extending about less than 100 nm to 5 μm depths into the surface.

Inelastic scattering produces secondary electrons, x-rays, auger electrons, phonons, transmitted electrons and cathodoluminescence; whilst backscattered electrons are caused by the elastic scattering. While all these signals are present in the SEM, not all of them are detected and used for information. The signals most commonly used are secondary electrons, backscattered electrons and x-rays. These interactions and effects are detected and transformed into an image (Lawes 1987).

Backscattered electrons are primary electrons emitted by changing trajectory of the incident electrons and escape from the sample as a result of elastic collisions with

the electrons of the specimen. Since their average energy is much higher than that of the secondary electrons, the sampling volume (sample depth) is also greater.

Secondary electrons have relatively lower energy (typically 2 to 5 eV). They are emitted from the outer shell of a specimen atom as a result of inelastic collisions with beam electrons. Secondary electrons escape from generally between 5 and 50 nm depth of the specimen due to their low energy. Secondary electrons are generated both by the beam entering the specimen and BSEs as they escape the specimen. Since the beam is only a few nanometres in diameter the resolution of the image is very good. Secondary electron imaging is the most common because it can be used with almost any specimen.

When the beam interacts with the sample, energy can be released in the form of x-ray radiation. The x-ray sample depth interval is approximately (0.1 to 100 μm). These signals can be utilized for imaging as well as the identification of elements within the sample volume. The absolute concentrations of individual elements can be calculated by comparing spectra with others collected from samples of known composition.

SEM can generate relative concentration maps for multiple elements. The electron beam is scanned across the sample, stopping at regular intervals to count the number of x-rays within a predefined energy window arriving at the detector. The number of counts at each stop (pixel) can then be displayed as a map.

Scanning electron microscopy instrument is designed for direct studying of the surfaces of solid objects. In a typical SEM a stream of monochromatic electrons is emitted from tungsten, lanthanum hexaboride LaB_6 cathode by heating of a metallic filament or via filed emission and attracted through an anode (WEB_11 2005). The first condenser lens is used to both form the beam and limit the amount of current in the beam. It works with the condenser aperture to eliminate the high-angle electrons from the beam. The electrons take a form of a thin, tight, coherent beam by using the second condenser lens. A user selectable objective aperture performs further elimination of high-angle electrons from the beam. A set of coils then scan the beam over the specimen in a series of lines and frames called a raster, just like the (much weaker) electron beam in a television. The scan coils are energized by varying the voltage and create a magnetic field, which deflects the beam back and forth in a controlled pattern. The varying voltage is also applied to the coils around the neck of the Cathode-ray tube (CRT) that produces a pattern of light deflected back and forth on the surface of the CRT. An image is built up simply by scanning the electron beam across the specimen in

exact synchrony with the scan of the electron beam in the cathode ray tube (WEB_12 2005). Figure 1.17 represents a schematic diagram of a scanning electron microscope.

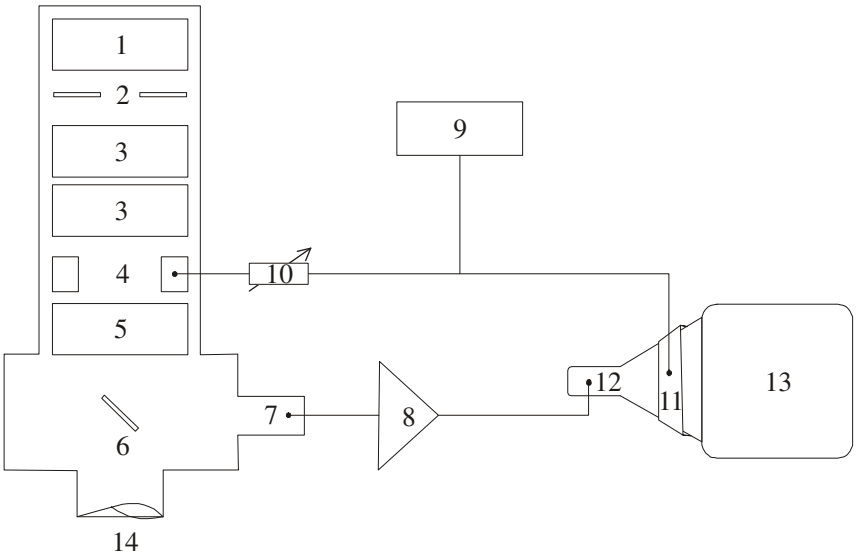

Electron optical column Display / electronics

1. Electron gun
2. Anode disc
3. Condenser lens
4. Scan coil
5. Objective lens
6. Specimen
7. Detector
8. Signal amplifier
9. Waveform generator
10. Magnification control
11. Scan coils
12. CRT brightness control
13. CRT display screen
14. Vacuum Connection

Figure 1.17. Schematic drawing of a scanning electron microscope (Lawes 1987)

The scan coils are used for controlling the position of the beam on the sample, scanning of the beam to produce an image, determining magnification of the image, electronic shifting of the imaged area, and positioning a probe for x-ray analysis.

Magnification is independent of the lenses, that is adjusted by changing the size of the area scanned on the specimen while the monitor or film size is held constant. Thus a smaller area scanned on the sample will produce a higher magnification. A typical magnification range for the SEM is 10x to 100,000x.

In the SEM, sample is mounted using conductive tape. Carbon tape is commonly used that is essentially graphite.

Since the SEM uses electrons to produce an image, most conventional SEM's require that the samples be electrically conductive. All metals are conductive and

require no preparation to be viewed using an SEM. In order to view non-conductive samples the sample must be covered with a thin layer of a conductive material using a sputter coater.

Materials with volatile or high-vapor-pressure components must be prepared for viewing in the SEM. Elimination of water from specimens may employ freeze drying, critical point drying, or chemical means (Lawes 1987).

In the SEM equipped for energy dispersive x-ray microanalysis, x-rays can also be detected. The nature and quantity of different elements in the material is measured accurately by computer analysis of the wavelength or energy pattern (WEB_13 2005).

1.5.3.3 Fourier Transform Infrared Spectroscopy (FTIR)

Fourier Transform Infrared Spectroscopy is an analytical technique used for identifying chemical bonds (functional groups) in a molecule by producing an infrared absorption spectrum. FTIR is most useful to identify chemicals that are either organic or inorganic. Solids, liquids, and gases can be analyzed by this technique after they are prepared for the analysis by an appropriate method. FTIR can be used to quantitate some components of an unknown mixture. In addition to identification of unknown materials, it can determine the quality or consistency of a sample and the amount of components in a mixture.

Fourier Transform Infrared Spectrometer measures the absorption of various infrared light wavelengths by the material of interest. These IR absorption bands identify specific molecular components and structures. Absorption bands in the region of 4000 - 1500 cm^{-1} are induced by the functional groups, e.g. -OH, C=O, N-H, CH_3, etc. Absorption bands range of 1500 - 400 cm^{-1} caused by intra-molecular phenomena forms the fingerprint region and are highly specific for each material. The unknown IR absorption spectrum is compared with standard spectra in computer databases or a spectrum obtained from a know material to determine the identity of the material being analyzed. It is applied to identify foreign materials (such as particulates, fibers, residues), bulk materials, constituents in multi-layered materials and also to quantify silicone, esters, etc. as contamination on various materials (WEB_14 2005).

Quantitative concentration of a compound can be determined from the area under the curve in characteristic regions of the IR spectrum after calibrated concentration curve is established from spectra for samples of known concentrations.

Michelson Interferometer is the most important part of an FTIR Spectrophotometer, which built around the sample chamber. Radiation from an IR source is directed through the sample cell to a beam splitter. Half of the radiation is reflected from a fixed mirror while the other half is reflected from a mirror that moved continuously over a distance of about 2.5 μm. When the two beams are recombined at the detector, an interference pattern is produced. A single scan of the entire distance takes about 2 seconds and is stored in the computer. In order that several scans may be added, they must coincide exactly. A helium-neon laser can be used to satisfy this requirement, which is directed through the Michelson Interferometer. The resulting signal is called an interferogram, which has the unique property that every data point (a function of the moving mirror position) makes up the signal has information about every infrared frequency which comes from the source. This means that as the interferogram is measured, all frequencies are being measured simultaneously. The measured interferogram signal cannot be interpreted directly, however, frequency spectrum (a plot of the intensity at each individual frequency) is required to identify species. This can be attained by a mathematical technique called the Fourier transformation. This transformation is performed by the computer, which then presents the user with a spectrum in percent transmittance (%T) vs. light frequency (cm^{-1}) (WEB_15 2005).

1.5.3.4 Mechanical Property Testing

To predict how a material will respond under real life loading can be possible known by testing of the material. Testing machines test materials in tension, compression or bending. The amount of tolerable deformation determines the performance of a structure. The product quality is measured by the mechanical properties that are tensile strength (as the maximum load value), yield strength (a point just beyond the beginning of permanent deformation) and Young's modulus of elasticity.

The primary function of a testing machine is to construct the stress-strain diagram. After generation of the diagram, yield strength, Young's Modulus, tensile strength or total elongation can be calculated. The Figure 1.18 represents a typical stress-strain curve.

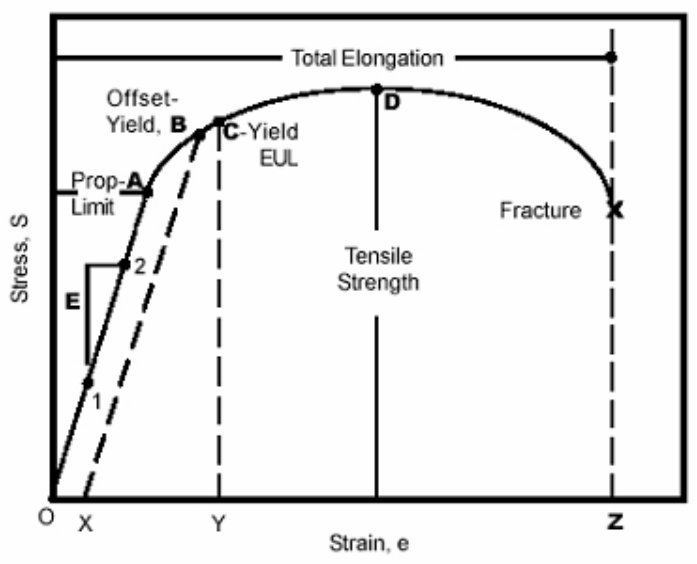

Figure 1.18. Stress - Strain diagram representing mechanical properties (Source: WEB_16 2005)

Stress is obtained by dividing the load (F) at any given time by the original cross sectional area (A_o) of the specimen.

$$\text{Stress} = F/A_o \tag{1.8}$$

Strain is obtained by dividing the elongation of the gauge length of the specimen (l) by the original gauge length (l_o).

$$\text{Strain} = \Delta l/l_o = (l - l_o)/l_o \tag{1.9}$$

In the diagram, Point A represents the proportional limit of a material, at which point, a permanent deformation begins to form when a material loaded in tension beyond point A is unloaded. Two practical measurements, offset yield strength (OYS) and yield by extension under load (EUL), are generally used instead of the proportional limit due to the practical ease. The initial portion of the curve below point A exhibits the elastic region and is approximated by a straight line. The slope of the curve in the elastic

region is referred to Young's Modulus of Elasticity (E) and is a measure of material stiffness.

$$E = \text{Stress} / \text{Strain} = (S_2-S_1)/(e_2-e_1) \quad (1.10)$$

Point B represents the offset yield strength and is found by constructing a line X-B parallel to the curve in the elastic region. The yield strength by extension under load (EUL) is exhibited by Point C, which is found by constructing a vertical line Y-C. Point D displays the ultimate tensile strength. Total elongation, which includes both elastic and plastic deformation, is the amount of uniaxial strain at fracture and is depicted as strain at point Z.

The shape and magnitude of the curve depend on the type of material being tested. A material with a lower value for Young's Modulus, E, and/or a higher value for yield strength will display greater shape distortion (WEB_16 2005).

CHAPTER 2

EXPERIMENTAL

2.1 Materials

2.1.1 Reactants

The reactants used to prepare $CaCO_3$ were Na_2CO_3 and anhydrous $CaCl_2$, which were purchased from Sigma (S-7795) and Horasan Chemicals, respectively. NaOH and HCl (purchased from Sigma (S-8045) and Merck (K32208717 328)) were used to adjust the pH of the solutions.

2.1.2 Organic Additives

The organic additives and the suppliers of the materials are as listed below. The chemical formulas of organic additives used in our studies were given in Figure 2.1 to 2.5.

Polyvinylpyrrolidone K 30, PVP, from Fluka Chemicals (81L120)

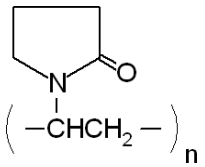

Figure 2.1. The chemical formula of PVP

Poly(diallyldimethylammonium chloride), PDDA, from Aldrich Chemicals (409014-1L)

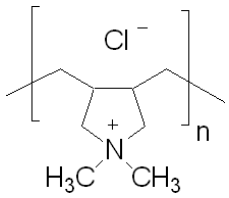

Figure 2.2. The chemical formula of PDDA

Poly(ethylene glycol), PEG, from Aldrich Chemicals (20,239-8)

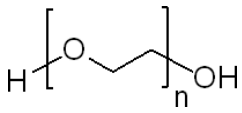

Figure 2.3. The chemical formula of PEG

Cetyltrimethylammonium bromide, CTAB, from Aldrich Chemicals (85,582-0)

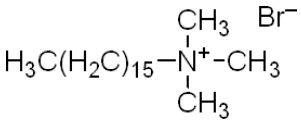

Figure 2.4. The chemical formula of CTAB

Ethylenediaminetetraacetic acid, EDTA, from Sigma-Aldrich (E9884-100G)

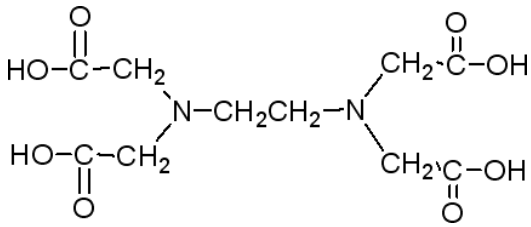

Figure 2.5. The chemical formula of EDTA

2.1.3 Materials for Surface Modification and Composite Fabrication

3-(Trimethoxysilyl) propyl methacrylate (98 %, 44.015-9) and hydrochloric acid (min. 30 %, 017-002-01-X) were purchased from Aldrich Chemicals and Birpa Chemicals, respectively. Thermoset polyester resin (Cam Elyaf (266)) was purchased from Cam Elyaf, Inc, Turkey.

2.2 Preparation of $CaCO_3$ Crystals in Aqueous Solution

Na_2CO_3 and $CaCl_2$ solutions were prepared as stock solutions at stated concentrations just before each experiment. 100 mL of $CaCl_2$ solution was poured into 250 mL erlenmeyer flask containing 100 mL Na_2CO_3 solution. The pH of the solution was adjusted to the desired value using 0.5 M NaOH and HCl solutions. The mixture was stirred for a minute and allowed to stand at indicated aging temperature in a thermostatic water bath for stated aging period. At the end of aging period, $CaCO_3$ crystals were filtered, washed three times with deionized water and dried at room temperature.

The effect of experimental parameters (initial concentration of reactants, pH, preparation temperature, aging temperature and aging time) on the morphology and crystal structure of prepared $CaCO_3$ particles were investigated by changing one parameter at a time and keeping all the other parameters constant.

The range of experimental values applied throughout the studies aiming at the examination of the effect of various parameters is provided in Table 2.1.

Table 2.1 Studied experimental conditions

PARAMETERS	RANGES
pH	7.0 – 12.0
Initial Concentration of Na_2CO_3&$CaCl_2$	0.01 – 0.20 M
Aging Time	30 min. – 1 week
Mixing Temperature	30 – 95^oC
Aging Temperature	- 20 – 80^oC

2.3 Preparation of $CaCO_3$ Crystals in the Presence of Organic Additives

In each experiment, 0.02 or 0.2 g organic additive was added into a 250 mL erlenmeyer flask containing 100 mL 0.05 M Na_2CO_3 solution. This mixture and 100 mL 0.05 M $CaCl_2$ solution prepared in another 250 mL erlenmeyer flask were brought to the desired preparation temperature separately. The pH of the solutions was adjusted by two different procedures. In the first procedure, the pH of Na_2CO_3 solution containing only organic additive was adjusted after it reached the preparation temperature then the $CaCl_2$ solution was poured into the pH adjusted solution. In the second procedure, the pH adjustment was performed after $CaCl_2$ solution was poured into the mixture. As a last step, solution containing $CaCO_3$ particles were kept in a thermostatic water bath at a specified aging temperature for various aging time. At the end of aging process, $CaCO_3$ crystals were filtered, washed three times with deionized water and dried at room temperature.

Throughout the relevant experiments, $CaCO_3$ particles were prepared at pH 9.0 and aging time of 24 hours. One set of the experiments was performed at the mixing and aging temperatures yielding calcite polymorph, and a second set was done at the experimental conditions yielding (mostly) aragonite polymorph. During these experiments, the following parameters were studied:

1- The effect of additive concentration; 0.1 g/L and 1.0 g/L.
2- The effect of the order of pH adjustment; in one part of the experiments, the pH was adjusted prior to the addition of the $CaCl_2$ solution to the solution medium containing the additive and Na_2CO_3, and in the second part the pH was adjusted after the addition of the $CaCl_2$ solution to the mixture.
3- For the purpose of comparison, in some cases, the effect of altering the pH values to 7.0 and 11.0 was also investigated.

In this part of the study, the crystallization of calcite and aragonite particles was investigated in the presence of the following additives:

1- Polyvinylpyrrolidone - (PVP)

2- Poly (diallyldimethylammonium chloride) - (PDDA)
3- Poly (ethylene glycol) - (PEG)
4- Cetyltrimethylammonium bromide - (CTAB)
5- Ethylenediaminetetraacetic acid - (EDTA)

2.4 Silane Treatment of Calcite Particles

While stirring, the pH of 0.170 g of deionized water in a beaker was adjusted to a value of 3.0 using hydrochloric acid. Silane (1.5 % of calcite by weight) was dissolved in the acidified water then calcite was added into the solution. After stirring the suspension for 30 minutes, the solid phase (treated - calcite particles) were filtered and dried at 85^{o} C in an oven.

2.5 Preparation of Calcite/Polyester Composites

Calcite/polyester composites having different weight fraction of calcite were prepared. 100 g polyester was used for each set and 5, 10, 20 weight percent of calcite particles were added into polyester resin. The mixtures were stirred using mechanical stirrer for 30 minutes. Prior to molding process, cobalt octoat (0.7 % of polyester by weight) and methyl ethyl ketone peroxide (1.5 % of polyester by weight) were added into the blends, sequentially. Polyester composites were molded and kept stand overnight. Finally, the composites were removed from the mold and post-cured in an oven at 100^{o}C for 2 hours.

2.6 Characterization Techniques

2.6.1 X-Ray Diffraction (XRD)

X-Ray powder diffraction analysis was carried out using a Philips X' Pert Pro diffractometer. Each $CaCO_3$ powder sample was mounted on a holder then introduced for analysis. XRD was carried out using a Cu Kα radiation (λ=1.54 Å) source. The accelerating voltage and the applied current were 45.0 and 40.0 mA, respectively. Data

was collected between 10-60^{o} 2θ values by scanning each sample with a step size of 0.03 and 10.16 s of time per step duration.

2.6.2 Scanning Electron Microscope (SEM)

Philips XL-30S FEG type instrument was employed for SEM characterization to obtain information about morphology and size of the crystals. The powder crystals were mounted on scanning electron microscopy stubs using conducting carbon tape and introduced for analysis. The surface of samples was displayed at different magnifications. Also, fracture surface of the composites after mechanical testing were examined.

2.6.3 Mechanical Testing Machine

Schimadzu AG-I 250 kN universal test machine was employed for tensile tests. A dumbbell shaped composite samples was prepared according to ASTM for testing. A cross-head speed of 2 mm/min was selected.

2.6.4 Differential Scanning Calorimeter (DSC)

A TA-Instruments DSC (model Q10) was employed to detect glass transition temperatures of polymer. Polyester composites were heated from 20 to 200^{o}C at a constant heating rate of 10^{o}C/min.

CHAPTER 3

RESULTS AND DISCUSSION

3.1 Effect of Experimental Conditions on the Polymorph and Morphology of $CaCO_3$

The precipitation reactions are known to be generally dependent on the concentrations of reactants, the temperature of the reaction medium, the prevailing pH conditions, and the aging time. In this study, a wide range of experimental factors were tested in order to establish the optimum parameters of $CaCO_3$ synthesis, primarily in the form of calcite. Literature resources contains a lot of data about the best reaction conditions for the synthesis of calcite (Cheng et al. 2004, Carmona et al. 2003, Loste et al. 2003), but most of the reported data either applies for small reaction volumes, or are not given in a collective manner, in away that reports the effects of different parameters in a single study. Moreover, by conducting the relevant experiments for the different factors affecting the synthesis of calcite, we aimed primarily at establishing a solid background for further studies, in particular those attempting to modify the morphology of the outcoming calcite in order to fit various industrial applications.

In addition, the conditions for the synthesis of aragonite polymorph were examined, in the absence of any additive. The importance of these experiments stems from the fact that this polymorph is well known to be synthesized with 100% purity only if Mg^{2+} is introduced into the reaction medium in large quantities. In those experiments the results of which are reported later in this chapter, we were able to synthesize aragonite with a purity that amounted to about 95%, merely by manipulating the reaction conditions without the addition of any 'foreign' chemical.

Throughout this study, the reactants were basically calcium chloride, $CaCl_2$, and sodium carbonate, Na_2CO_3, mixed under atmospheric PCO_2 pressure. The precipitation of $CaCO_3$ from those reactants is one of the most widely applied methods for that purpose. In the following sub-sections, the results of the effect of different factors on the synthesis of calcite and aragonite are reported in a consecutive manner.

3.1.1 Effect of pH

Throughout these experiments, the mixing and aging temperatures were kept at 30°C and the aging time was 24 h. The pH values were varied as 7.0, 9.0, 10.0, and 12.0 for two sets of reactant initial concentrations (0.01 M and 0.1 M) for both of $CaCl_2$ and Na_2CO_3. The XRD results (Figure 3.1) suggested that only calcite was formed within this range of pH and stated experimental conditions.

For both concentration values, i.e., 0.01 M and 0.1 M, well-defined rhombohedral calcite particles were best produced when the pH was 9.0. At the other pH values, however, structural and surface imperfections were widely observed, as illustrated by the SEM images given in Figure 3.2. Based on these images, the average particle size is seen to vary roughly in the range 5-10 μm within the studied pH range. From the above findings, the optimal pH value was selected to be 9.0 for the preparation of $CaCO_3$ particles; therefore the remaining experiments were performed at this initial pH value.

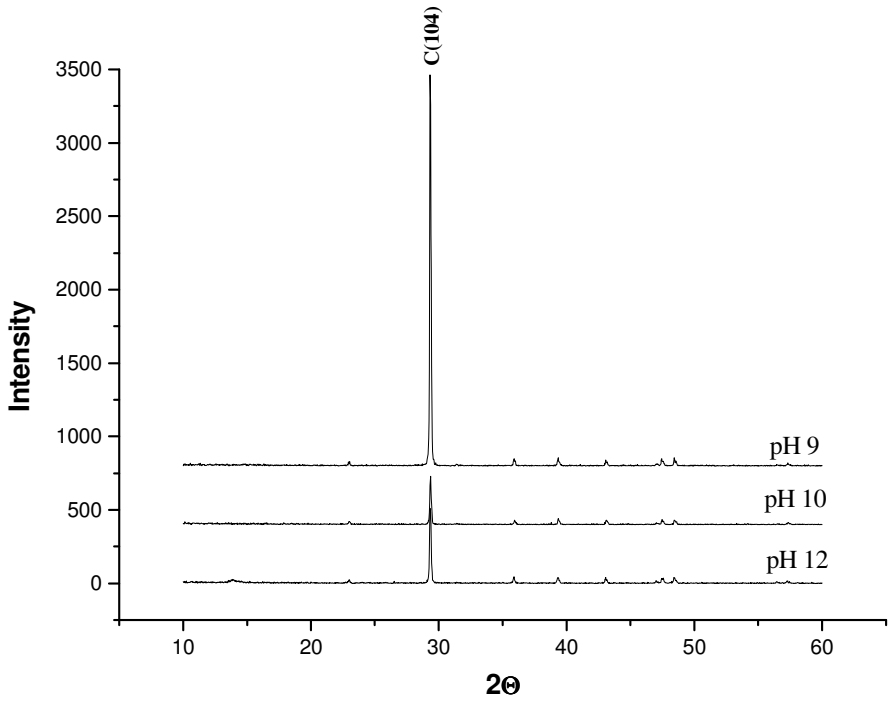

Figure 3.1. Typical XRD diagrams of calcite synthesized at different pH values ($[C_o]$=0.01 M, aging time=24 h, mixing and aging temperatures=30°C), C: Calcite

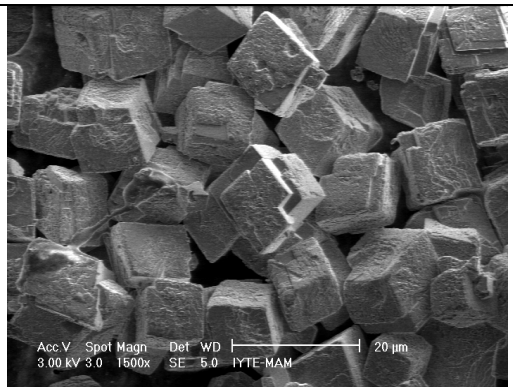

pH=7.0

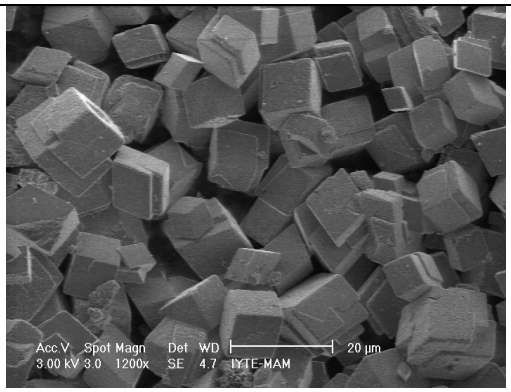

pH = 9.0

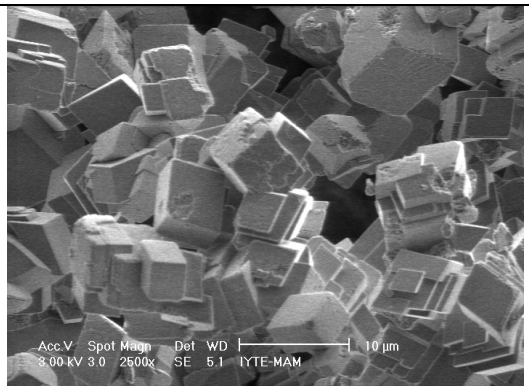

pH=10.0

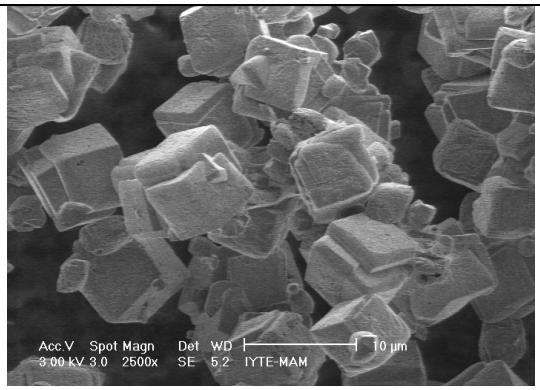

pH=12.0

Figure 3.2. SEM images of calcite precipitated at different pH values.

3.1.2 Effect of Initial Concentration of Reactants

The effect of various initial concentrations of $CaCl_2$ and Na_2CO_3 solutions was investigated at the values of 0.01 M, 0.05 M, and 0.20 M. During these experiments, the $CaCO_3$ particles were prepared at 30^oC mixing and aging temperatures and an aging time of 24 h. The XRD results indicated that the change in concentration of reactants yielded the formation of calcite in all cases, as seen in Figure 3.3. However, it was observed from the SEM micrographs, two of which are shown in Figure 3.4, that the particles produced at 0.05 M initial concentration possessed relatively smoother crystal surfaces and were smaller in size compared to the others. Based on the SEM images, the average particles size at this concentration was estimated to be around 5-6 µm.

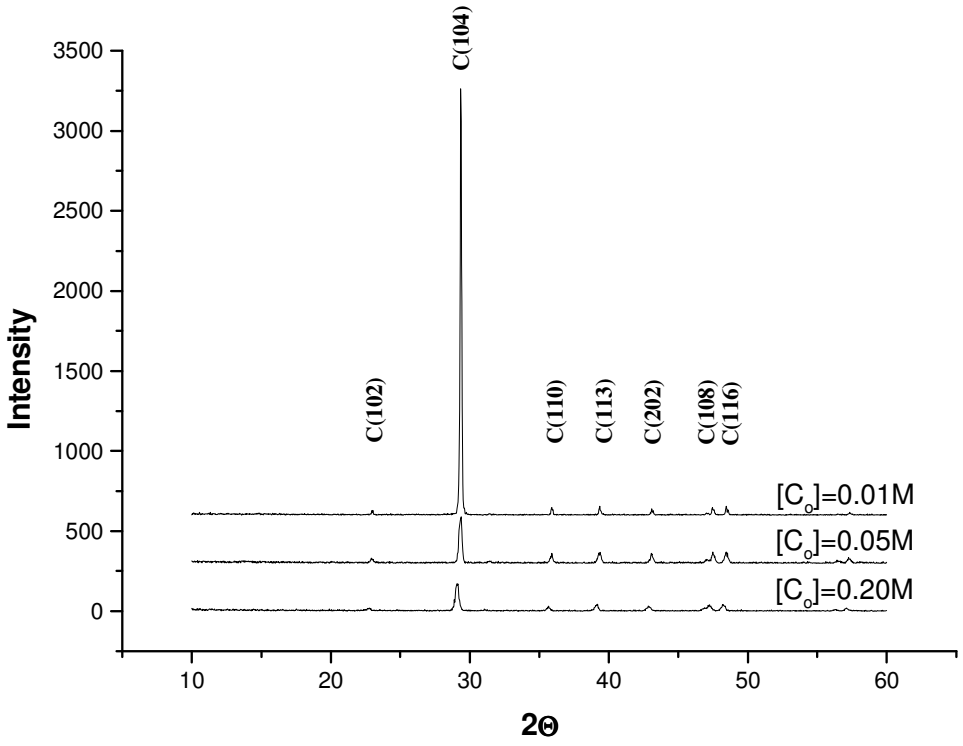

Figure 3.3. XRD patterns of $CaCO_3$ at different concentrations (pH=9.0, aging time=24h, mixing and aging temperature=30°C), C: calcite

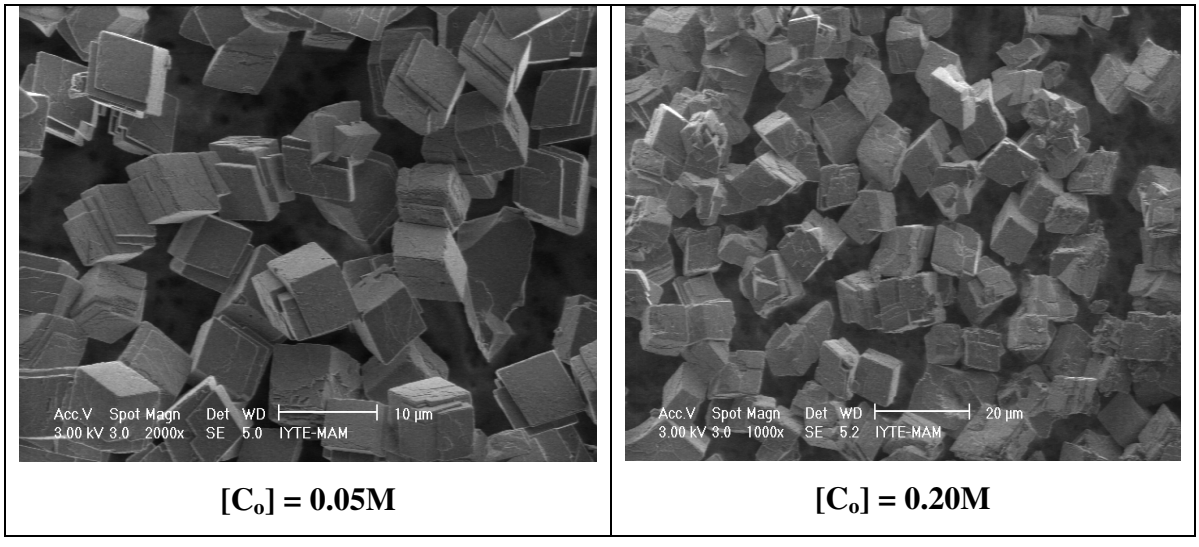

Figure 3.4. SEM images of $CaCO_3$ prepared at two different concentrations

3.1.3 Effect of Aging Time

These experiments were performed at 30°C mixing and aging temperatures, and the initial concentration of solution was 0.05 M with the pH fixed at 9.0. These conditions correspond to the optimum values of temperature, concentration, and pH, as discussed in the above sections. The aging time was changed from 6 hours up to 1 week. The results showed that throughout these experiments the produced $CaCO_3$ contained only calcite polymorph. In addition, the morphology of the calcite particles did not exhibit any obvious differences. Due to experimental practical considerations, 24 h aging time was preferred as optimal synthesis aging time for the remaining experiments, unless any other aging time was indicated. The XRD diagrams of the produced calcite at different aging times are given in Figure 3.5, and some typical SEM images are provided in Figure 3.6.

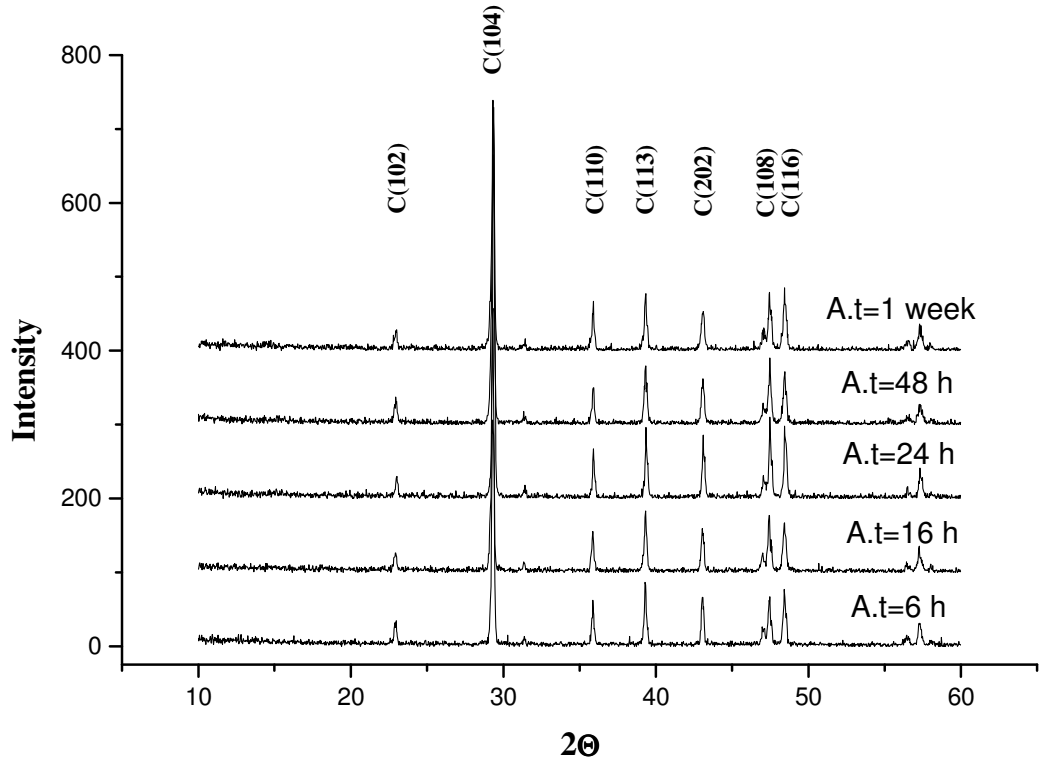

Figure 3.5. XRD diagrams of the produced $CaCO_3$ at different aging times ($[C_o]$=0.05M, pH=9.0, mixing and aging temperatures=30°C), C: calcite

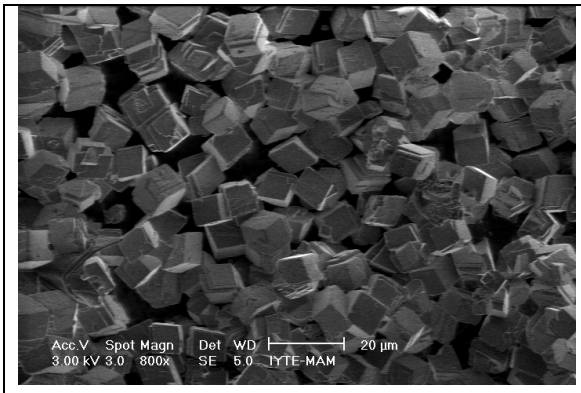

6 hours

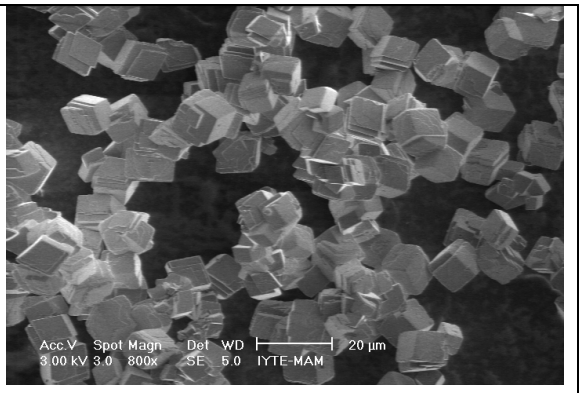

16 hours

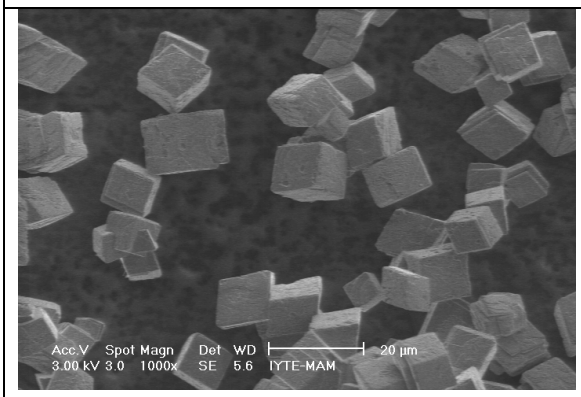

24 hours

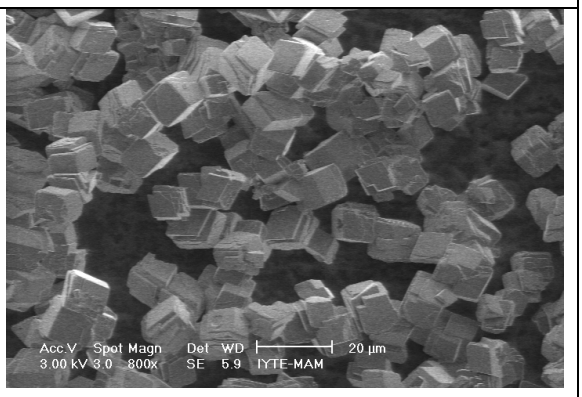

1 week

Figure 3.6. Typical SEM images of the produced $CaCO_3$ at different aging times

3.1.4 Effect of Temperature

After the optimal initial concentration, pH and aging time were determined, the effects of mixing and aging temperature were investigated.

3.1.4.1 Effect of Mixing Temperature

In the first stage, $CaCO_3$ particles were synthesized at 30°C, 50°C, 80°C, and 95°C mixing temperatures, while the aging temperature was kept at 10°C. The results showed that at the mixing temperature of 30°C and 50°C, rhombohedral calcite particles were formed. It should be noted here that at 50°C mixing temperature, calcite particles were observed to start to agglomerate with their surfaces possessing serious defects, and a few number of aragonite particles were also occasionally observed. Increasing the

mixing temperature to 80°C and 95°C promoted the formation of aragonite further, as revealed by the XRD diagrams in Figure 3.7. According to the SEM microimages (Figure 3.8), the aragonite particles possessed a *branch-like* shape, with average particle sizes of 5-6 μm. High temperature conditions are believed to hinder the crystal growth of calcite and enhance that of aragonite in reaction media (Hu and Deng 2004, Tai and Chen 1998, Liu et al. 1998). However in those studies it is stressed that stabilizing the aragonite polymorph requires the addition of $MgCl_2$.

Based on the intensity of the major reflections of aragonite and calcite, the percentage of aragonite and calcite crystals were calculated using the equation:

$$X_A = \frac{3.9S_A}{S_C + 3.9S_A} \tag{3.1}$$

Here, X_A corresponds to the calculated fraction of aragonite; S_A is the integrated intensity of aragonite (111) reflection (2θ=26.1), and S_C is the integrated intensity of calcite (104) reflection (2θ=29.2). The percentages of aragonite crystals formed in the $CaCO_3$ powders were 79% and 84% for mixing temperatures 80°C and 95°C, respectively.

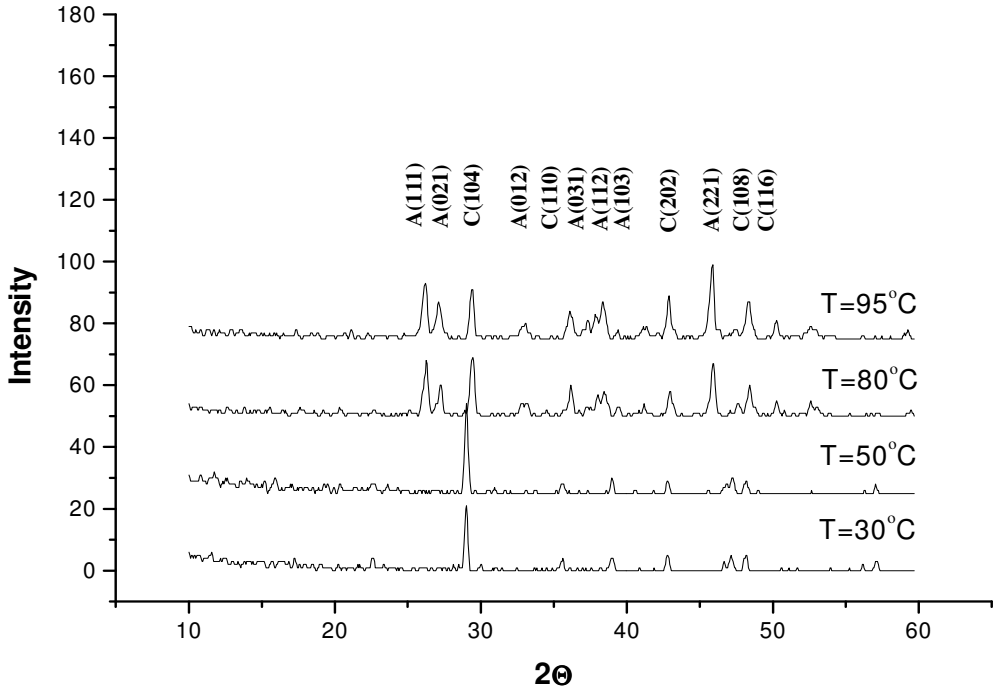

Figure 3.7. XRD diagrams of $CaCO_3$ prepared at different mixing temperatures ($[C_o]$=0.05 M, pH=9.0, aging time=24 h, aging temperature=10°C), A: aragonite, C: calcite

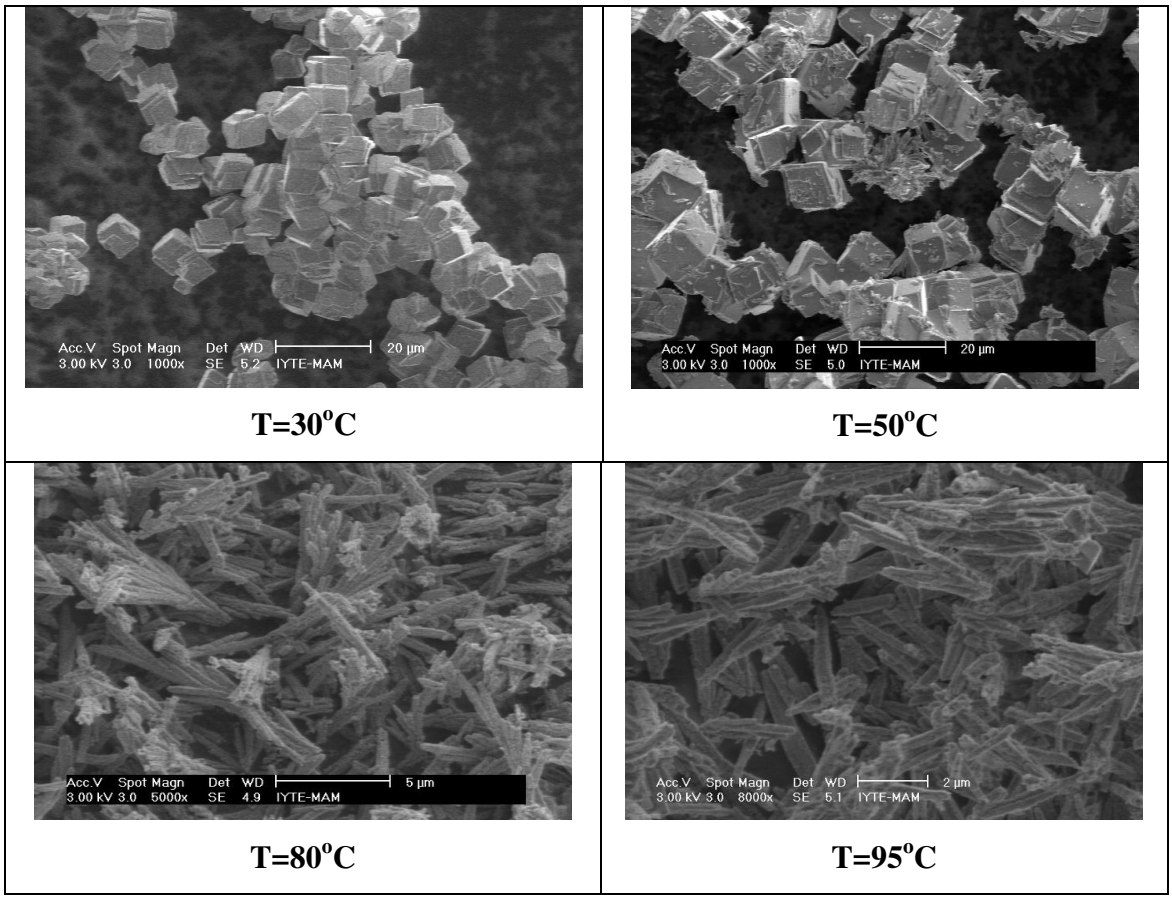

Figure 3.8. SEM images of $CaCO_3$ prepared at different mixing temperatures

The formation of aragonite is considered to be responsible for the activation of the symmetric stretching mode (ν1) in the FTIR spectra of $CaCO_3$, which is shown in Figure 3.9. The D_{3h} symmetry of free carbonate ion is lowered to D_3 in the case of calcite and C_s in the case of aragonite the thing that leaves the carbonate vibrational modes unchanged in the case of calcite but activates the ν1 mode in aragonite (Nakamoto 1986). Figure 3.9 gives the FTIR spectra of a $CaCO_3$ sample entirely compose of calcite (a), and that of the $CaCO_3$ sample composed of aragonite and calcite. The clear increase in the intensity of the ν1 band in (b) can be used as an indicative of the presence of aragonite in the powder.

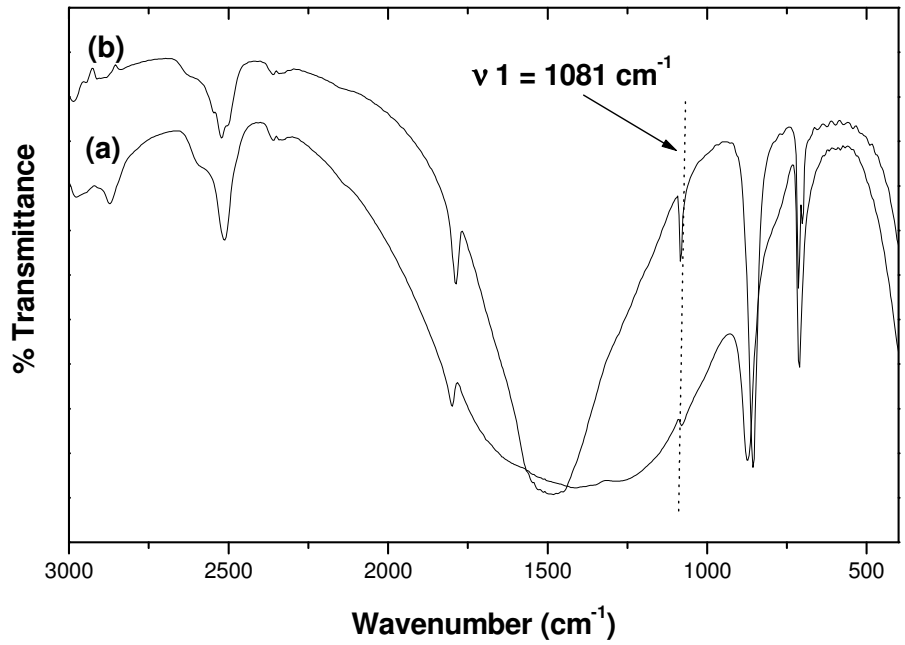

Figure 3.9. FTIR spectra of $CaCO_3$ prepared at mixing temperatures of: (a) 30°C; calcite polymorph, and (b) 90°C; both of calcite and aragonite polymorphs.

3.1.4.2 Effect of Aging Temperature

The second stage of the investigation of the effect of temperature on the outcoming polymorph type of $CaCO_3$ and the corresponding morphologies was devoted to studying the effect of the aging temperature. These experiments were carried out at the same optimum conditions reported above, i.e. 0.05 M initial concentrations of $CaCl_2$ and Na_2CO_3 solutions, pH of 9.0 and aging time of 24 h. The experiments concentrated on revealing whether changing the aging temperature would affect the amount of aragonite polymorph. Aragonite crystals are applied in different industries like plastics, paper making, and rubber filling (Hu and Deng 2004). So far, researchers has reported successful synthesis of aragonite by applying inorganic/organic additives believed to inhibit calcite growth in favor of the growth of aragonite while the reaction medium is generally kept at a high temperature. Among such additives are sodium sulfate (Hu and Deng 2003), Mg-containing compounds (Hu and Deng 2004, Tai and Chen 1998, Liu et al. 1998), silicate to produce self-organized formation of porous aragonite (Imai et al. 2002), soluble proteins extracted from nacre (Feng et al. 2000), aging in the presence of urea at 90°C (Wang et al. 1999). In our experiments, however, the primary aim was to

maximize the yield of outcoming aragonite in the absence of any inorganic/organic additive. Therefore the reactants were mixed at 90^{o}C, and then they were kept at various aging temperatures, i.e., 70^{o}C, 50^{o}C, 30^{o}C, 10^{o}C, 0^{o}C, -20^{o}C. According to the quantification analysis based on XRD patterns (Figure 3.10), in all cases the prepared crystals were dominated by aragonite polymorph, and no significant difference in aragonite content was observed at the various aging temperatures. However, these studies revealed clearly that although the aging temperature did not essentially influence aragonite fraction, the same thing might not be valid for the aspect ratio (defined as ratio of length to diameter of the aragonite crystal) values, which seemed to show a slight increase as the aging temperature was decreased ranging from 8-12. Aragonite possessing a high aspect ratio is favored as a biomedical material and as filler for the improvement of the mechanical properties of paper and polymer material (Richter et al. 1995). The fractions of aragonite in $CaCO_3$ obtained at different aging temperatures are provided in Table 3.1. The SEM pictures of crystals showed that the obtained aragonite particles possessed a *needle-like* morphology in addition to the *branch-like* morphologies reported earlier in this text. Typical SEM images are provided in Figure 3.11.

Table 3.1. The fractions of aragonite in $CaCO_3$ obtained at different aging temperatures

Aging Temperature (^{o}C)	**Aragonite Fraction (%)**
70	97
50	93
30	93
10	93
0	93
-20	92

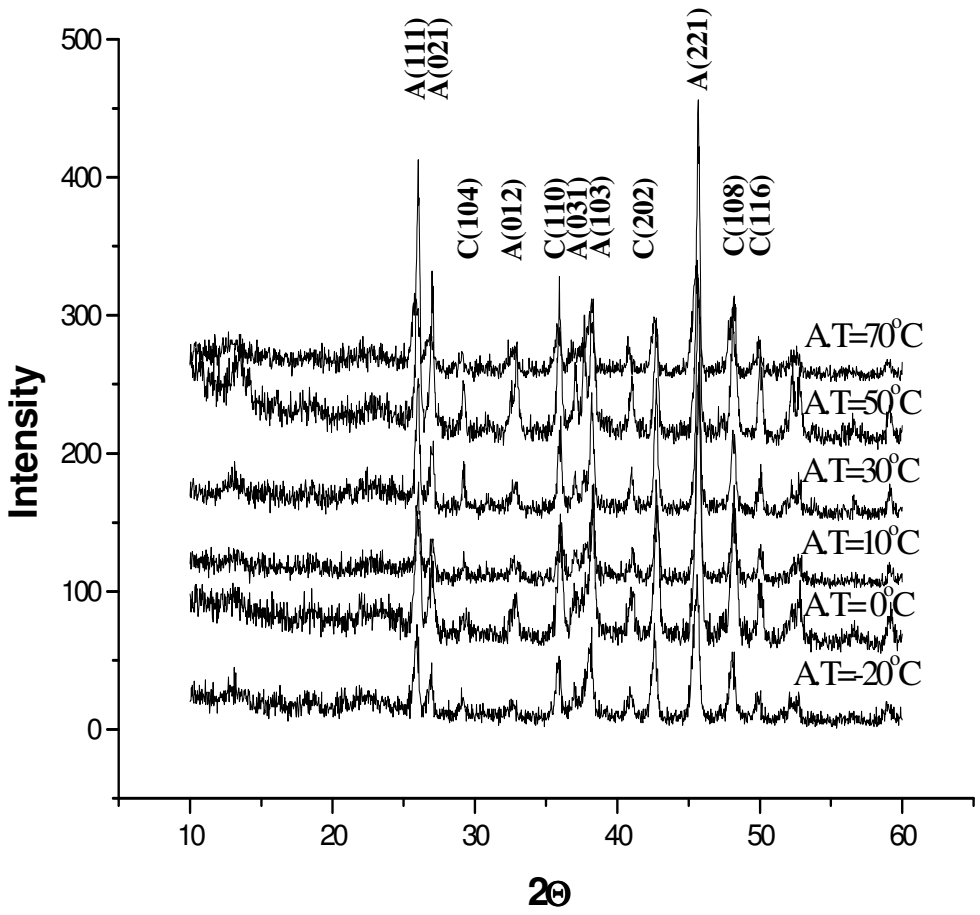

Figure 3.10. XRD diagrams of $CaCO_3$ prepared at a mixing temperature of 90°C, and different aging temperature ($[C_o]$=0.05 M, pH=9.0, aging time=24 h, mixing temperature=90°C), A: aragonite, C: calcite

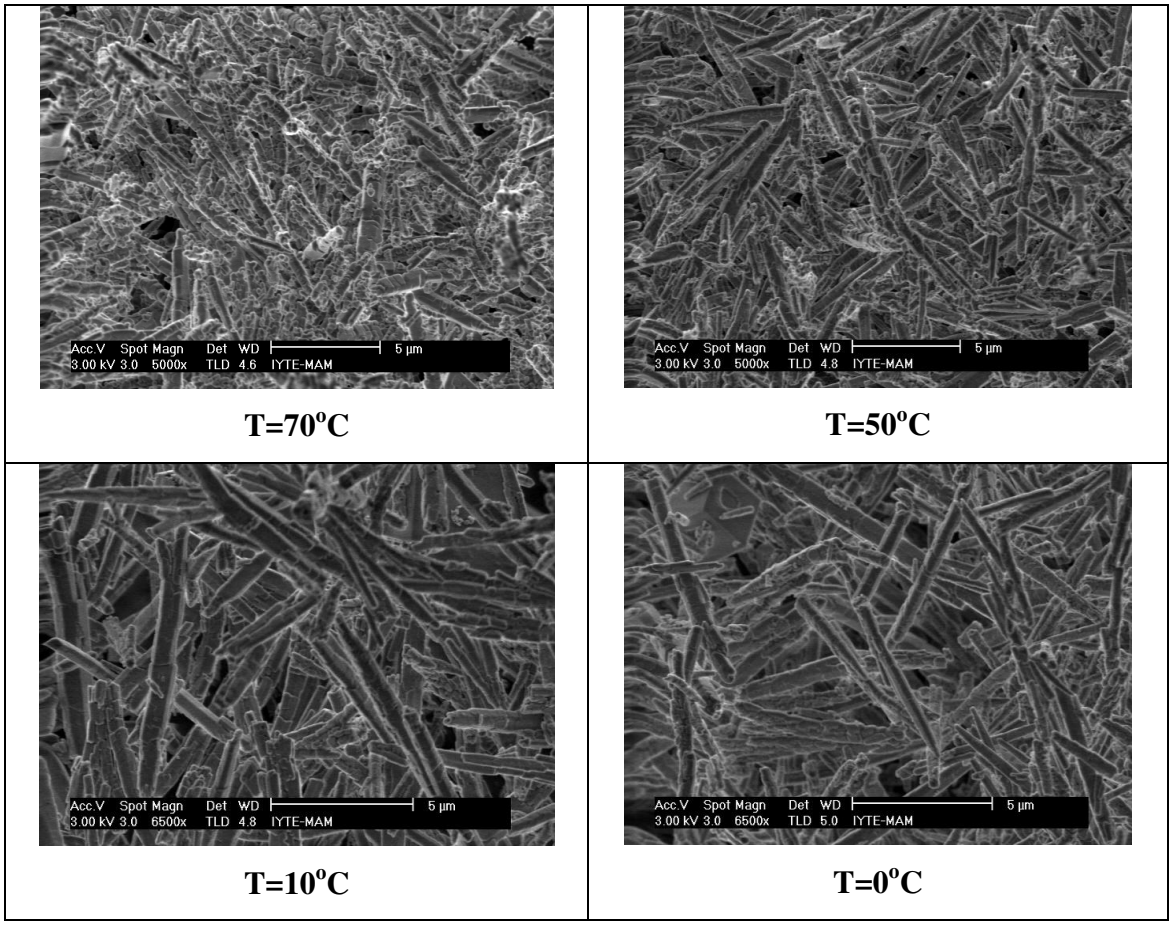

Figure 3.11. Typical SEM images for aragonite crystals prepared at a mixing temperature of 90°C, and different aging temperature.

As a final stage for elucidating the effect of temperature, the $CaCO_3$ crystals were synthesized at the optimal values of concentration, pH and aging time (reported previously) while the mixing and aging temperature values were simultaneously changed. In these experiments, the mixing and aging temperatures were 80°C, 70°C, 60°C 50°C, 40°C, 30°C and 20°C. From the XRD data, shown in Figure 3.12, the aragonite fraction in $CaCO_3$ prepared at 80°C, 70°C, 60°C mixing and aging temperatures were calculated as, 50%, 48% and 30%, respectively. As expected, the decrease in preparation temperature resulted in a decrease in aragonite fraction in $CaCO_3$ crystals. Below a temperature of 50°C, the resulting $CaCO_3$ was composed of cubic and rhombohedral calcite crystals. By analyzing the relevant SEM images recorded at different magnifications, it was observed that the average particle size of calcite crystals prepared at the mixing and aging temperatures of 50°C, 40°C, 30°C and

20°C, increased gradually from about 8 μm to about 12 μm as the temperature changed from 50°C down to 20°C. Hence, it seems from those results that decreasing the medium temperature leads to an increase in the size of the calcite particles, however, a full elaboration of the topic requires further experiments. Typical SEM microimages of calcite are given in Figure 3.13.

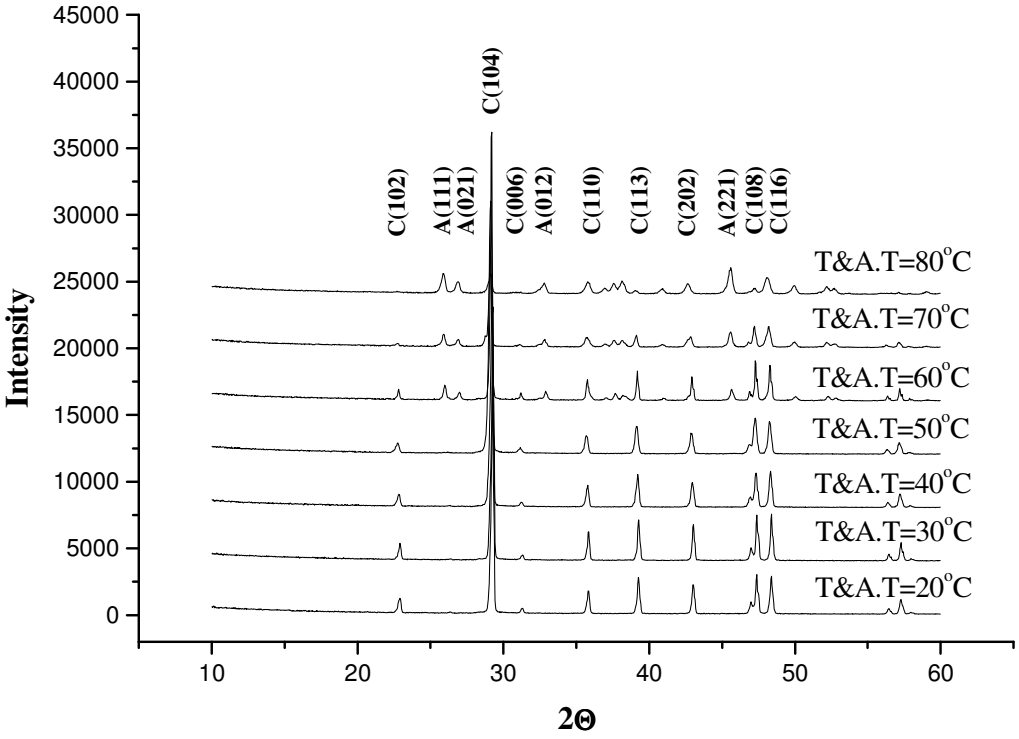

Figure 3.12. XRD patterns of $CaCO_3$ samples prepared at various temperatures ($[C_o]$=0.05 M, pH=9.0, aging time=24 h, mixing and aging temperature are changed simultaneously), A: aragonite, C: calcite

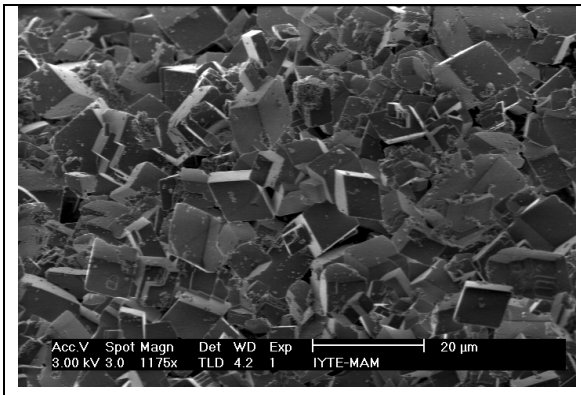

T= 50°C

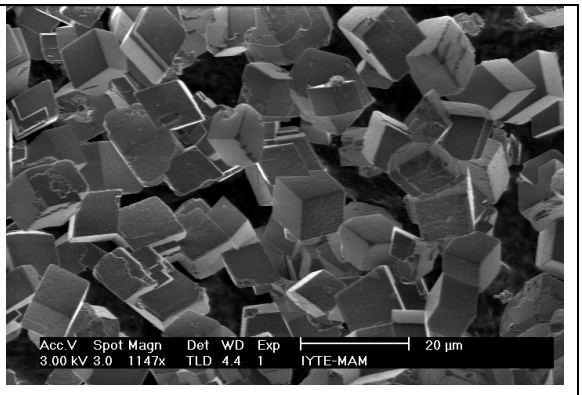

T= 40°C

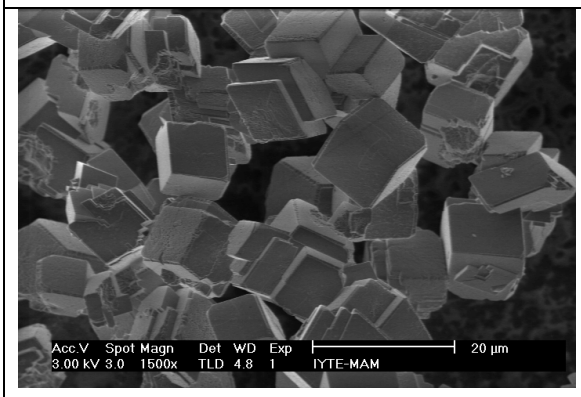

T= 30°C

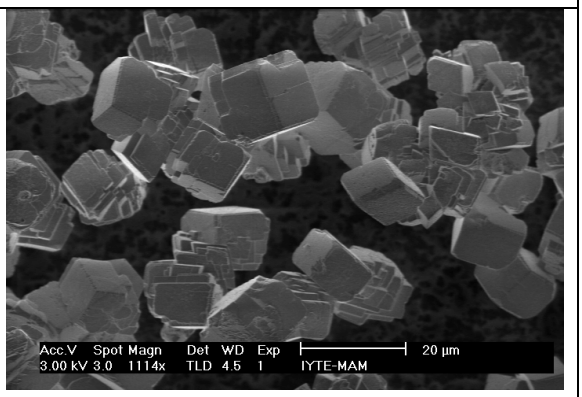

T= 20°C

Figure 3.13. Typical SEM images of calcite crystals prepared at different temperatures.

3.1.5 Effect of Mixing Temperature and Aging Time on Aragonite Fraction

In these experiments, the effect of aging time on the extent of aragonite formation was studied. For this purpose, facile precipitation of $CaCO_3$ was carried out at mixing temperatures of 70°C, 80°C and 90°C and various aging times (30 min, 2 h, 6 h and 24 h). The initial reactant concentration, pH and aging temperature were 0.05 M, 9 and room temperature, respectively. The amount of aragonite (%) in the samples prepared at the indicated experimental conditions is summarized in Table 3.2. According to the obtained results, the highest value of aragonite fraction seems to be obtained at the lowest aging time; i.e. 30 min, for each mixing temperature. Generally, there is a decrease in the aragonite amount as the aging time is increased within the first 24 hours. However, when the aging time is raised to 24 hours, an increase in aragonite

fraction is observed. It is also seen that aragonite content in the samples prepared at 30 min aging time increased with the increase in mixing temperature. Typical XRD diagrams corresponding to a mixing temperature of 90^{o}C are presented in Figure 3.14.

The samples were again analyzed one month after their preparation (stored under ambient conditions) to check the morphological stability over time. The XRD patterns of the samples indicated no serious change in the fraction of aragonite as well as in the particle morphology. SEM micrographs, some of which are presented in Figure 3.15, suggested that resultant crystals exhibited a mixture of needle-like and whisker morphologies. The aspect ratios of the crystals, calculated from the SEM pictures, ranged from 6-10. In general, shorter aging times resulted in higher aspect ratio at each mixing temperature, but this difference was more pronounced at 70^{o}C and decreased as the mixing temperature increased.

Table 3.2 The amount of aragonite (%) in the samples prepared at [C_o] = 0.05 M, pH=9.0, and aging temperature = room temperature

Aging Time (hour) / Aging Temperature (^{o}C)	**0.5**	**2**	**6**	**24**
70	86	73	76	82
80	91	81	83	87
90	92	80	69	-

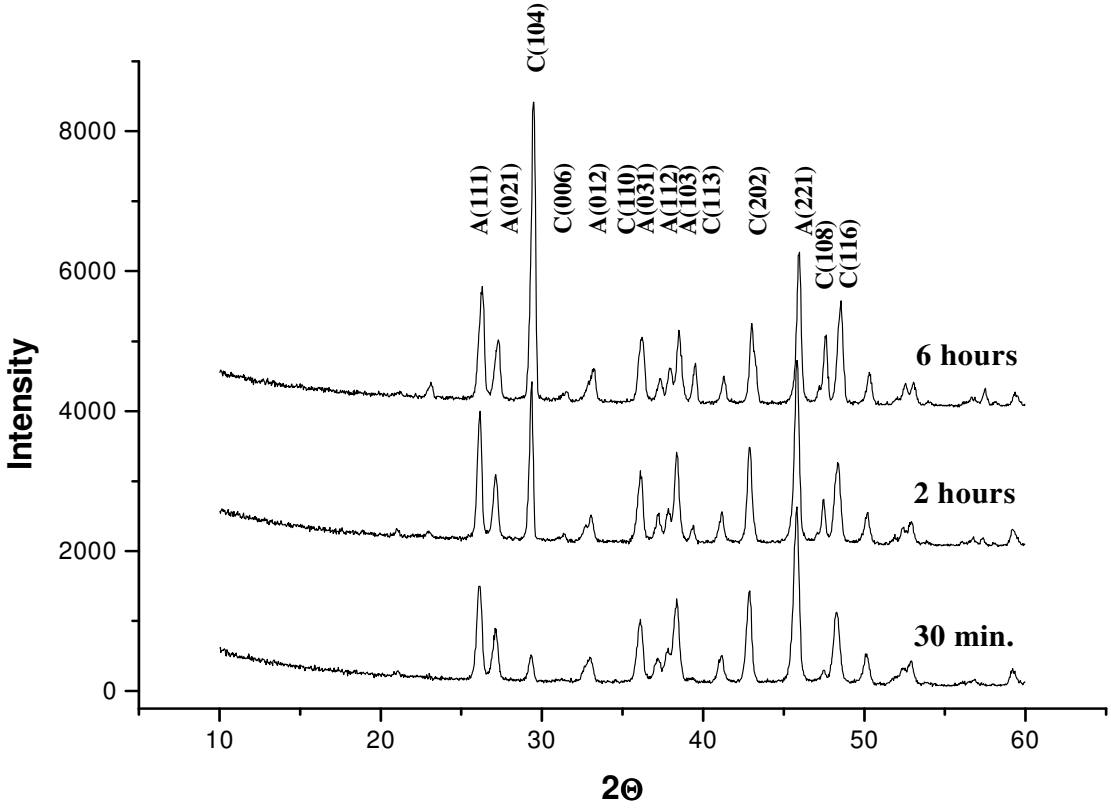

Figure 3.14. The XRD diagrams of the samples prepared at various aging times ($[C_o]$=0.05 M, pH=9.0, mixing temperature=90°C and aging temperature=room temperature), A: aragonite, C: calcite

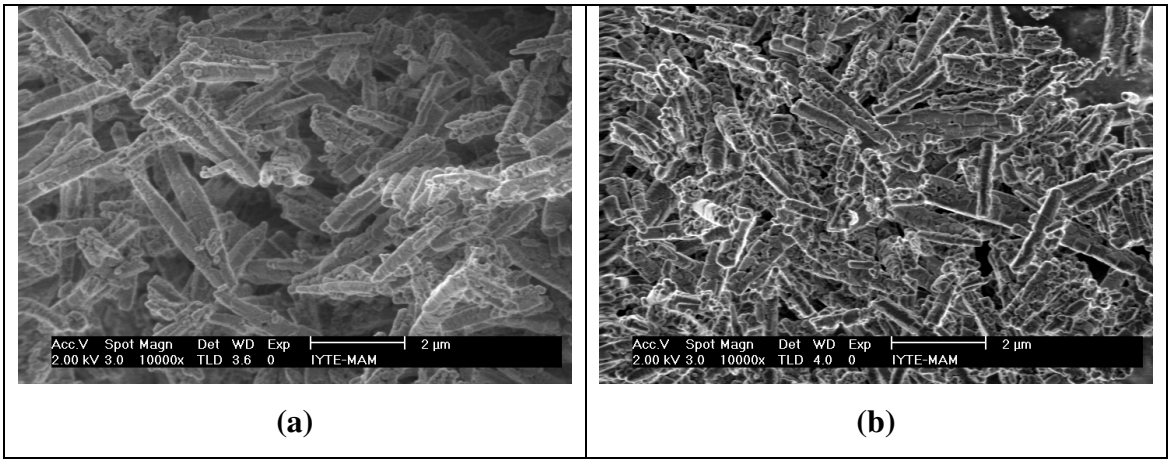

Figure 3.15. SEM images of $CaCO_3$ particles prepared at $[C_o]$=0.05 M, pH=9.0, mixing temperature=70°C, aging temperature=room temperature and at different aging times; (a) 30 min, (b) 24 hours

To summarize, from the detailed results given in this section (3.1), it can be concluded that within the investigated experimental conditions, the most appropriate pH value for calcite preparation was 9.0, and a concentration of 0.05 M seems to be appropriate for obtaining calcite crystals with smooth surfaces. The most suitable mixing and aging temperatures for the production of this polymorph is around 30^{o}C, and the aging time seems to have insignificant effect on the yield of calcite, as long as the temperature is not changed beyond 50^{o}C. Under the above conditions the morphology of calcite is dominated by rhombohedral and cubic shapes in addition to plate-like crystals formed to a comparatively lesser extent. When the mixing and aging temperatures are raised beyond 50^{o}C, the formation of aragonite driven. The quantity of this polymorph in the outcoming $CaCO_3$ samples was seen to be directly proportional with increasing temperature, and reached a mass percentage of about 97 when the mixing temperature was 90^{o}C. The aging temperature showed less effect on the amount of aragonite formed compared to the mixing temperature, the thing expected due to the short time scale of the nucleation and crystal growth processes, the intervals during which one polymorph might be kinetically stabilized over another. Nevertheless, decreasing the aging temperature was observed to increase the aspect ratio of the synthesized aragonite.

Another interesting aspect of aragonite formation is the fact that the synthesis of this polymorph would be driven further if the aging time were kept short. It seems that longer aging times affect the kinetic stability of this polymorph with respect to calcite. Within the above experimental conditions, aragonite morphology was dominated by *branch-like* and to some extent by *needle-like* shapes and, occasionally, *flower-like* shape was observed

3.2 Effect of Organic Additives on the Morphology of Calcite and Aragonite

The study of the effect of organic additives on the crystal type and on the corresponding morphologies of $CaCO_3$ polymorphs is important from the industrial viewpoint due to the role of such additives in the production of unusual morphologies in addition to affecting the transformations of the polymorphs $CaCO_3$. In general, additives may affect the nucleation steps and the crystal growth of $CaCO_3$ by virtue of their

molecular structure framework and solvating abilities. This is reported to take place by blocking of growth sites and confining the reactant solution with organized media possibly leading to high-localized accumulation of ionic charge with high spatial density, the thing that will determine the size, shape, and organization of the crystal forms (Lei et al. 2006). This will ultimately have direct effects on the ionic availability of Ca^{2+} and CO_3^{2-} ions in the medium, and the way these ions interact and build a particular structure, however, little information are available about the mechanistic details of such effects.

The general strategy for obtaining unusual morphologies of $CaCO_3$ polymorphs is to use organic additives with complex functionalization patterns to template the nucleation, growth, and alignment of $CaCO_3$ through electrostatic matching and structural and stereochemical complementarity at inorganic/organic interface (Lei et al. 2006).

In general, the additives inhibition of crystal growth depends on (Westin and Rasmuson 2005b);

1. Extent of complexation of Ca^{2+} in solution.
2. Type of adsorption of the complexing agent or additive to the surface of $CaCO_3$ (flexible adsorption vs rigid adsorption). Less inhibition is generally observed when adsorption is more flexible.
3. Type of polymorph; its atomic structure determining whether more or less Ca^{2+} is exposed to complexing agents (more retardation is usually observed for aragonite compared to calcite).
4. Additive concentration; more concentration causes more inhibition.

In this part of the study, the effects of the presence of some organic additives and the factors indicated in Section 2.3 on the morphology or particle size in addition to some effects observed on the polymorph type of precipitated $CaCO_3$ are discussed below.

3.2.1 Effect of PVP

3.2.1.1 Effect of PVP on Calcite Polymorph

The addition of PVP did not affect the polymorph type of $CaCO_3$, i.e. the resulting particles were composed of calcite. Moreover, minimal effect on morphology or crystal size was detected when the concentration of PVP was increased from 0.1 g/L to 1.0 g/L. However, the order of pH adjustment was seen to affect the morphology of the crystals. When the pH was altered in Na_2CO_3 solution containing PVP prior to the addition of $CaCl_2$ solution, particles had average sizes of around 7 μm, but when the pH was adjusted after $CaCl_2$ solution was added, the particles size on the average was approximately 10 μm, as estimated from SEM images. In addition, the latter case attributed smoother and well-defined rhombohedral surface to the crystals, while in the previous case, the corners of some particles were dissolved, as can be seen in Figure 3.16 (a, b).

Changing the pH value to 11.0 did not influence the phase structure and particle morphology of calcite. But when the pH was reduced to 7.0, the morphology seemed to undergo a transition towards spheroidal-like shape, as shown in Figure 3.16 (c, d). It must be noted that such a change was observed when the pH is altered after the addition of $CaCl_2$.

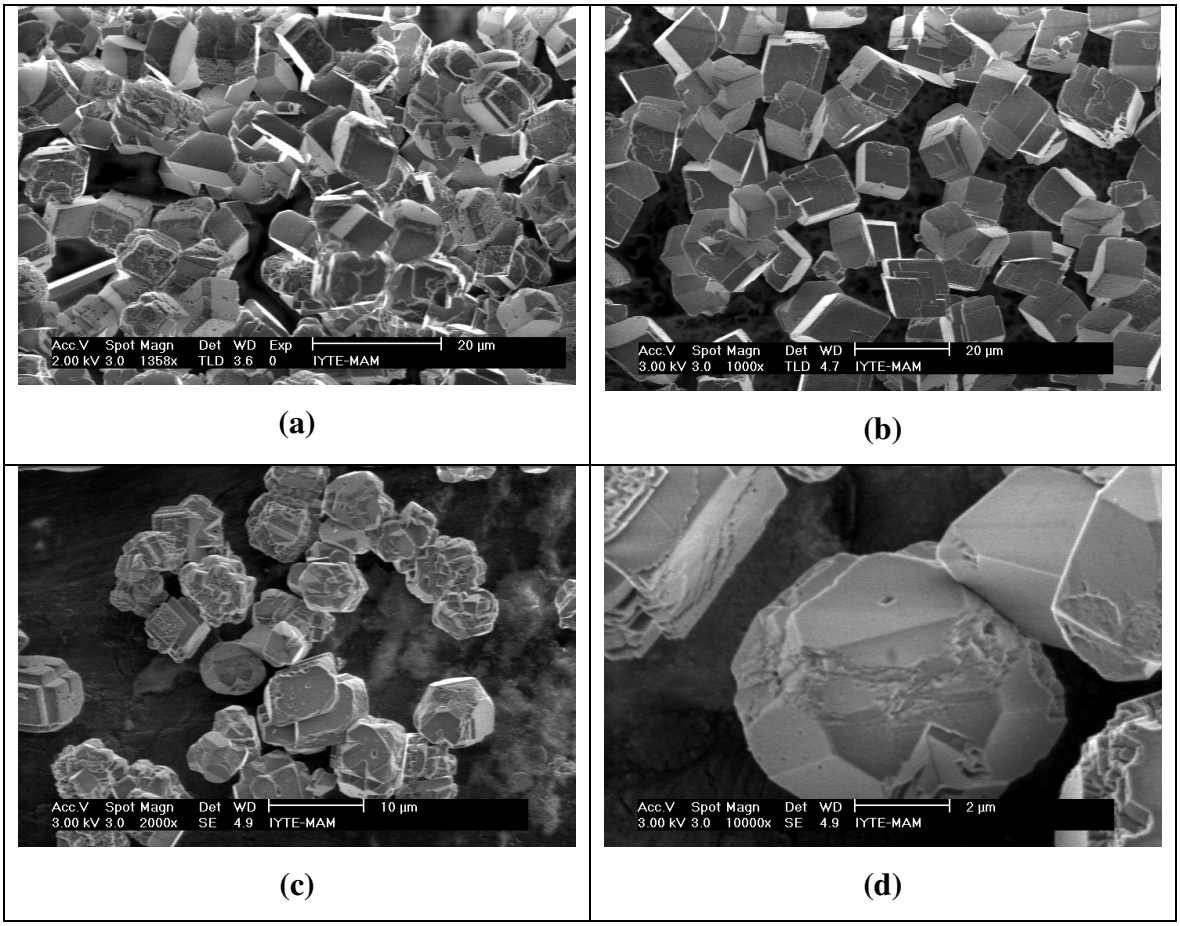

Figure 3.16. SEM micrographs of calcite particles obtained at an additive concentration of 1.0 g/L, pH adjusted; (a) to 9.0 before the addition of $CaCl_2$, (b) to 9.0 after the addition of $CaCl_2$ solution, (c, d) to 7.0 after the addition of $CaCl_2$ solution.

3.2.1.1 Effect of PVP on $CaCO_3$ Dominated by Aragonite Polymorph

In these experiments, $CaCO_3$ particles were prepared at 90°C mixing and 10°C aging temperature in the presence of PVP. As was reported in section 3.1, these conditions leads to the formation of aragonite dominated $CaCO_3$. According to the results, the presence of PVP leads to no obvious change in aragonite fraction and morphology. In addition, changing the concentration of PVP, and the order of pH adjustment did not yield significant changes in particle morphology, but some decrease in the aspect ratio of the crystals seemed to take place. Aragonite fractions and aspect

ratios of resultant particles obtained from the XRD data and SEM pictures are given in Table 3.3. Typical SEM images of the samples are shown in Figure 3.17.

Table 3.3. Aragonite percentage in $CaCO_3$ and the corresponding aspect ratios obtained in the presence of PVP; (a) pH was adjusted prior to the addition of $CaCl_2$, and (b) pH was adjusted after the addition of $CaCl_2$

	(a)		**(b)**		
	0.1 g/L PVP	**1.0 g/L PVP**	**0.1 g/L PVP**	**1.0 g/L PVP**	**No PVP**
Aragonite (%)	83	89	91	87	93
Aspect Ratio	14	12	9	11	11

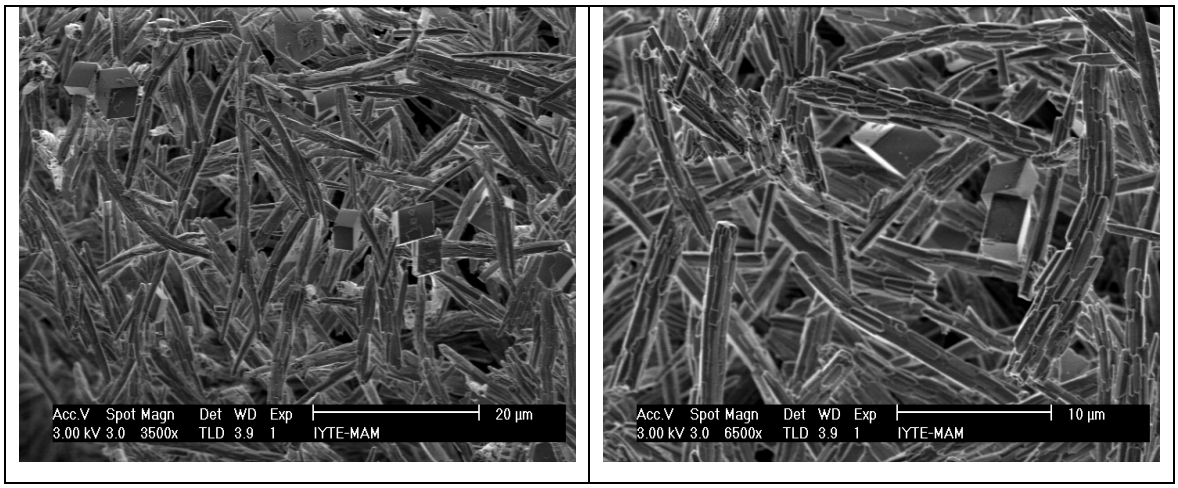

Figure 3.17. Typical SEM images of aragonite crystals obtained in the presence of PVP

3.2.2 Effect of PDDA

3.2.2.1 Effect of PDDA on Calcite Polymorph

PDDA is one of the polycationic additives the effect of which on the morphology and polymorphs of $CaCO_3$ has not been studied to date. In this part, $CaCO_3$ particles were prepared at the optimal experimental conditions of calcite. In all cases, the XRD results indicated that only calcite was formed in the presence of PDDA. The variation of the added amount of PDDA did not lead to significant changes in the particle morphology of calcite. The order of pH adjustment, however, influenced the morphology of calcite particles. When the pH was adjusted after the addition of $CaCl_2$ solution, no change in the morphology and the average particle size of calcite particles was observed as shown in Figure 3.18 (a). In the figure, the rhombohedral calcite particles appear without surface defects with an average particle size amounted to approximately 8 μm. Alternatively, when the pH was adjusted prior to the addition of $CaCl_2$ solution, a kind of particle agglomeration was observed and surface defects were observed. A typical SEM image is given in Figure 3.18 (b).

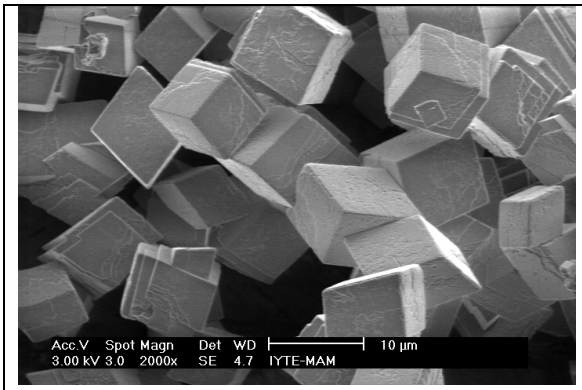

(a)

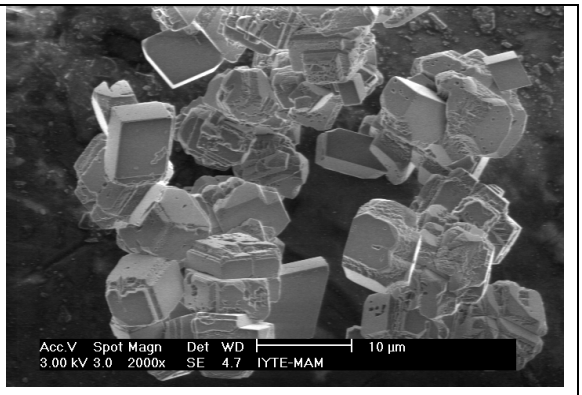

(b)

Figure 3.18. Typical SEM images of calcite prepared in the presence of PDDA; pH adjusted; (a) after the addition of $CaCl_2$ solution, (b) before the addition of $CaCl_2$.

3.2.2.2 Effect of PDDA on $CaCO_3$ Dominated by Aragonite Polymorph

When $CaCO_3$ particles were prepared at the optimal experimental conditions of aragonite and in the presence of PDDA, the XRD patterns indicated that the order of the pH adjustment influenced the morphology and the phase structure of the precipitated $CaCO_3$ particles. The pH adjustment prior to the addition of $CaCl_2$ in the presence of 0.1 g/L of PDDA suppressed the formation of aragonite, leading to a decrease in the formed aragonite to 25%. The remaining aragonite particles exhibited a *rod-like* morphology with their aspect ratio being around 13 (ranged from 5 to 20) as presented in Figure 3.19 (a). As a result of the further addition of PDDA, i.e., 1 g/L, aragonite particles vanished completely and only calcite particles were present in the precipitated sample. This is an important result since it points to the ability of stabilizing calcite at high temperature, an observation that was never reported in literature. The average particle size of the obtained particles was approximately 9 μm, with a *rectangular-prism* like morphology as shown in Figure 3.19 (b). It is crucial to note that the pH adjustment must be performed prior to the addition of $CaCl_2$ for aragonite precipitation to vanish leading to stabilization of calcite at higher mixing temperature. When the pH adjustment is performed after the addition of $CaCl_2$, it was observed that PDDA lost its effect on the morphology and the crystal phase of $CaCO_3$ particles completely when the concentration of PDDA was 0.1 g/L and the aragonite percentage was calculated as 92%. Increasing the concentration of PDDA to 1.0 g/L decreased the aragonite fraction to 79%. For both concentration values aragonite particles exhibited *a branch-like* shape, as shown in Figure 3.19 (c). Moreover, Figure 3.20 illustrates the effect of the order of pH adjustment on the obtained XRD diagrams of the samples.

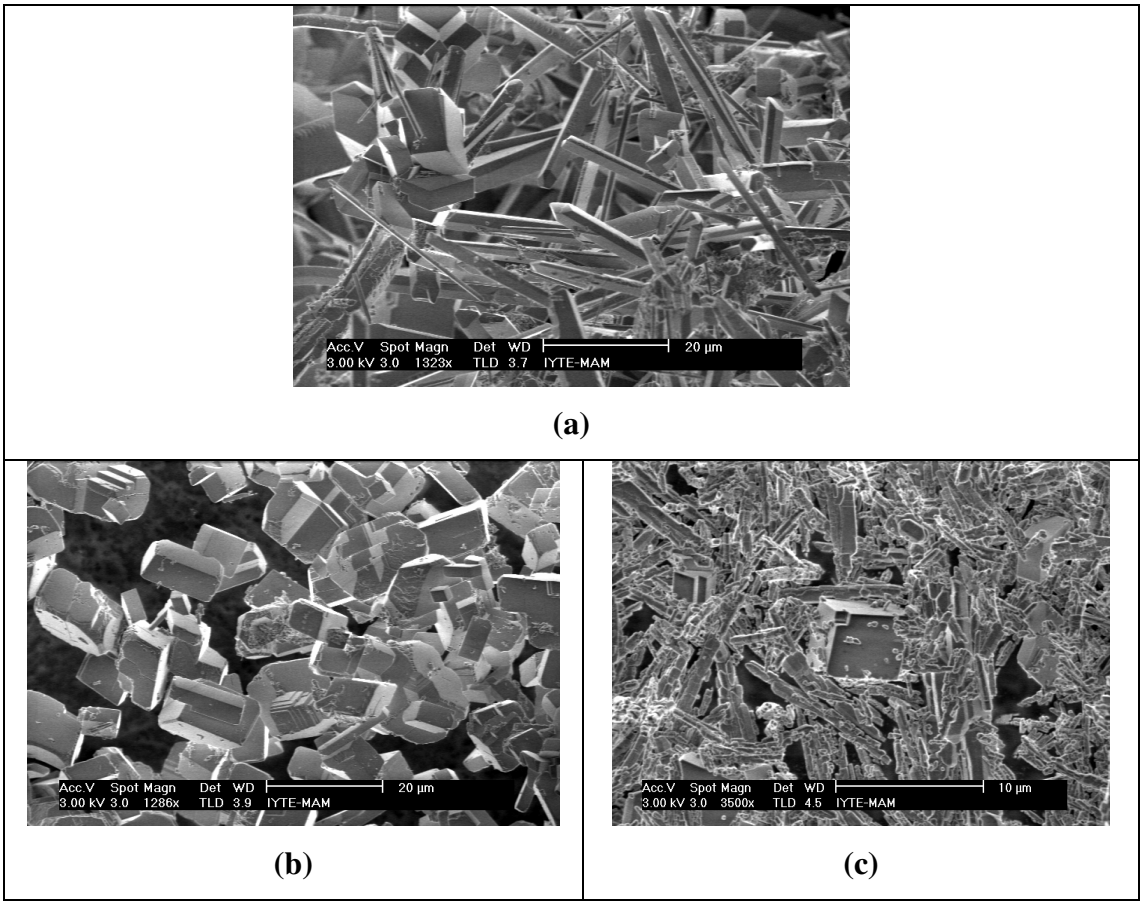

Figure 3.19. SEM images of $CaCO_3$ precipitated in the presence of PDDA; (a) aragonite with rod-like shape, (b) calcite with rectangular-prism shape, and (c) aragonite with branch-like shape.

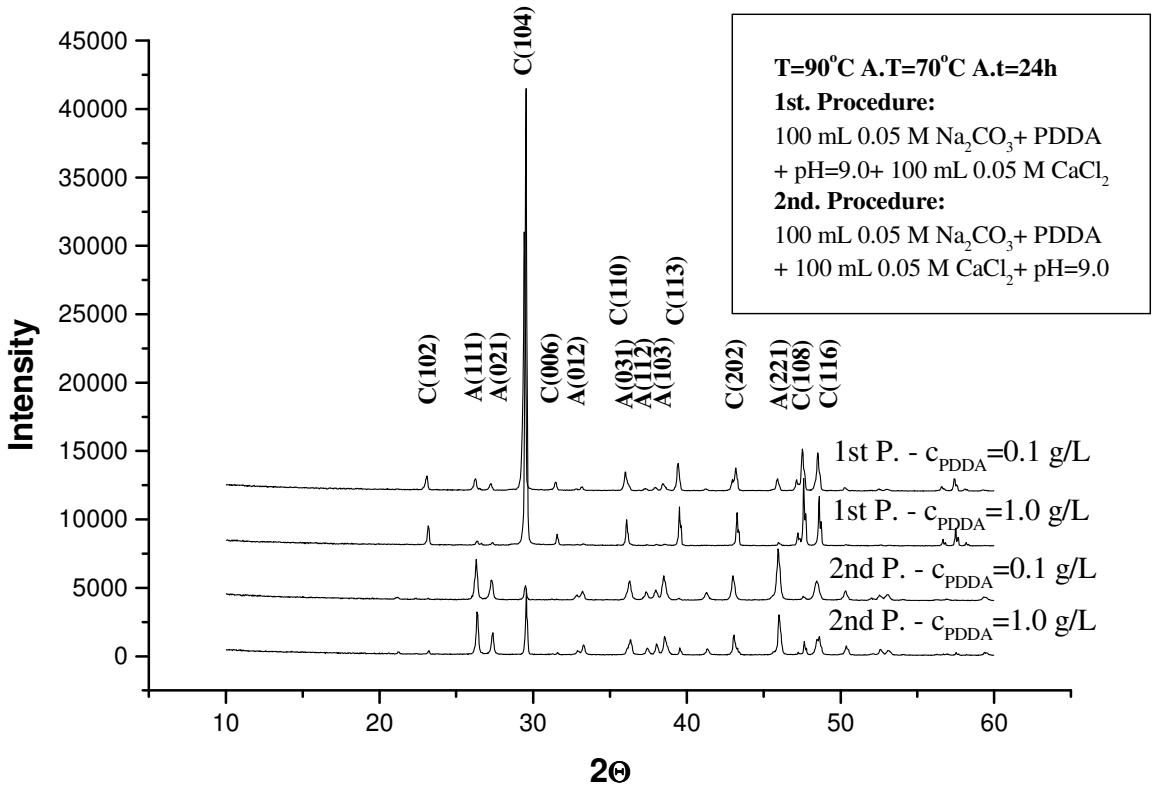

Figure 3.20. Effect of the order of pH adjustment on aragonite fraction in $CaCO_3$ precipitated in the presence of PDDA, A: aragonite, C: calcite

3.2.3 Effect of PEG

3.2.3.1 Effect of PEG on Calcite Polymorph

The results of these experiments indicated that the presence of PEG and the variation of its concentration resulted in some effects on the particle morphology and that the crystal size of calcite particles averaged to approximately 8-9 μm. Under the experimental conditions, PEG dissolved the higher energy points on the crystal surface like edges and corners and caused the crystals to be acquire a rounded shape, as long as the pH is adjusted prior to the addition of $CaCl_2$ solution to the reaction mixture (Figure 3.21 (a)). Changing the order of pH adjustment caused PEG to greatly loose its effect on the precipitated calcite crystals, which seemed to be dominated by the typical rhombohedral shape (Figure 3.21 (b)) with an average particle size of about 10 μm regardless of the concentration of the additive.

In addition, the effect of pH on the morphology of calcite particles in the presence of PEG was examined at the pH values of 7.0 and 11.0. The pH adjustment to 7.0 prior to the addition of $CaCl_2$ solution resulted in an increase in the average particle size to about 18 μm. Particles having smaller average particle size of approximately 8 μm were obtained if the pH was adjusted to 7.0 after the addition of $CaCl_2$. In both cases, dissolution of corners and edges of rhombohedral calcite faces were observed. Adjustment of pH to 11.0 had no effect on the resultant calcite particles and the precipitation reactions yielded rhombohedral calcite particles with particle sizes ranging 5-8 μm.

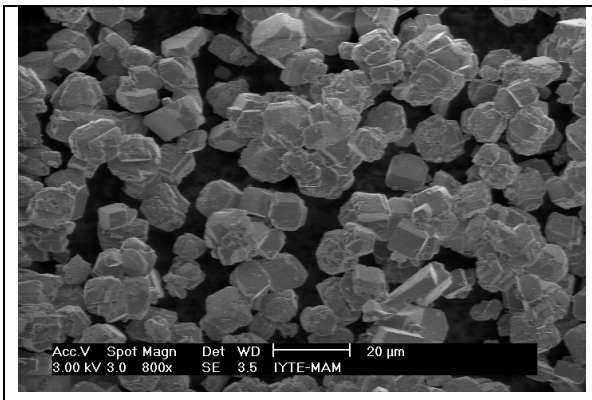

(a)

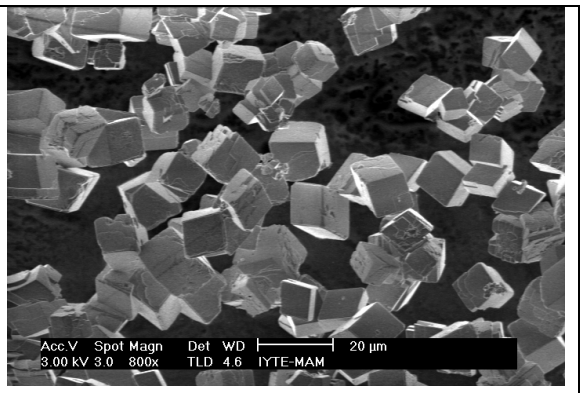

(b)

Figure 3.21. Typical SEM images of calcite prepared in the presence of PEG. pH adjusted; (a) before the addition of $CaCl_2$ solution, (b) after the addition of $CaCl_2$

3.2.3.2 Effect of PEG on $CaCO_3$ Dominated by Aragonite Polymorph

In these experiments, it was observed that when the particles were prepared at optimal conditions leading, in the absence of additives, to formation aragonite dominated $CaCO_3$ that PEG had an influence on the extent of aragonite formation, similar to that reported above for the effect of PDDA. The addition of PEG partially suppressed the aragonite formation leading to stabilization of aragonite at the temperature of mixing, i.e. 90°C. Based on XRD diagram, Figure 3.22, the $CaCO_3$ crystals contained 43% and 31% aragonite for the PEG concentrations of 0.1 g/L and 1.0 g/L, respectively, compared to about 90% yield obtained in the absence of PEG. The

morphology of aragonite looked as *columnar-prismatic* with an approximate aspect ratio of 15 (Figure 3.23 (a)), while calcite particles assumed irregular shapes (Figure 3.23 (b)). The above results are obtained if the pH is adjusted prior to adding $CaCl_2$ to the reaction mixture. However, if the pH is adjusted following the addition of $CaCl_2$, then again the suppression effect of PEG will still be observed but to a lesser extent. Quantitatively, in the presence of 0.1 g/L of PEG the aragonite amount was 79%, while at 1.0 g/L PEG only 65% aragonite is obtained.

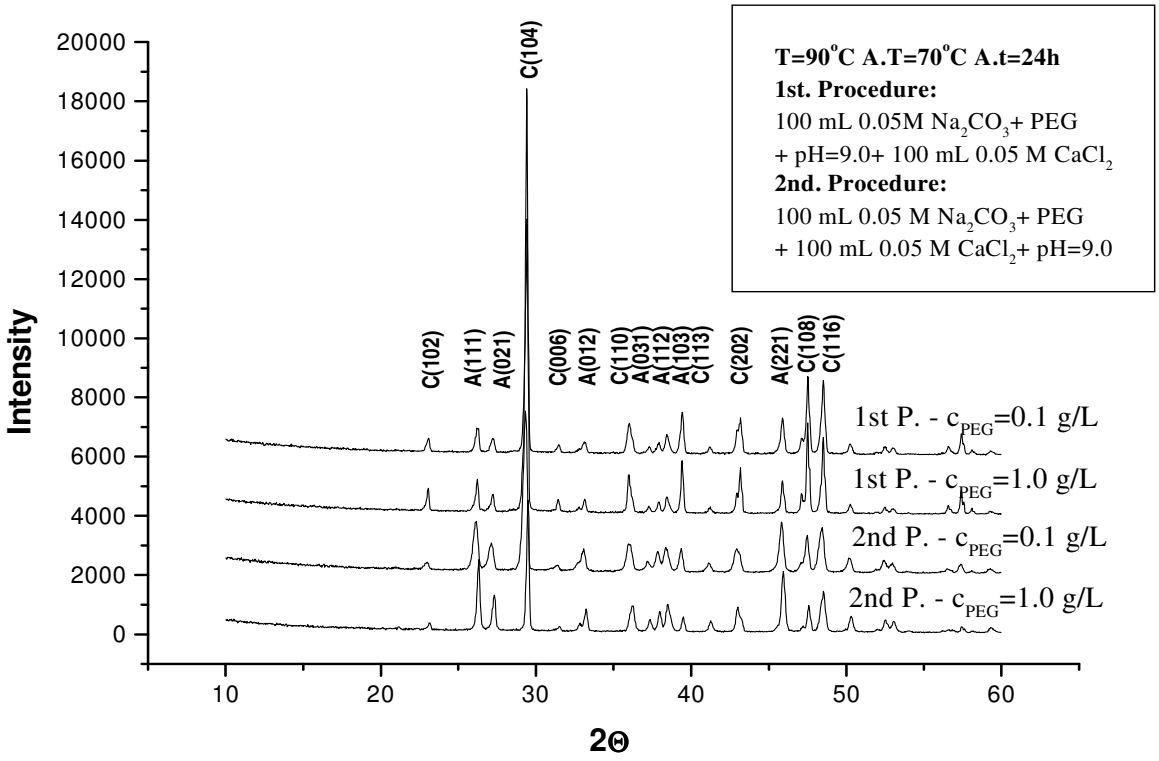

Figure 3.22. Effect of the order of pH adjustment on aragonite fraction in $CaCO_3$ precipitated in the presence of PEG, A:aragonite, C: calcite

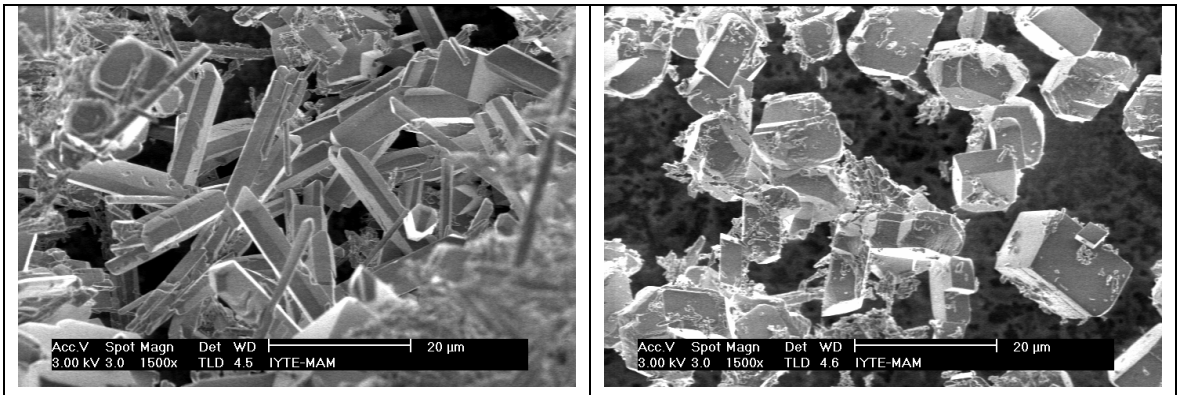

(a) **(b)**

Figure 3.23. SEM images of $CaCO_3$ precipitated in the presence of PEG; (a) aragonite with columnar-prismatic shape, (b) calcite with irregular shape

3.2.4 Effect of CTAB

3.2.4.1 Effect of CTAB on Calcite Polymorph

The results indicated that the presence of CTAB in the reaction medium causes the calcite crystals to aggregate. In the presence of 0.1 g/L CTAB, deformed rhombohedral calcite seems to start aggregation, and when CTAB concentration is increased to 1.0 g/L, calcite aggregation lead to formation of rods with an aspect ratio of 2-3. Typical SEM images are shown in Figure 3.24. This effect is observed if the pH is adjusted before the addition of $CaCl_2$. As seen in other additives, if the pH is adjusted after the addition of $CaCl_2$, CTAB will loose its effect on the morphology of calcite particles and regardless of the CTAB concentration, rhombohedral calcite particles were formed with the average particle size range of about 7 µm.

When the pH is altered to 7.0 in the presence of CTAB, deterioration in the crystal morphology is observed accompanied with a tendency to form spheroidal particles (Figure 3.25 (a)). The presence of CTAB had no effect on the calcite particles when the pH was adjusted to 11 and the size of the resulting rhombohedrons was about 8 µm (Figure 3.25 (b)).

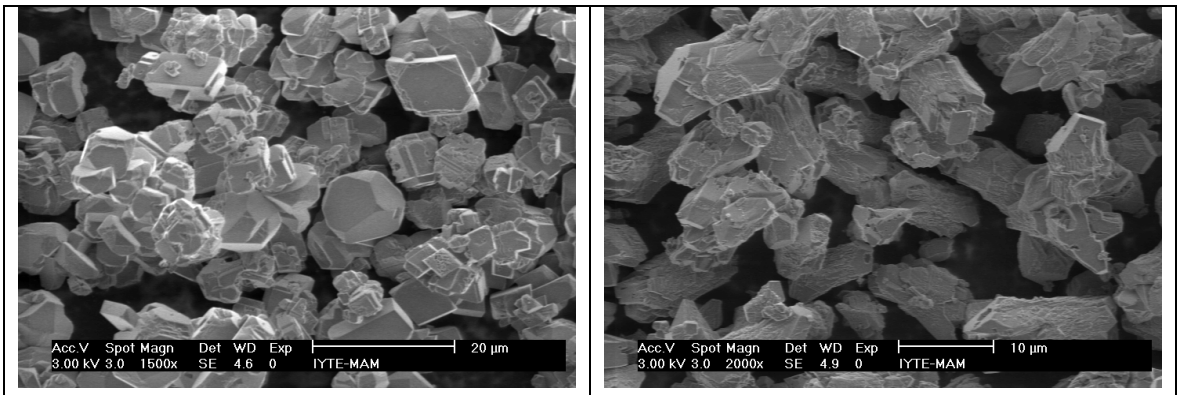

(a) **(b)**

Figure 3.24. Typical SEM images in the presence of: (a) 0.1 g/L CTAB, and (b) 1.0 g/L CTAB

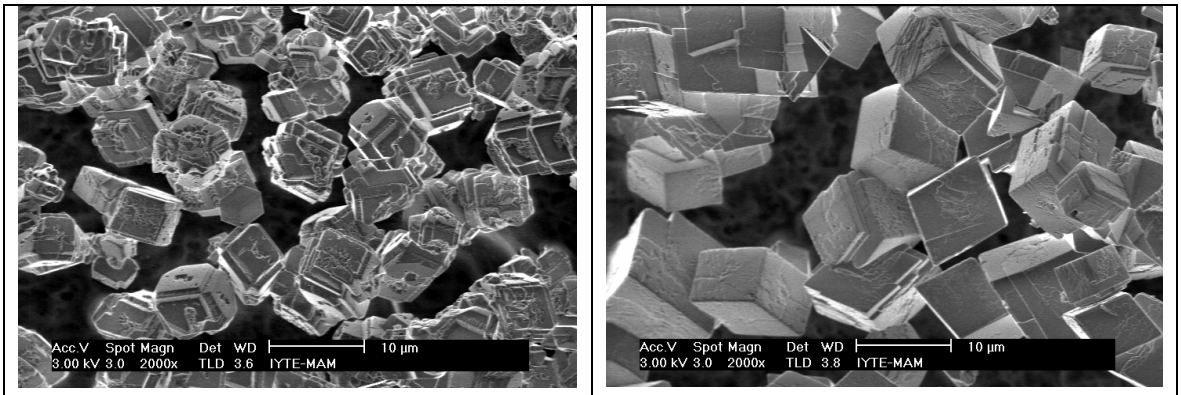

(a) **(b)**

Figure 3.25. SEM images of calcite crystals at pH of: (a) 7.0, (b) 11.0.

3.2.4.2 Effect of CTAB on $CaCO_3$ Dominated by Aragonite Polymorph

The presence of CTAB in the reaction mixture under the conditions that leads to aragonite formation caused a decrease in the amount of formed aragonite. According to the quantification based on XRD diagrams (Figure 3.26), the percentage of aragonite in the precipitated $CaCO_3$ were 14% and 19% for the CTAB concentration of 0.1 g/L and 1.0 g/L, respectively. The morphology of aragonite under such conditions appeared to be *rod-like* with an aspect ration of 25, and calcite crystals appeared to be *plate-like* with part of them assuming a pentagonal shape (Figure 3.27 (a)). As expected from the

experience with earlier additives, adjusting the pH following the addition of $CaCl_2$ caused CTAB to loose its effect on the morpho-synthesis of $CaCO_3$. According to XRD diagrams, under such condition, the percentage of aragonite were 82 and 92% were calculated for the concentrations of 0.1 g/L and 1.0 g/L of CTAB, and the morphology appears to be the typical branch-like (Figure 3.27 (b)).

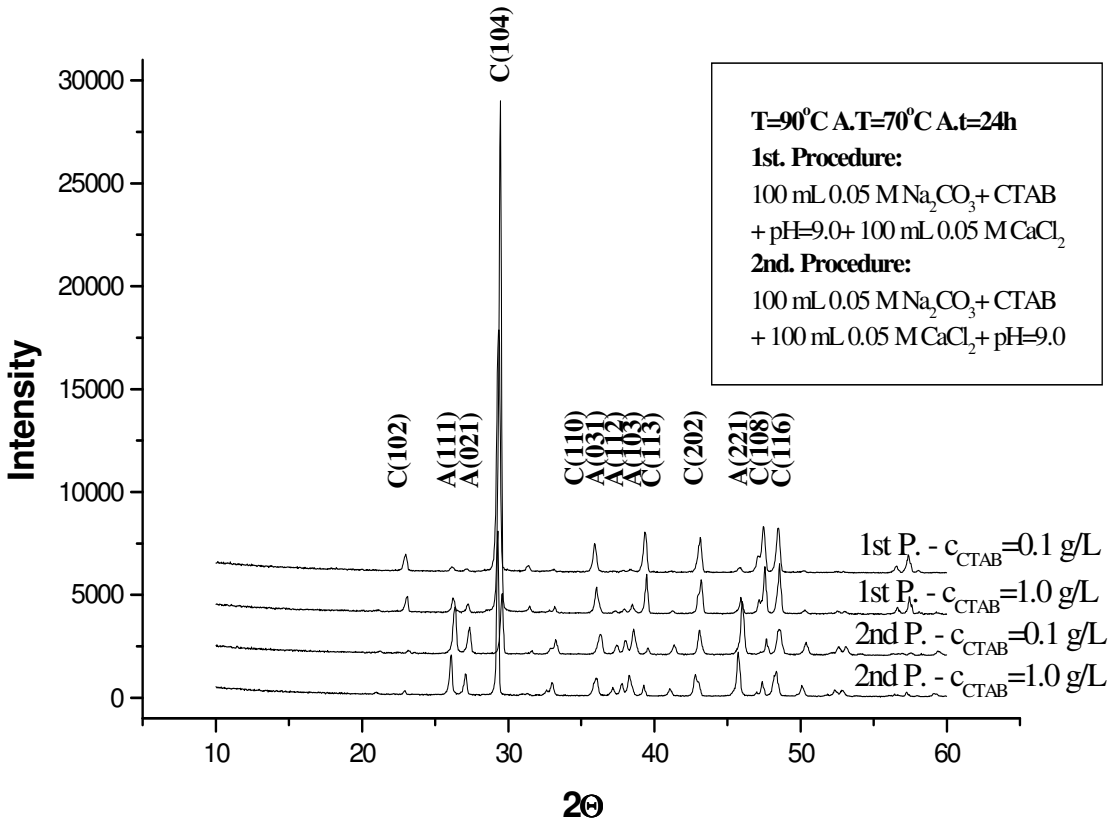

Figure 3.26. XRD diagrams of $CaCO_3$ prepared in the presence of CTAB

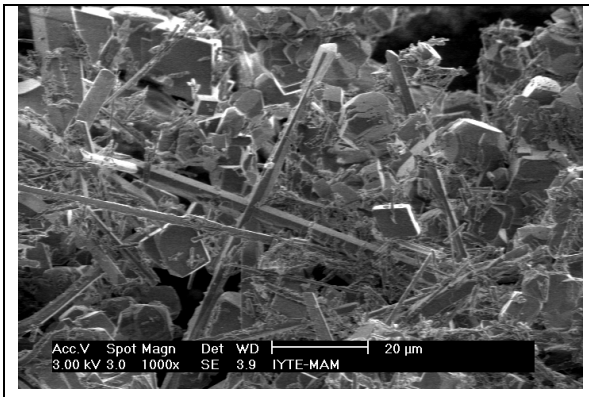

(a)

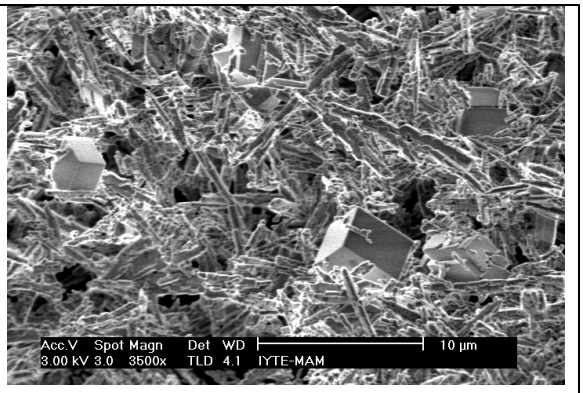

(b)

Figure 3.27. SEM images of $CaCO_3$ precipitated in the presence of CTAB; (a) pH adjusted before the addition of $CaCl_2$, (b) pH adjusted after the addition of $CaCl_2$

3.2.5 Effect of EDTA

3.2.5.1 Effect of EDTA on Calcite Polymorph

Among the various additives studied in this work, EDTA was the one that showed the highest impact on the morphology of calcite. When calcite is precipitated with the pH adjustment performed prior to adding $CaCl_2$ to the reaction medium and the concentration of EDTA is kept at 0.1 g/L, the particles had a tendency to aggregate. However, increasing EDTA concentration to 1.0 g/L yielded the well-defined calcite *apple core-types* with an aspect ratio of 4, as shown in Figure 3.28. The top of the particles exhibited smooth surface while the sides were rough. Similar morphology of calcite particles was reported by Donners et al. 2002 where they were obtained by utilization of the sodium salts of poly(L-isocyanoalanyl-D-alanine) and poly(L-isocyanoalanyl-D-alanine) and reported an aspect ratios of 1.87 and 2.2, respectively. When the pH was adjusted to 9.0 after the $CaCl_2$ addition, EDTA was lost its effect on the calcite particles where they gained their typical rhombohedral morphology with the average particle size of 7-8 µm in the presence of 0.1 g/L EDTA. An increase in the concentration of EDTA to 1.0 g/L exhibited no significant effect except some deformation on the rhombohedral calcites.

In the presence of EDTA, reducing the pH to 7.0 yielded again the apple core-type calcites with an aspect ratio range of 3-4, while increasing the pH to 11.0 yielded the calcite polygons with average particle size range of 8-10 μm. Typical SEM graphs are given in Figure 3.29. It is interesting to note that the order of the pH adjustment had no significant influence on the synthesized calcite particles.

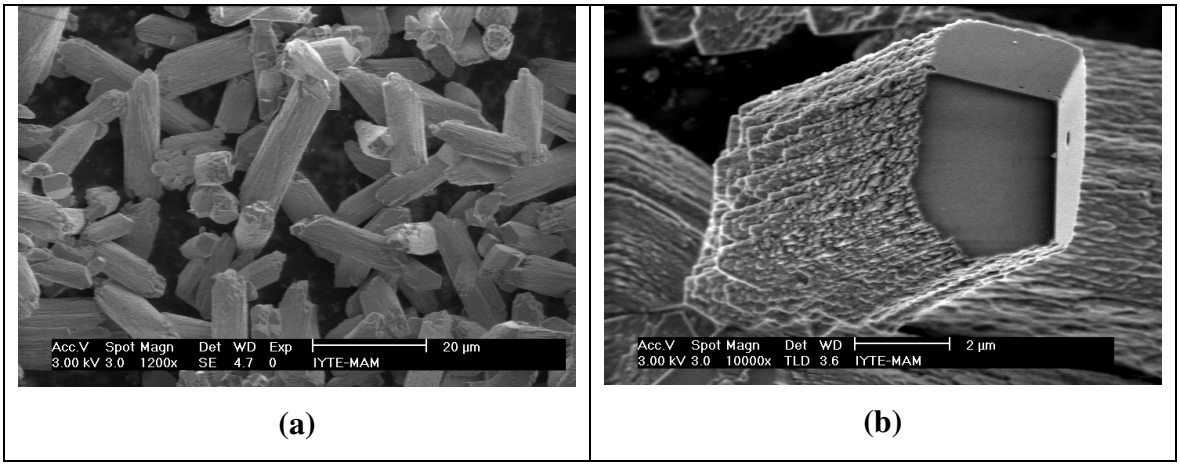

(a) **(b)**

Figure 3.28. SEM microimages of calcite particles prepared in the presence of EDTA.

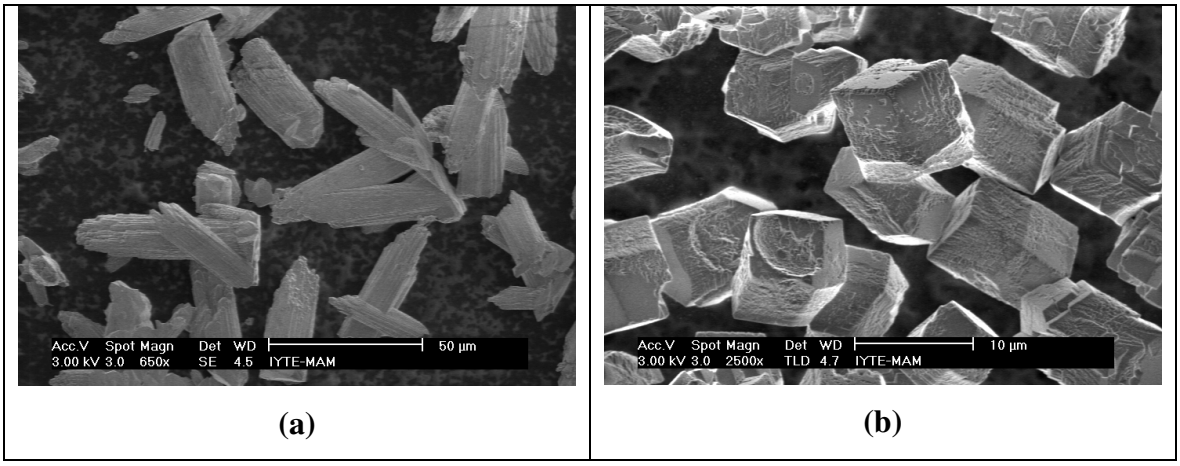

(a) **(b)**

Figure 3.29. SEM images of calcite precipitated in the presence of EDTA; (a) pH=7.0, (b) pH=11.0.

3.2.5.2 Effect of EDTA on $CaCO_3$ Dominated by Aragonite Polymorph

In these experiments the precipitation of $CaCO_3$ at the optimal conditions of aragonite formation was carried out in the presence of EDTA. According to the obtained results, EDTA suppressed the formation of aragonite and promoted the formation of calcite. The percentage of aragonite obtained at the indicated conditions is given in the Table 3.4. The XRD patterns used in the quantification analysis are provided in Figure 3.30.

Aragonite synthesized with the pH being adjusted to 9.0 prior to the addition of $CaCl_2$ demonstrated interesting morphologies in the presence of EDTA. When the concentration of EDTA was 0.1 g/L, sub-micron plates of the mineral appeared to stack yielding rods with approximately 2-3 μm lengths (Figure 3.31 (a, b)). An increase in the concentration of EDTA to 1.0 g/L yielded a mixture of well-defined spheres and rods. The spheres had a diameter of ca. 20 μm and the aspect ratios of rods were 2-3 (Figure 3.31 (c, d)). Alternatively, the preparation of the crystals with the pH adjusted to 9.0 following the addition of $CaCl_2$ resulted in an aggregation of the rhombohedral particles regardless of the variation of EDTA concentration.

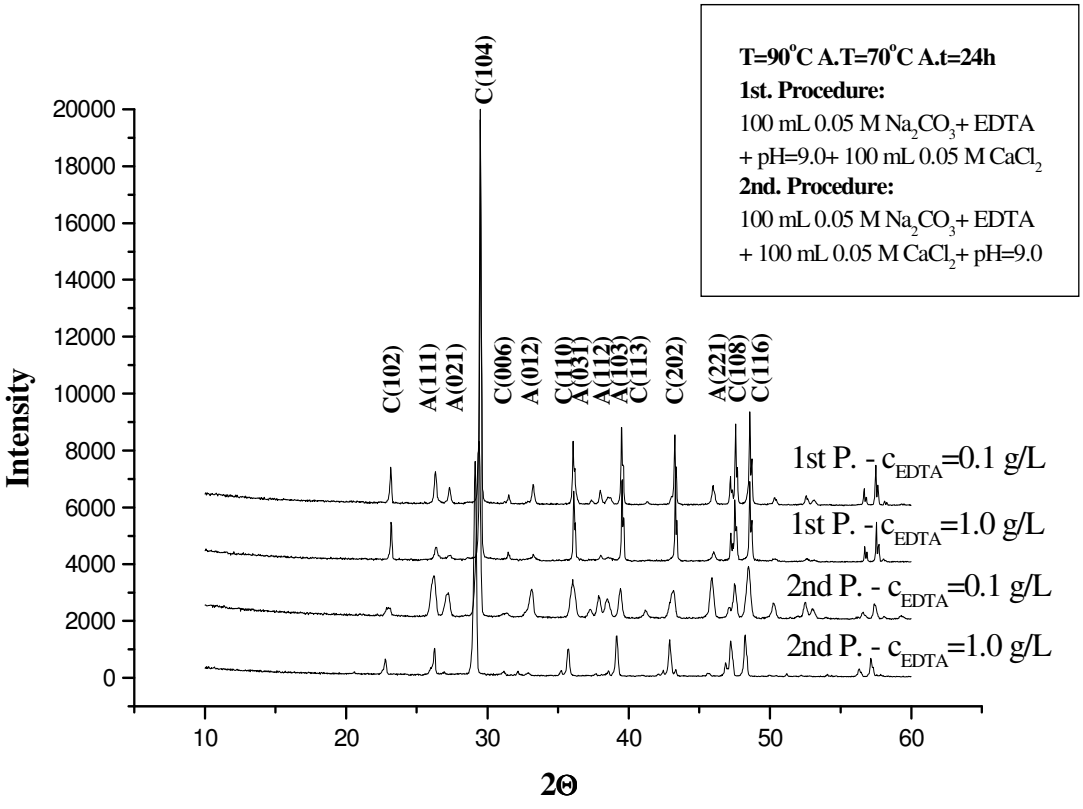

Figure 3.30. XRD patterns of $CaCO_3$ precipitated in the presence of EDTA

Table 3.4. The percentage of aragonite obtained in the presence of EDTA, (a) pH was adjusted to 9.0 prior to the addition of $CaCl_2$, (b) pH was adjusted to 9.0 after the addition of $CaCl_2$

	(a)		**(b)**	
	0.1 g/L EDTA	**1.0 g/L EDTA**	**0.1 g/L EDTA**	**1.0 g/L EDTA**
Aragonite %	38	30	56	41

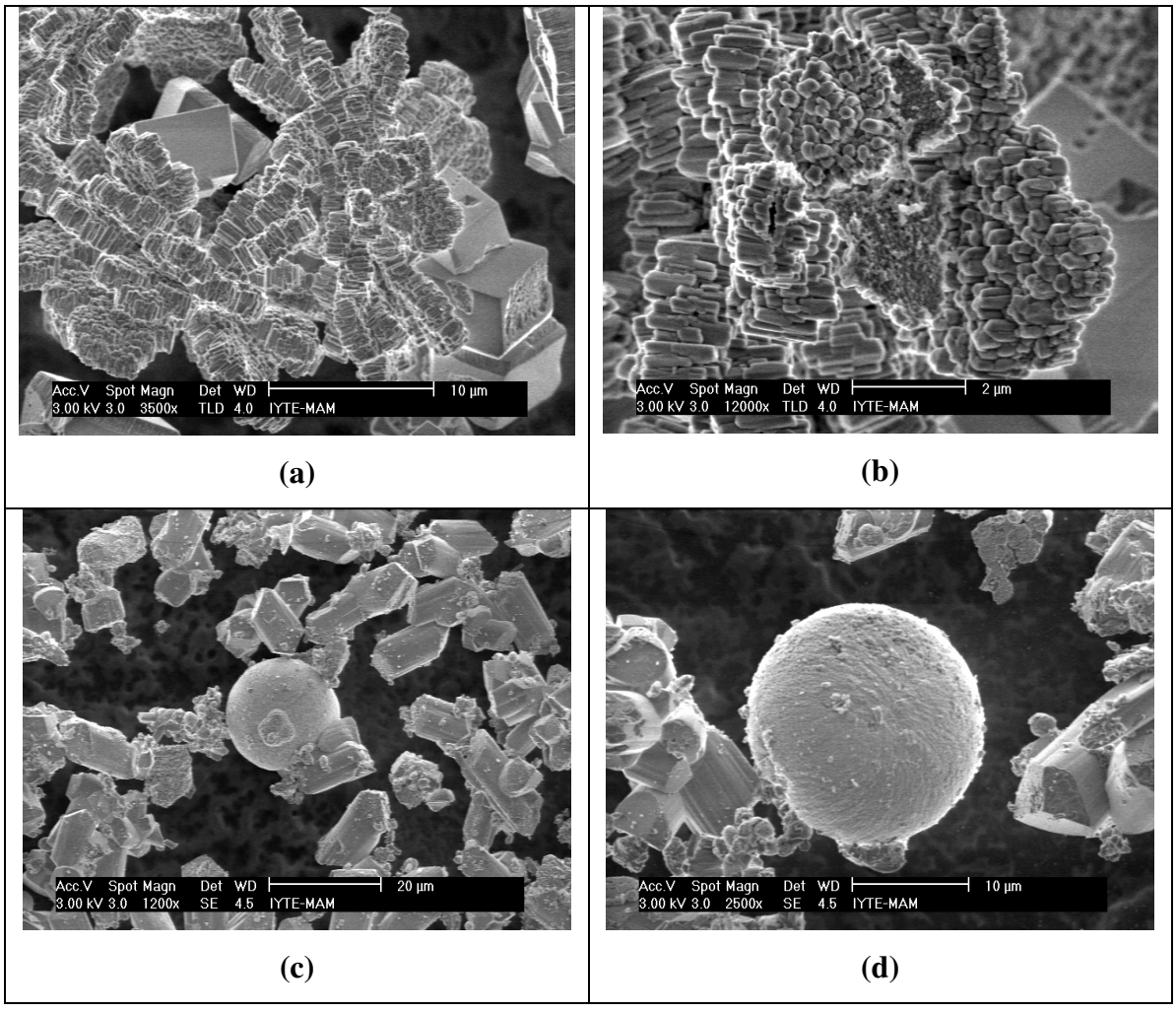

Figure 3.31. SEM images of $CaCO_3$ (aragonite polymorph) precipitated in the presence of EDTA; (a, b) 0.1 g/L EDTA, and (c, d) 1.0 g/L EDTA.

3.3 Properties of Calcite Filled Polyester Composites

$CaCO_3$ is extensively utilized as filler in many industries as paints, plastics, rubber and paper (Yu et al. 2006). The aim in these experiments is to incorporate the calcite synthesized under the optimum conditions (Section 3.1) as filler in a polyester polymer matrix and to examine the effects of calcite particles on the mechanical properties of composites. In addition, the effect of the silane-treatement of calcite on the composites was studied. For this purpose, polyester resins were loaded with unsilanized and silanized calcite fillers at the weight fractions of 5, 10, and 20 %.

Figure 3.32 (a) and (b) shows the Young's modulus and the tensile strength of composites as a function of calcite weight fraction.

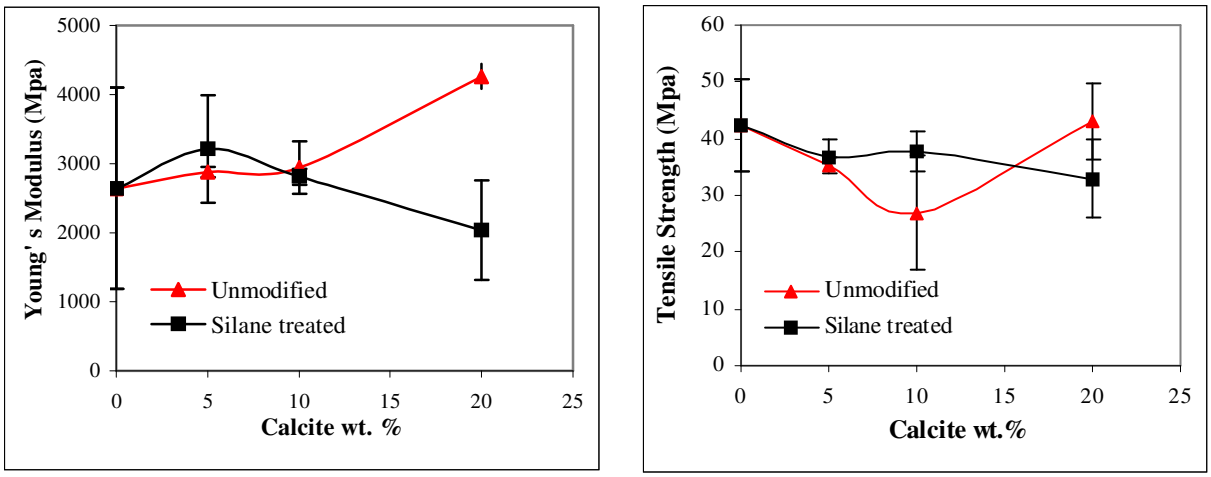

(a) **(b)**

Figure 3.32. Young' s modulus (a) and tensile strength (b) of polyester composite loaded with unsilanized and silanized calcite

It is evident from the figures that the Young's modulus of the polyester composites increases slightly with unmodified calcite particle loading. In contrast, the presence of modified calcite particles enhances the Young's modulus values only at low concentration; however this value decreases as the concentration of modified filler is increased.

As shown in Figure 3.32 (b) the tensile strength of the composite decreases slightly with increasing calcite content for modified particles. However, this value

decays for unmodified particles up to 10 wt. % and rises again at 20 wt.% and approaches to the value of neat polyester. Up to 10 weight percent of calcite it was obvious that silanization of particles provides almost equal strength or of neat polyester. For further concentrations, it seems that the high concentration of silanes reduces the adhesion at the interface. It was reported that the presence of adhesion between the polymer and the filler results in an increase in tensile strength value (Şen and Nugay 2000).

Demjen 1998 reported that 3-(trimethoxysilyl) propyl methacrylate, when used in polypropylene/$CaCO_3$ composites, exhibited the mechanical properties of composites basically unchanged. In our study, the calcite particles were treated at pH 3, within which the small bicarbonate concentration develops OH functional groups at the surface. Some enhancements on the mechanical properties may be attributed to the interactions between the minor OH functional groups formed at the calcite surface and silane coupling agents.

SEM analyses were carried out on the fracture surfaces of the composite samples to assess the dispersion of the filler in the composites. The samples were sputter-coated with a thin layer of gold to obtain a conductive surface. SEM images of fracture surfaces of neat polyester, unmodified and silane-treated $CaCO_3$/Polyester composites are shown in Figure 3.33 to 3.35 for neat polyester. The images indicated some aggregation of calcite particles, regardless of the amount of filler and the effect of silanation. In addition, clear surfaces of the filler particles indicate a weak adhesion between the filler and polymer matrix. The tendency of calcite particles to aggregate in addition to the weak interaction between the calcite particles and the polyester resins is considered to be responsible for the decrease in the tensile strength composites.

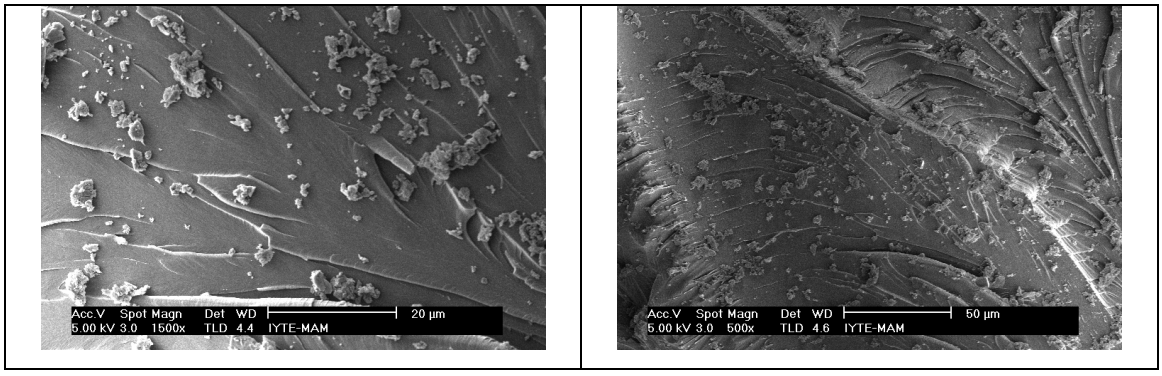

Figure 3.33. SEM micrographs of fracture surface of neat polyester

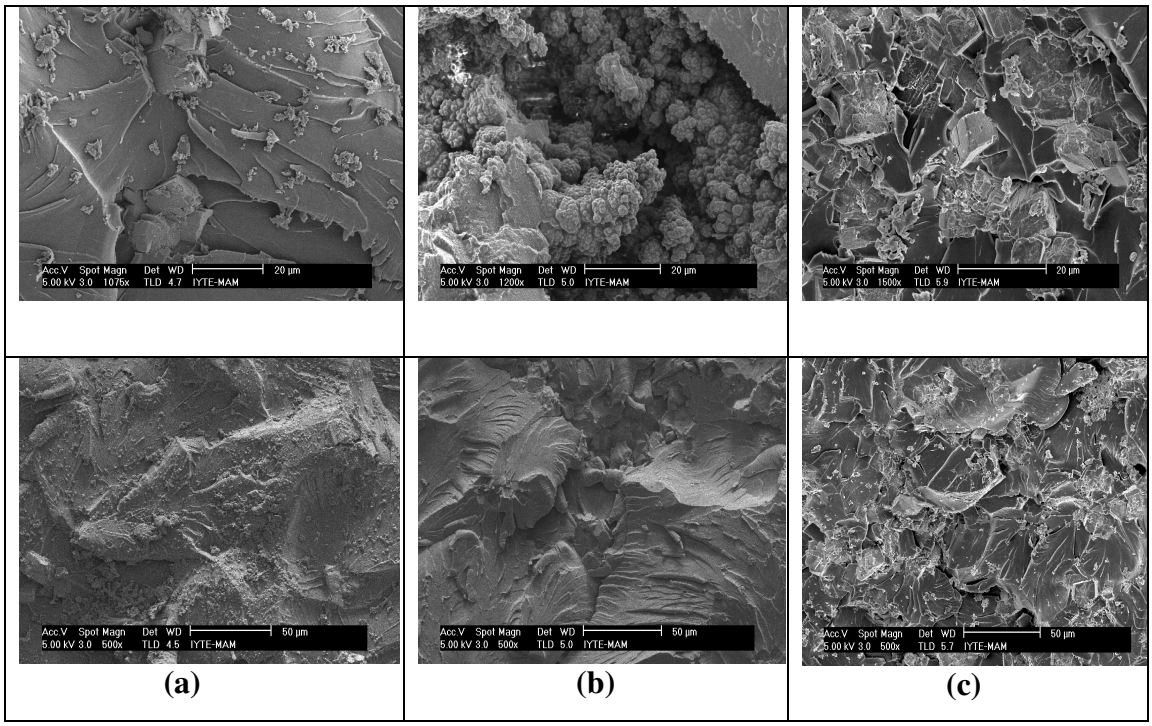

Figure 3.34. SEM micrographs of fracture surface of (a) 5 wt.%, (b) 10 wt.%, and (c) 20 wt. % unmodified calcite added polyester composite

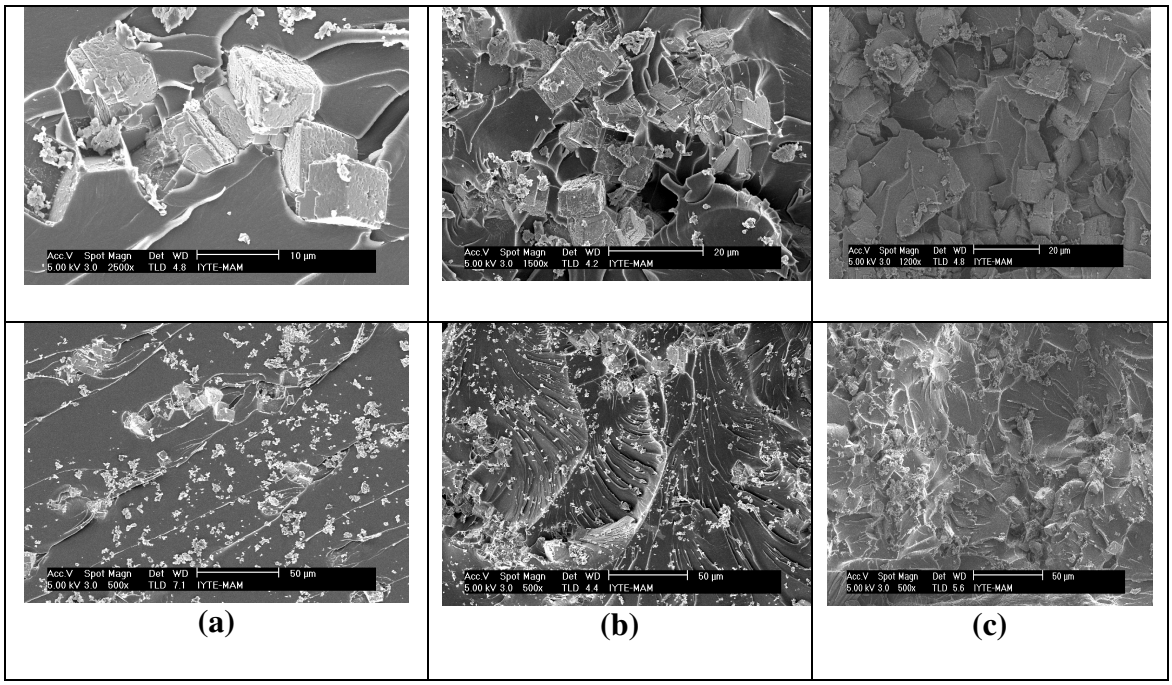

Figure 3.35. SEM micrographs of fracture surface of (a) 5 wt.%, (b) 10 wt.%, and (c) 20 wt. % silanized calcite added polyester composite

The glass transition temperature (Tg) of modified calcite particle added polyester composites were measured by differential scanning calorimeter (DSC). The results are given in Table 3.5. According to the DSC results, the addition of the calcite particles into the polyester systems does not significantly affect the Tg. However, it was observed that the presence of modified calcite at 10wt.% increases the Tg by 2-3^{o}C.

Table 3.5 DSC results of the silane modified calcite / polyester composites

Weigth % of Modified $CaCO_3$ Particles in Polyester	**Tg (^{o}C)**
Neat polyester	115.8
5	114.3
10	118.4
20	115.8

Based on the results of mechanical tests and thermal analyses, it can be concluded that the addition of calcite particle has no significant reduction on the mechanical properties and the glass transition temperature of the polyester resins. As a result, calcite seems to be a good candidate that can be potentially used as a filler in polyester resins. Moreover, the economic feasibility and the expected enhancement in the thermal properties of the polymer, in particular the improvement of the inflammability characteristics, are expected to contribute to the applicability of calcite as a filler in polyester matrices.

CHAPTER 4

CONCLUSION

The findings of this work showed that, within the investigated experimental conditions, the most appropriate pH value for calcite preparation was 9.0, and a concentration of 0.05 M seems to be appropriate for obtaining calcite crystals with smooth surfaces. The most suitable mixing and aging temperatures for the production of this polymorph is around 30^{o}C, and the aging time seems to have insignificant effect on the yield of calcite, as long as the temperature is not changed beyond 50^{o}C. Under the above conditions the morphology of calcite is dominated by rhombohedral and cubic crystal shapes in addition to plate-like crystals formed to a comparatively lesser extent. When the mixing and aging temperatures are raised beyond 50^{o}C, the formation of aragonite is driven. The quantity of this polymorph in the outcoming $CaCO_3$ samples was seen to be directly proportional with increasing temperature, and reached a mass percentage of about 97 when the mixing temperature was 90^{o}C. The aging temperature showed less effect on the amount of aragonite formed compared to the mixing temperature, the thing expected due to the short time scale of the nucleation and initial phases of crystal growth processes, the intervals during which one polymorph might be kinetically stabilized over another. Nevertheless, decreasing the aging temperature was observed to increase the aspect ratio of the synthesized aragonite.

Another interesting aspect of aragonite formation is the fact that the synthesis of this polymorph would be driven further if the aging time were kept short. It seems that longer aging times affect the kinetic stability of this polymorph with respect to calcite. Within the above experimental conditions, aragonite morphology was dominated by *branch-like* and to some extent by *needle-like* shapes and, occasionally, *flower-like* shape was observed.

The presence of various additives in the reaction medium leading to the facile precipitation of $CaCO_3$ appeared to affect, to various extents, the morphologies of calcite and aragonite in addition to the polymorph stability of aragonite. Among the studied additives, PVP exhibited the least influence on the morphology and phase structure of the produced $CaCO_3$ particles. At the optimal calcite formation condition

when pH was adjusted prior to the addition of $CaCl_2$, PDDA and CTAB caused to the formation of aggregates, while PEG produced rounded calcites. In the presence of EDTA apple core-type calcites were formed. At the optimal aragonite formation condition PEG, CTAB and EDTA suppressed the formation of aragonite and promoted the formation of calcite. This effect was more pronounced in the case of PDDA, which caused, under high concentration conditions, a complete vanishing of aragonite polymorph. The particles in the presence of EDTA exhibited sphere and rod morphologies, and polygon-calcites were observed when the pH was raised to 11. The pH modification prior to the addition of $CaCl_2$ to the reaction mixture caused the additives to be much more effective on the precipitated crystals compared to the situation in which such an adjustment is made after the addition of $CaCl_2$. This is indicating clearly that the time scale of additive action on $CaCO_3$ morphology and/or phase stability is very short.

The results of the studies on the application of calcite as a filler in polyester polymer showed that calcite has no significant effect on the mechanical properties of the polyester resins. As a result, calcite seems to be a good candidate that can be potentially used as a filler in polyester resins. Moreover, the economic feasibility and the expected enhancement in the thermal properties of the polymer, in particular the improvement of the inflammability characteristics, are expected to contribute to the applicability of calcite as a filler in polyester matrices. The detailed investigation of the effect of calcite addition on the thermal properties of polyester can be a topic for future works.

REFERENCES

Abdel-Aal, N. and Sawada K. 2003. "Inhibition of adhesion and precipitation of $CaCO_3$ by aminopolyphosphonate", *Journal of Crystal Growth*, Vol.256, pp.188-200.

Addadi, L. and Weiner, S. 1985. *Proc Natl. Acad. Sci. USA*. Vol.82, p.4110.

Andreassen, J.-P. 2005. "Formation mechanism and morphology in precipitation of vaterite-nano-aggregation or crystal growth?", *Journal of Crystal Growth*, Vol.274, pp.256-264.

Büchel, K.H., Moretto, H.H., Woditsch, P., 2000. *Industrial Inorganic Chemistry*, (Wiley-VCH), pp.535-547.

Carmona, J.G., Morales, J.G. and Clemente, R.R. 2003. "Morphological control of precipitated calcite obtained by adjusting the electrical conductivity in the $Ca(OH)_2$-H_2O-CO_2 system", *Journal of Crystal Growth*, Vol.249, pp.561-571.

Cheng, B., Lei, M., Yu, J. and Zhao, X. 2004. "Preparation of monodispersed cubic calcium carbonate particles via precipitation reaction", *Materials Letters*, Vol. 58, pp. 1565-1570.

Cölfen, H. 2003. "Precipitation of carbonates: recent progress in controlled production of complex shapes", *Current Opinion in Colloid and Interface Science*, Vol.8, p. 23.

Cullity, B.D., 1978. *Elements of X-Ray Diffraction,* (Addison-Wesley Publishing Company, Inc., USA) pp.84-87.

Demjén, Z., Pukánszky, B., Földes, E. and Nagy, J. 1997. "Interaction of Silane Coupling Agents with $CaCO_3$", *Journal of Colloid and Interface Science*, Vol.190, p.427.

Demjén, Z., Pukánszky, B., and Nagy, J. 1998. "Evaluation of interfacial interaction in polypropylene/surface treated $CaCO_3$ composites", *Composites* Part A 29 A, pp. 323-329.

Donners, J.J.J., Nolte, R.J.M., and Sommerdijk N.A.J.M. 2002. "A Shape-Persistent Polymeric Crystallization Template for $CaCO_3$", *J.Am.Chem. Soc.*, Vol. 124, pp. 9700-9701.

Feng, Q. L., Pu, G., Pei, Y., Cui, F. Z., Li, H. D. and Kim, T. N. 2000. "Polymorph and morphology of calcium carbonate crystals induced by proteins extracted from mollusk shell", *J. Cryst. Growth,* Vol. 216, p. 459.

Gutjahr, A., Dabringhaus, H., and Lacmann, R. 1996. "Studies of the growth and dissolution kinetics of the $CaCO_3$ polymorphs calcite and aragonite II. The influence of divalent cation additives on the growth and dissolution rates", *Journal of Crystal Growth*, Vol.158, pp.310-315.

Hu, Z. and Deng, Y. 2003. "Supersaturation control in aragonite synthesis using sparingly soluble calcium sulfate as reactants*", J. Colloid Interf. Sci.,*Vol. 266, p.359.

Hu, Z. and Deng, Y. 2004. "Synthesis of needle-like aragonite from calcium chloride and sparingly soluble magnesium carbonate", *Powder Technology*, Vol.140, pp.10-16.

Imai, H., Terada, T., Miuro, T. Yamabi, S. 2002. "Self-organized formation of porous aragonite with silicate", *J. Cryst. Growth*,.Vol. 244, p.200.

Khoshkhoo, S. and Anwar, J. 1993. "Crystallization of Polymorphs: the effect of solvent", *J. Phys. D: App. Phys.*, Vol.26, pp.B90-B93.

Lawes, G., 1987. *Scanning Electron Microscopy and X-Ray Microanalysis*, (John Wiley & Sons, London), pp. 2-53.

Lei, M., Li, P.G., Sun, Z.B. and Tang, W.H. 2006. "Effects of organic additives on the morphology of calcium carbonate particles in the presence of CTAB", *Materials Letters*, In press.

Liu, Q.S., Liu, W.Y., Chen, B. and Chen, W. 1998. Proc. Int. Symp. Electr. Insul. Mater., Inst. Elec. Eng., Japan, Tokyo, pp 159-161.

Loste, E., Wilson, R.M., Seshadri, R. and Meldrum, F.C. 2003. "The role of magnesium in stabilizing amorphous calcium carbonate and controlling calcite morphologies", *Journal of Crystal Growth*, Vol. 254, pp.206-218.

Mann, S., Dldymus, J.M., Sanderson, N.P., Heywood, B.R. and Samper, E.J. 1990. *J. Chem. Soc. Faraday Trans*, Vol.86, p.1873.

Mansour, S.H. and Abd-El-Messieh, S.L. 2002. "Electrical and Mechanical Properties of Some Polymeric Composites", *Journal of Applied Polymer Science*, Vol.83, pp. 1167-1180.

Naka, K. and Chujo, Y. 2001. "Control of Crystal Nucleation and Growth of Calcium Carbonate by Synthetic Substrates", *Chem. Mater.*, Vol.13, pp.3245-3259.

Nakamoto, K. 1986. *Infrared and Raman Spectra of Inorganic and Coordination Compounds*, (John Wiley & Sons), pp. 86-87.

Osman, M.A., Atallah, A. and Suter, U.W. 2004. "Influence of excessive filler coating on the tensile properties of LDPE-calcium carbonate composites", *Polymer*, Vol.45, pp.1177-1183.

Öktem, G.A.1991. *The Properties of Perlite Filled High Density Polyethylenes*, *PhD. Thesis,* (Ankara*).*

Petrucci, R.H. and Harwood, W.S., 1997. General Chemistry, (Prentice-Hall, Inc., New Jersey), p.776.

Qi, L., Li, J. and Ma, J. 2002. "Biomimetic Morphogenesis of Calcium Carbonate in Mixed Solutions of Surfactants and Double-Hydrophilic Block Copolymers", *Advanced Materials*, Vol.14, No.4, pp.300-303.

Richter, A., Betzold, D., Hofman, H., Ulfrich, N. 1995. *Chem. Technol.* Vol. 6, p.306.

Sinkankas, J., 1964. *Mineralogy*, (Van Nostrand Reinhold Company, New York), pp. 57-69.

Swinney, L.D., Stevens J.D., and Peters, R.W. 1982. "Calcium carbonate Crystallization Kinetics*", Ind. Chem. Eng. Fundam*., Vol.21, p.31.

Şen, S. and Nugay N. 2000. "Uncured and Cured State Properties of Fly Ash Filled Unsaturated Polyester Composites", *Journal of Applied Polymer Science*, Vol.77, p.1128.

Tai, Y.T. and Chen, F.B. 1998. "Polymorphism of $CaCO_3$ Precipitated in a Constant - Composition Environment", *AlChE Journal*, Vol.44, No.8, pp.1790-1798.

Verdoes, D., Kashichhiev, D., and van Rosmalen, G.M. 1992. *Journal of Crystal Growth*, Vol.118, p.401.

Wang, L., Sondi, I., and Matijević, E. 1999. "Preparation of Uniform Needle-Like Aragonite Particles by Homogeneous Precipitation", *Journal of Colloid and Interface Science*, Vol.218, pp.545-553.

WEB_1, 2005. European Industrial Minerals Association, 07/11/2005. http://www.ima- eu.org/en/CalCarb05.pdf

WEB_2, 2005. United Kingdom Institute for Conservation of Historic and Artistic Works, 07/11/2005. http://palimpsest.stanford.edu/ukic/fw/cn/75-2.htm

WEB_3, 2005. University of Oregon, 07/11/2005. http://darkwing.uoregon.edu/~jrice/geol_311/xtalg row.html

WEB_4, 2005. Paperloop, 07/11/2005. http://www.paperloop.com/db_area/archive/ppi_mag/2004/09/06.html

WEB_5, 2005. About, 08/12/2005. http://metals.about.com/library/bldef-Composite-Material.htm

WEB_6, 2005. Wikipedia, 30/11/2005. http://en.wikipedia.org/wiki/Bragg%27s_law

WEB_7, 2005. EDDNET Chemistry, 31/11/2005.
http://www.chm.bris.ac.uk/webprojects2000/dedmonds/Dave's%20Documents/chemistry/xray7.html

WEB_8, 2005. Princeton University, 31/11/2005.
https://webdb.princeton.edu/dbtoolbox/query.asp?qname=RigakuXRD

WEB_9, 2005. USGS, 30/11/2005.
http://pubs.usgs.gov/of/of01-041/htmldocs/xrpd.htm

WEB_10, 2005. Binghamton University,30/11/2005.
http://materials.binghamton.edu/labs/xray/xray.html

WEB_11, 2005. Wikipedia, 02/12/2005.
http://en.wikipedia.org/wiki/Scanning_electron_microscope

WEB_12, 2005. University of Nebraska, 02/12/2005.
http://www.unl.edu/CMRAcfem/em.htm

WEB_13, 2005. ACEPT, 02/12/2005.
http://acept.la.asu.edu/PiN/rdg/elmicr/elmicr.shtml

WEB_14, 2005. Materials Evaluation and Engineering, Inc., 07/12/2005.
http://www.mee-inc.com/ftir.html

WEB_15, 2005. Massachusetts Institute of Technology, 05/12/2005.
http://ocw.mit.edu/NR/rdonlyres/Chemistry/5-32Intermediate-Chemical-ExperimentationSpring2003/CA6722BA-7333-4A99-B4AB1F7B880080C6/0/Appendix_1_Qual_Instrumentation_03.pdf

WEB_16, 2005. ADMET, 08/12/2005.
www.admet.com/articles.htm

Wray, J.L. and Daniels F. 1957. “Precipitation of Calcite and Aragonite”, *Journal of the American Chemical Society*, Vol.79, No.9, pp.2031-2034.

Wei, H., Qiang, S., Zhao Y., Wang, D.J. and Xu, D.F. 2003. “Influence of polyvinyl pyrrolidone on the precipitation of calcium carbonate and on the transformation of vaterite to calcite”, *Journal of Crystal Growth*, Vol.250, pp.516-524.

Wei, H., Qiang, S., Zhao Y., Zhou, Y., Wang, D.J. and Xu, D. 2004a. “Crystallization habit of calcium carbonate in presence of sodium dodecyl sulfate and/or polypyrrolidone”, *Journal of Crystal Growth*, Vol.260, pp.545-550.

Wei, H., Qiang, S., Zhao Y., Zhou, Y., Wang, D.J. and Xu, D. 2004b. “Effect of anionic surfactant-polymer complexes on the crystallization of calcium carbonate”, *Journal of Crystal Growth*, Vol.264, pp.424-429.

Westin, K.J. and Rasmuson, Å.C. 2005a. ”Nucleation of calcium carbonate in presence of citric acid, DTPA, EDTA and pyromellitic acid”, *Journal of Colloid and Interface Science*, Vol.282, pp.370-379.

Westin, K.J. and Rasmuson, Å.C. 2005b. *Journal of Colloid and Interface Science*, “Crystal growth of aragonite and calcite in presence of citric acid, DTPA, EDTA and pyromellitic acid”, Vol.282, pp.359-369.

Xie, A.J., Yuan, Z.W. and Shen, Y.H. 2005. “ Biomimetic morphogenesis of calcium carbonate in the presence of a new amino-carboxyl-chelating-agent “, *Journal of Crystal Growth*, Vol.276, pp.265-274.

Yu, J., Ming, L., Cheng, B. and Zhao, X. 2004. “Facile preparation of calcium carbonate particles with unusual morphologies by precipitation reaction”, *Journal of Crystal Growth*, Vol.261, pp.566-570.

Yu, Q., Ou, H., Song, R., Xu, A. 2006. “The effect of polyacrylamide on the crystallization of calcium carbonate: Synthesis of aragonite single-crystal nanorods and hollow vatarite hexagons”, *J.Cryst.Growth*, Vol, 286, p.178.

Zhou, B., Ji, X. Sheng, Y., Wang, L. and Jiang Z. 2004. “Mechanical and thermal properties of poly-ether ether ketone reinforced with $CaCO_3$”, *European Polymer Journal*, Vol. 40, pp. 2357-2363.